SCUOLA DOTTORALE IN

GEOLOGIA DELL'AMBIENTE E DELLE RISORSE

XXV CICLO SEZIONE GEOLOGIA DELL'AMBIENTE E GEODINAMICA

RELATIONSHIP BETWEEN CURVED THRUST BELTS, RIFT INVERSION, OBLIQUE CONVERGENCE AND STRIKE-SLIP FAULTING. AN EXAMPLE OF EASTERN CORDILLERA IN COLOMBIA

presented by

GIOVANNY JIMENEZ DIAZ

Prof. Claudio Faccenna, examiner

Dr. Fabio Speranza, co-examiner

ROME, 2013

Table of contents

Chapter 1

INTRODUCTION 1

Chapter 2

Paleomagnetism and magnetic fabric of the Eastern Cordillera of Colombia: Evidence for oblique convergence and non-rotational reactivation of a Mesozoic intra-continental rift. 5

Abstract 5

1.0 Introduction 6
2.0 Setting and evolution of NW South America and the Colombian cordilleras 10
2.1 Structure, shortening estimates, and evolution of the Eastern Cordillera of Colombia. 11
2.2 Previous Paleomagnetic data from the northern Andes. 16
3.0 Sampling strategy and Methods 17
4.0 Results 19
4. 1 Anisotropy of magnetic susceptibility 19
4. 2 Magnetic Mineralogy 22
4. 3 Paleomagnetic Directions 23
4. 4 Oroclinal Test 28
5.0 Discussion 27
6.0 Conclusions 35
References 37

Chapter 3

Magnetic stratigraphy of the Bucaramanga alluvial Fan: Evidence for a ≤ 3 mm/yr slip rate for the Bucaramanga-Santa Marta Fault, Colombia 52

Abstract 53
1.0 Introduction 49
2.0 Characteristics of the Bucaramanga-Santa Marta Fault 55
2.1 The Bucaramanga Fan 59
2.2 The deep seismicity of the Bucaramanga Nest 60
3.0 Sampling and Methods 61
4.0 Results 62
4.1 Magnetic Mineralogy 62
4.2 Paleomagnetism 63
5.0 Discussion and Conclusions 68
References 72

Chapter 4

Emplacement of the Paleocene-Eocene Santa Marta Batholith (Santa Marta Massif-Northern Colombia): Constraining the Cenozoic tectonic evolution of the Caribbean arc. 78

1.0 Introduction 78
2.0 Geological framework 80
3.0 Sampling strategy and Methods 83
4.0 Results 85
4.1 Anisotropy of magnetic susceptibility 85
4.2 Foliations and Lineations 87
4. 3 Faults 88
5.0 Discussion and conclusions 89
References 92

Chapter 5

Rift inversion during oblique convergence insight from analog modeling 97

1.0 Introduction 97
2.0 Methods 98
2.1 set up 98
3.0 Results 100
3.1 Brittle-ductile 0º 100
3.2 Brittle-ductile 15º 100
3.3 Brittle-ductile 30º 101
3.4 Brittle-ductile 45º 102
References 104

Chapter 1

INTRODUCTION

The northern Andes mountain belt in Colombia is a complex tectonic region close to the triple junction of the continental plate of South America with the Caribbean and the Nazca oceanic plates. In this complex region, the South Caribbean tectonic evolution reflects the interaction between the Caribbean plate and the Northwestern border of South America since Late Cretaceous times (Cortes et al, 2005). The Mesozoic tectonic evolution of the NW Andes has been related to the accretion of several tectonostratigraphic terranes of both oceanic and continental origin (Barrero, D; 1979, Etayo, F; 1983, Toussaint, F y Restrepo, J; 1989). The Eastern Cordillera (EC) is a Mesozoic rift inverted since Miocene; as well as the EC is a regional curved thrust belt with regional change in the strike of local structures (faults and folds). By considering the regional strike of EC, this thrust belt can be defined by three domains. (1) In the southern zone the NS strike domain, (2) the central zone the NE strike domain and (3) to the north the NW strike domain. Those changes in strike could be related to rotations of blocks in the younger phases of shortening or to accommodation of the deformation in the shortening phases, controlled by faults in the Jurassic and early Cretaceous basement, likely related to the rift phase. At least two hypotheses can explain the curved shape of the EC: (1) orocline hypothesis or (2) non-rotational chain with rift structures controlling the subsurface to surface geometry.

In order to gain insights in some of these problems, a detail structural, paleomagnetism, anisotropy of magnetic susceptibility (AMS) and analog modeling study will be carried out. Paleomagnetism and AMS technics were focus on the EC, Bucaramanga Fan, Santa Marta Massif. Analog modeling technic was used to explore the tectonic inversion into the brittle and ductile regimens under oblique convergence.

The paleomagnetism is the main technique allowing a quantification of rotation and

translation of blocks. Ferromagnetic minerals record the ancient direction of the earth's magnetic field. The anisotropy of magnetic susceptibility (AMS) is considered an important proxy for the strain characterizing a rock. Sediments have a magnetic foliation sub-parallel to bedding. Deformation phases modify primary fabrics developing magnetic lineation, and this lineation can be related with strain ellipsoids and major tectonic structures. AMS is very sensitive to the pristine tectonic phases occurring early after diagenesis. Therefore the AMS study of sediments of different age may provide the evidence for different tectonic episodes developing synchronous with the geologic history of an orogen. A model - either analog or numerical - is a simplified scaled representation of nature, though on a more convenient geometric and temporal scale (smaller and faster). The purpose of models is not simply to reproduce natural observation, but primary to test by controlled experiments hypotheses as to the driving mechanisms of tectonic processes. The main advantage of analogue modeling lies in the fact that a correctly constructed model passes through an evolution, which is the physical response of the system to the applied experimental conditions. These advantages of laboratory models make this methodology a valid tool for the advancement of our understanding of structural and geodynamic processes.

This work was focus in four topics: the spatial evolution of the EC, the Bucaramanga Fault, Santa Marta Fault and rift inversion. Each topic is presented in the next chapters. Chapter 2 shows the paleomagnetic and AMS results of Cretaceous to Cenozoic units of the EC and Cucuta zone. 23 sites reveal no rotation of the EC range with respect to stable South America. Magnetic lineations from AMS analysis do not trend parallel to the chain, but are oblique to the main orogenic trend. By also considering GPS evidence of a ~1 cm/yr ENE displacement of central-western Colombia accommodated by the EC, we suggest that the Miocene-recent deformation event of this belt arises from ENE oblique convergence reactivating a NNE rift zone. Oblique shortening was likely partitioned in pure dip-slip

shear characterizing thick-skinned frontal thrust sheets. Finally, the 35°±9° clockwise rotation observed in four post-Miocene magnetically overprinted sites from the Cucuta zone reflects late Cenozoic and ongoing right-lateral strike-slip displacement occurring along buried faults parallel to the Boconó fault system.

Chapter 3 shows a paleomagnetic investigation of a continental alluvial, Bucaramanga fan juxtaposed to the Bucaramanga Fault, and horizontally displaced by 2.5 km with respect to its feeding river. Nine reliable paleomagnetic directions define a succession of six different magnetic polarity zones that, lacking additional age constraints, can be correlated with several tracks of the Plio-Pleistocene magnetic polarity time scale. The Bucaramanga Fan can be reasonably dated at 0.8 Ma (Brunhes-Matuyama chron transition), translating into a maximum 3 mm/yr slip rate for the Bucaramanga Fault. Older age models would obviously yield smaller slip rates. Paleomagnetic sites, located at 4-10 km from the fault, do not show significant rotations, implying weak fault coupling and/or ductile upper crust behavior adjacent to the Bucaramanga Fault.

Chapter 4 shows structural and AMS results of Cretaceous metamorphic and Paleogene intrusive rocks. Foliations, lineations, faults and AMS reveal ductile and brittle regimens. Foliations and lineations in Metamorphic and granitic rocks shows ductile deformation related to NE extension during the Paleogene. Brittle deformation is related to regional wrench faults as the Santa Marta and Oca faults. AMS and faults kinematic solutions show a NW-SE (aprox) compression vector. Finally, chapter 5 shows the results for experiment in sand box for brittle and ductile-brittle regimens. Rift inversion mechanism was evaluated in 3D for brittle and ductile regimen in oblique convergence for 0º, 15º, 30º and 45º. The brittle experiments show a rift inversion located in the principal normal fault plane. During the 45º experiment, rift inversion reveals strike-slip component. On the other hand the ductile-brittle experiments reveal a positive flower for all experiments, as well as, in 30º and 45º convergence develop a strike-slip component.

Overall the results of the four chapters highlight the importance of the basin geometry, structures related and dextral strike-slip component to explain the non-rotational curved thrust belt. Deformation related to the strike-slip Bucaramanga Fault occurs with low slip rate during the last 0.8 ma. The Cretaceous metamorphic rocks in the Santa Marta Massif, records NE-SW extensional structures related to Paleogene intrusions. The strike-slip Santa Marta Fault deforms the intrusive rocks in brittle regimens with a normal component. Finally ductile layers in normal to oblique convergence develop a positive flower during rift inversion

Chapter 2

Paleomagnetism and magnetic fabric of the Eastern Cordillera of Colombia: Evidence for oblique convergence and non-rotational reactivation of a Mesozoic intra-continental rift.

Abstract

We report on the paleomagnetic and anisotropy of magnetic susceptibility (AMS) investigation of 58 sites from Cretaceous to Miocene marine and continental strata gathered in the Eastern Cordillera (EC) and the Cucuta zone, at the junction between the Santander Massif and the Merida Andes of Colombia. The EC, widely investigated in the past for hydrocarbon exploration, is a NNE-trending double vergent intra-continental thick-skinned range inverting a Triassic-early Cretaceous rift zone. Twenty-three sites reveal no rotation (on average) of the EC range with respect to stable South America. Our data show that the EC inverted a NNE-oriented rift zone, and that the locations of the Mesozoic rift and the mountain chain roughly correspond. Surprisingly, magnetic lineations from AMS analysis do not trend parallel to the chain, but are oblique to the main orogenic trend. By also considering GPS evidence of a ~1 cm/yr ENE displacement of central-western Colombia accommodated by the EC, we suggest that the Miocene-recent deformation event of this belt arises from ENE oblique convergence reactivating a NNE rift zone. Oblique shortening was likely partitioned in pure dip-slip shear characterizing thick-skinned frontal thrust sheets (well-known along both chain fronts), and by range-parallel right-lateral strike-slip fault(s), which have not been identified yet and likely occur in the axial part of the EC. Finally, the 35°±9° clockwise rotation observed in four post-Miocene magnetically overprinted sites from the Cucuta zone reflects late Cenozoic and ongoing

right-lateral strike-slip displacement occurring along buried faults parallel to the Boconó fault system, possibly connected with the right-lateral faults inferred along the axial part of the EC.

1.0 Introduction

The NW corner of South America is characterized by a system of mountain chains, spreading northward in Colombia and Venezuela from the complex Andean belt observed at equatorial latitudes (Fig. 1).

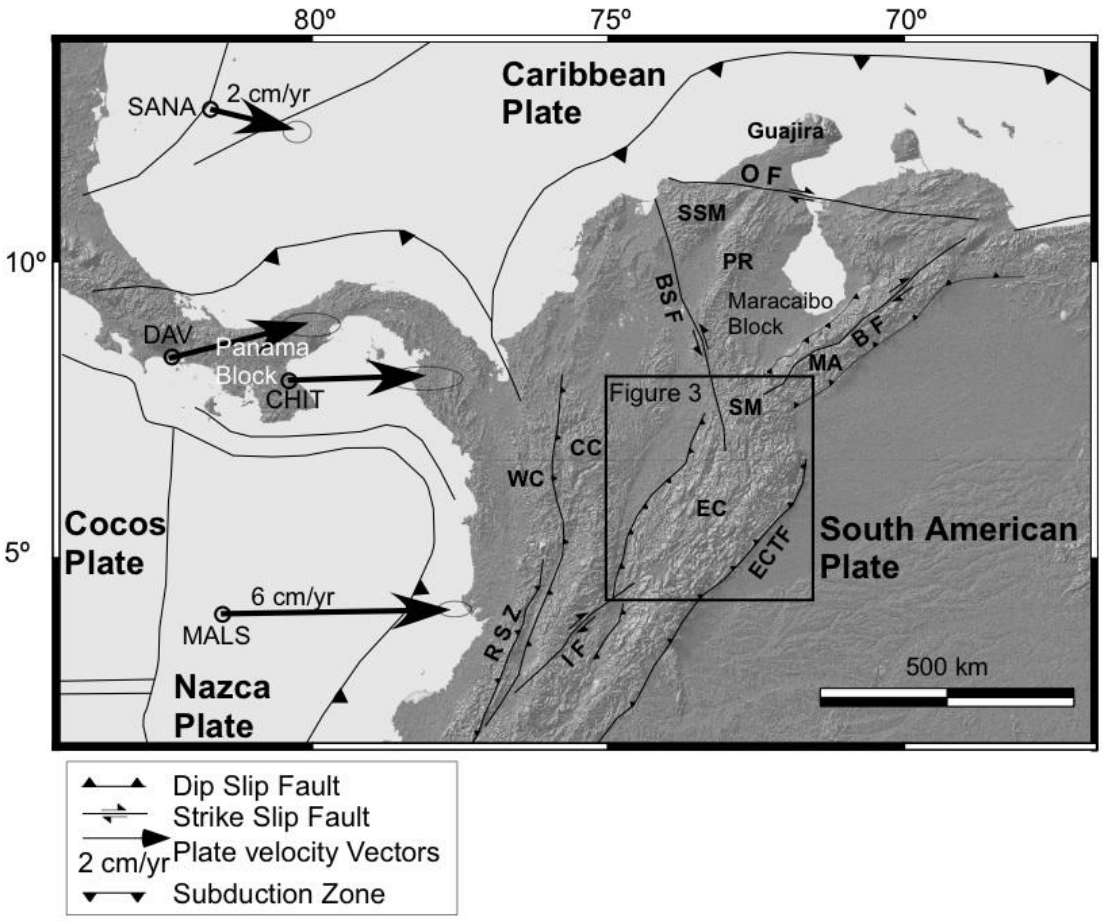

Figure 1. Major tectonic and structural features of the NW margin of South America. Plate velocity vectors with respect to stable South America are from Trenkamp et al. (2002). WC = Western Cordillera, CC = Central Cordillera, EC = Eastern Cordillera, SM = Santander Massif, SSM = Santa Marta Massif, PR = Perijá Range, MA = Merida Andes, ECTF = Eastern Cordillera thrust front, RSZ = Romeral suture zone, IF = Ibagie Fault, BSF = Bucaramanga-Santa Marta Fault, OF = Oca Fault, BF = Boconó Fault.

The narrow Andean chain of Ecuador evolves northward into three distinct mountain chains (Western, Central, and Eastern Cordillera). Farther north, the Western Cordillera turns westward and is connected with the Panama Arc, while the Eastern Cordillera (EC) terminates northward with the triangular-shaped Maracaibo block, bounded at its three sides by strike-slip faults and associated orogenic belt systems (Santander Massif (SM), Santa Marta Massif and Mérida Andes).

The orogenic complexity of NW South America is the result of the interaction between the Nazca, Caribbean, and South American plates, further complicated by the eastward indentation of the Panama-Chocó block since Oligocene (Farris et al., 2011) to mid-Miocene times (Pindell et al., 1988; Taboada et al., 2000; Cortés et al., 2005). Relative plate velocities with respect to South America are fairly well constrained with GPS observations (Trenkamp et al., 2002). The fast eastward Nazca motion at 6 cm/yr is largely accommodated at the oceanic trench west of South America, while the 2-3 cm/yr E-ESE drift of the Panama Arc and the Caribbean plate seems to be progressively absorbed by both the South Caribbean accretionary wedge and other chain systems of NW South America.

Unraveling the genesis and evolution of such a complicated belt should take advantage of several different data sets, such as plate motion reconstructions during the geological past (Pindell et al., 1988), geology and tectonics of the chain (Montes et al., 2005; Cortés et al., 2005, Sarmiento-Rojas et al., 2006, Bayona et al., 2008, Mora et al., 2008, 2010, Parra et al., 2012), present-day deformation given by geodesy and seismicity (Trenkamp et al., 2002, Taboada et al., 2000), and deep chain structure documented by seismic reflection profiles (Colletta et al., 1990; Dengo and Covey., 1993, Cooper et al., 1995). However, previous studies have not addressed so far the causes of for the along strike changes in the structural trends Eastern Cordillera, from N-S, south of Bogotá, to NE, north of Bogotá, and finally to NNW to the north of the Eastern Cordillera and SM.

In this framework, paleomagnetism and anisotropy of magnetic susceptibility (AMS) are expected to give a significant contribution, as they can document rotations and bending of given portions of mountain belts, and provide valuable strain proxies for different rock units. These analyses have contributed to understand the setting and evolution of several mountain chains such as the Apennines (Mattei et al., 1995; Speranza et al., 1997; Muttoni et al., 1998), the Pyrenees (Larrasoaña et al., 2003; Pueyo et al., 2003), the Rocky Mountains (Eldredge and Van der Voo, 1988; Jolly and Sheriff, 1992), and the Andes (Arriagada et al., 2000, 2003, 2006; Butler et al., 1995; Maffione et al., 2009; McFadden et al., 1995; Rapalini et al., 2001; Randall et al., 1996, 2001; Roperch et al., 1992, 1999, 2000; Somoza et al., 2002; Taylor et al., 2005, among many others).

By considering vertical-axis rotations and orogenic trends (e.g. Carey (1955), Marshak (1988), Macedo and Marshak (1999) Sussman et al., (2004), Weil and Sussman (2004), Cifelli et al., (2008)) arcs, which do not undergo vertical-axis rotations are primary arcs; the paleomagnetic declinations remain parallel along the arc, and do not correlate with changes in thrust and fold-axis trend (Fig. 2a). Former rectilinear belts subsequently bent are called “oroclines”; the paleomagnetic declinations change following changes in thrust and fold-axis trend with a perfect correlation (Fig. 2b). Progressive curves are those where rotations and thrusting occur simultaneously (Fig. 2c).

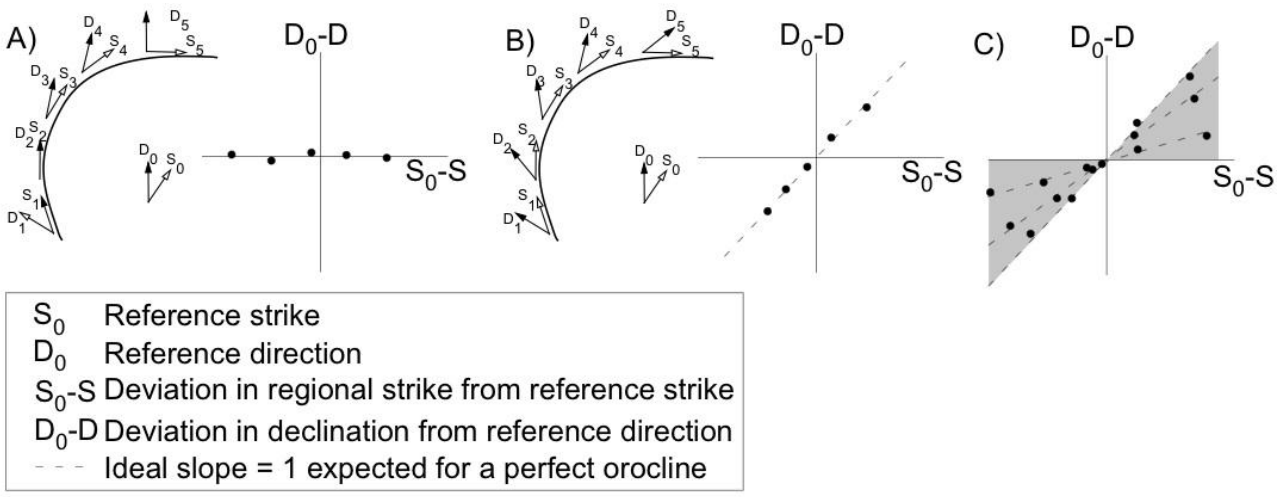

Figure 2. Scheme of the distribution of paleomagnetic declinations as a function of the structural trend in (a) a primary arc, (b) an orocline and (c) a progressive arc (modified from (Cifelli et al. 2008)). (See text for details).

In this paper we report the results of an extensive paleomagnetic investigation of the Eastern Cordillera of Colombia. The Eastern Cordillera is an intra-continental orogen extending from southern Colombia to the southern vertex of the Maracaibo block. When considering also the Santander Massif (Fig. 3), the Eastern Cordillera might resemble an orogenic salient encircling the Magdalena salient to the west and the Cocuy salient to the east (Fig. 1). Thus the initial aim of our paleomagnetic investigation was to address the non-rotational vs. oroclinal nature of the Eastern Cordillera (Fig.2), to better constrain orogenic displacements and paleogeography. Since there is wide evidence that the Eastern Cordillera inverted a Triassic-Cretaceous rift system (Colletta et al., 1990; Cooper et al., 1995; Sarmiento-Rojas, 2001; Mora et al., 2006; Mora et al., 2009), our investigation was also addressed to try to constrain the location of the chain with respect to the original rift basin.

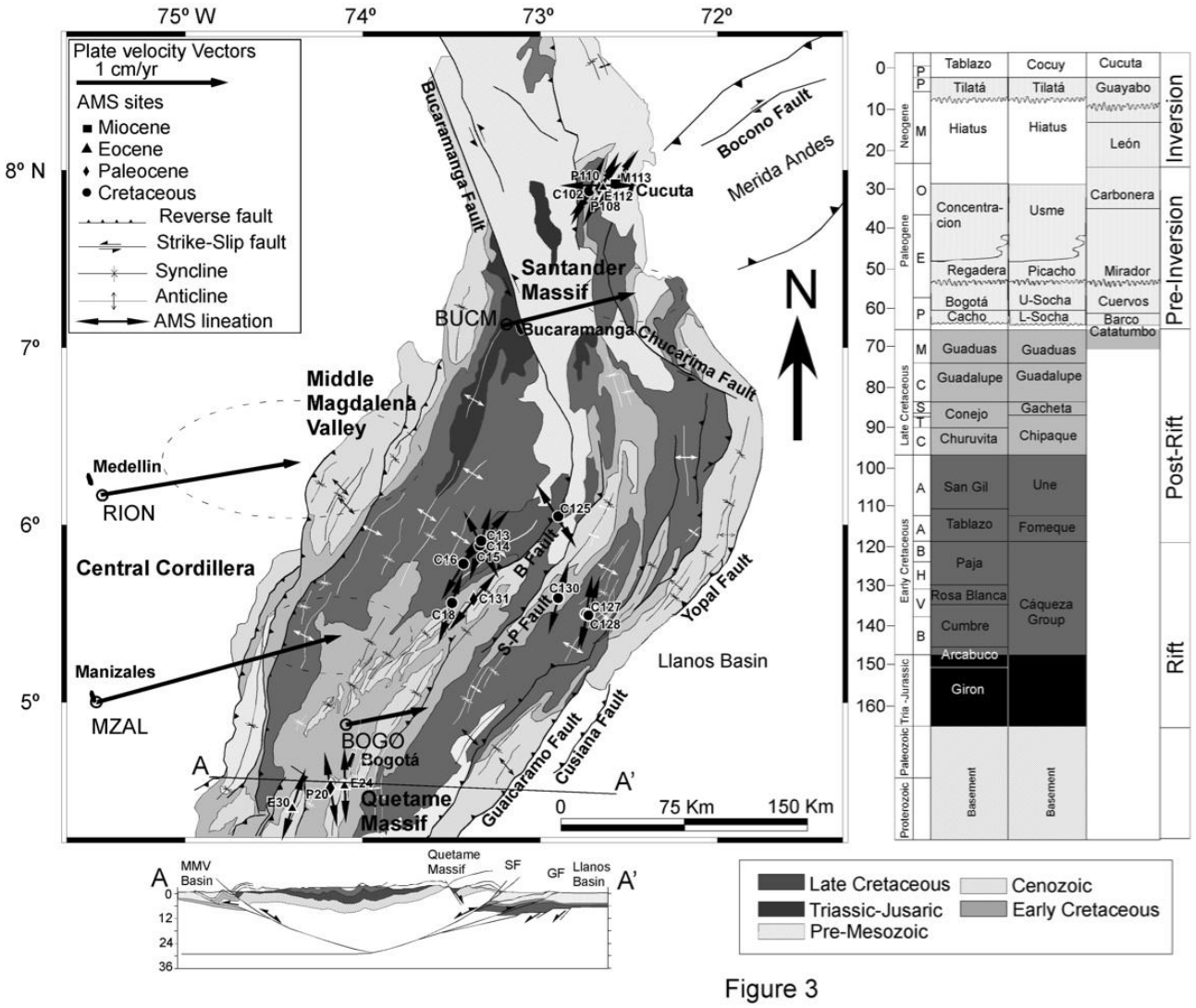

Figure 3

Figure 3. Geological map of the Eastern Cordillera and adjacent zones (see Figure 1 for location). Black double arrows represent the site-mean magnetic lineation directions (numbers are site codes, see Table 2), white arrows are plate velocity vectors with respect to South America (Trenkamp et. al, 2002). B Fault = Boyacá Faut, S-P Fault = Soapága-Pesca Fault.. Cross section A-A' (modified from (Mora et al.,2008)). Meso-Cenozoic stratigraphy of the Eastern Cordillera and Cucuta area

2. 0 Setting and evolution of NW South America and the Colombian cordilleras

While the subduction of the Farallon plate beneath South America has been continuously occurring since Late Paleozoic to early Mesozoic times (Case et al., 1990; Restrepo-Pace, 1995), the accretion of oceanic terranes of the Western Cordillera along the Romeral fault system occurred since Maastrichtian–Early Paleocene (Barrero, 1979). Eastward

subduction of the Caribbean plate (Bayona et al., 2012) and oceanic terrane accretion caused the onset of uplift of the continental margin (Central Cordillera-Santa Marta Massif; Gomez et al., 2003; Bayona et al., 2011), and intraplate deformation and volcanism encompassing from the Magdalena Valley to the present Llanos basin due to the reactivation of basement structures in a transpressive setting (Montes et al., 2003; Cortés et al., 2006; Bayona et al., 2012). A late Paleocene- middle Eocene unconformity in the Eastern Cordillera has been associated with the accretion of the San Jacinto Terrane in northern Colombia (Taboada et al., 2000), and the relative shift from eastward to northward movement of the Caribbean plate (Bayona et al., 2012). The regional tectonic setting of the South Caribbean region changed in Miocene times (25 Ma), as the Farallón plate broke up and formed the Nazca and Cocos plates (Hey, 1977). As a result of plate reorganization, the convergence direction between Nazca and South America changed abruptly, from SW–NE to W–E (Pilger, 1983). The middle to Late Miocene collision of the Panama arc with NW Colombia has been related with the main Andean tectonic phase of shortening in the Eastern Cordillera (Duque-Caro, 1990; Taboada et al., 2000).

2.1 Structure, shortening estimates, and evolution of the Eastern Cordillera of Colombia.

The Eastern Cordillera of Colombia is a double-verging mountain system inverting a Mesozoic rift, and bounded by major reverse faults that locally involve crystalline and metamorphic Precambrian–Lower Paleozoic basement rocks, as well as Upper Paleozoic–Cenozoic sedimentary and volcanic sequences (Colletta et al., 1990, Cooper et al., 1995; Mora et al., 2009). To the north, the Eastern Cordillera terminates against the Maracaibo block (Fig. 1), and it is split into the Santander Massif (adjacent to the left-lateral Bucaramanga strike-slip fault), and the Merida Andes. The Merida Andes grew since

Oligocene times (Bermúdez et al., 2010), and are considered the result of strain partitioning and tectonic escape mainly related to the right-lateral shear occurring along the Boconó fault, well documented by both GPS (Trenkamp et al., 2002) and focal mechanisms of shallow earthquakes (Audemard et al., 2005; Monod et al., 2010). The interaction between the Boconó fault and the Eastern Cordillera thrust front is defined as a basement structural high, called Pamplona indenter (Boinet et al., 1985). The Santander Massif is characterized by Precambrian and Paleozoic metamorphic rocks, which are intruded by Triassic-Jurassic igneous rocks. Locally, sedimentary rocks of Late Paleozoic to Early Cretaceous age are also exposed, while a Cenozoic sequence occurs in the flanks of the massif (Ward et al., 1973; Evans, 1977). Fabre (1987) and Ayala-Calvo et al., (2012) suggested that uplift occurred since Paleocene time, whereas fission-track analyses indicate kilometer-scale (3.5 km) erosion from early Miocene to Pliocene (Ross et al., 2009).

The first tectono-stratigraphic events characterizing the Eastern Cordillera-Santander massif date back to Triassic-Early Cretaceous times, when continental rifting originated the Tablazo-Magdalena rift to the west and the Cocuy half-rift to the east, separated by the Floresta-Santander high (Fabre, 1987; Cooper et al., 1995). A back-arc setting and tectonic subsidence dominated during the Early Cretaceous (Hebrard, 1985; Fabre, 1987; Sarmiento-Rojas et al., 2006).

The Syn-rift sequence is dominated by continental red beds in the Tablazo-Magdalena basin (Giron-Cumbre formations) and by shallow-marine sediments in the Cocuy basin (Caqueza Group) (Fig. 3). The Rosa Blanca Formation marks the change between continental to marine sedimentation (Cooper et al., 1995). The syn-rift sequence finished with the restricted marginal marine mudstones (Paja Formation) (Fig.3).

The Late Cretaceous was a period of thermal subsidence, and continuous subduction of

the Farallon plate beneath the western margin of South America (Cooper et al., 1995; Sarmiento-Rojas et al., 2006). Mountain building and deformation started in the Maastrichtian to Early Paleocene in the Western and Central Cordillera (Gomez et al., 2003). The post-rift sequence or back-arc sequence (Copper et al., 1995) in the Tablazo sub-basin is dominated by organic-rich marine mudstones, limestones and sandstones (Tablazo and San Gil formations) (Fig. 3). In the Cocuy sub-basin, deposition was characterized by shallow-marine sands (Fomeque Formation) (Cooper et al., 1995). A regional transgression is represented by muddy and marine mudstones with subordinate thin carbonates (San Gil Formation) and shallow-marine silici-clastic shelf over a wide area, including the Santander high (Une Formation) (Fig. 3). The marine sequence continued with mudstones, cherts, and phosphates (La luna-Churuvita-Conejo, Gacheta and Chipaque formations) (Fig. 3). According to Cooper et al., (1995), a fall in relative sea level deposited high energy, quartz-rich, shoreface sandstones (Guadaupe Formation).

Mountain building and deformation started in the Maastrichtian to Early Paleocene in the Western and Central Cordillera (Gomez et al., 2003). At that time, the domain of the present-day Eastern Cordillera was a foreland basin segmented by minor uplifts (Bayona et al., 2008; Parra et al., 2012). Finally, post-early Oligocene shortening (increasing in Miocene time during the Andean tectonic phase) caused positive tectonic inversion of pre-existing normal faults on both flanks of the Eastern Cordillera (Colletta et al., 1990; Cooper et al., 1995, Mora et al., 2006, 2008, 2010a), uplift of the Santander Massif (Ross et al., 2009) and Merida Andes (Bermudez et al., 2010).

Pre-inversion to inversion sequences are represented by continental paralic to fluvial interbedded sandstone and shales. According to Bayona et al., (2008), five sequences can be identified. The first sequence corresponds to late Maastrichtian–Paleocene composed by amalgamated quartzarenites that abruptly grade upward to organic-rich fine-grained beds (Guaduas Formation) and black shales and mudstones (Catatumbo Formation). The

second is the Lower to upper Paleocene sequence; correspond to light-colored mudstones interbedded with litharenites (Cacho, Bogotá, Lower and Upper Socha, Barco and Cuervos) (Fig. 3). The third sequence corresponds to conglomeratic quartzes sandstones deposited during early to middle Eocene time (Regadera, Picacho and Mirador) (Fig. 3). The fourth sequence corresponds to Upper Eocene to Middle Miocene. The sequence vary laterally from laminated dark-gray mudstone with thin seams of coal and bioturbated fine-grained sandstones, in the axial zone of the Eastern Cordillera (Usme and Concentración formations) to amalgamated sandstones in the Llanos Basin (Carbonera Formation) (Fig. 3). Finally the fifth sequence from Middle Miocene to Pliocene. The sequence consists of dark-colored laminated mudstone and shale (Leon Formation) and varicolored mudstone, lithic-bearing sandstone, and conglomerates (Guayabo Formation). Neogene units are restricted to the synclinal inliers within the orogen (Tilatá Formation), but much more extensive in the foreland (Mora et al., 2008) (Fig.3).

The Eastern Cordillera is characterized by shallow thrust-type earthquakes at both range fronts, while a few strike-slip events have been recorded at the axial-western part of the chain, ~100 km north of Bogota (Fajardo-Peña, 1998 and Taboada et al., 2000). A well-known nest of deep seismicity at 100-200 km depth below the Bucaramanga town (Zarifi et al., 2007) has been mostly interpreted as occurring within the subducting Caribbean plate (Taboada et al., 2000; Cortés et al., 2005). GPS data show that most of the 6 cm/yr eastward motion of the Nazca plate is absorbed at the oceanic trench, but that central-western Colombia still drifts ENE-ward with respect to South America at a rate exceeding 1 cm/yr (Fig. 3; Trenkamp et al., 2002).

Shortening estimates proposed for the Eastern Cordillera by authors interpreting seismic reflection profiles and cross sections vary from 58 km (Mora et al., 2008) (Fig. 3), to 170 km (Roeder and Chamberlain, 1995), while the intermediate values of 68, 105, and 140 km were proposed by (Cooper et al., 1995), Colletta et al., (1990), and Dengo and Covey

(1993), respectively. Sarmiento-Rojas et al., (2001) proposed a southward decrease of regional shortening, in agreement with the evidence that the Eastern Cordillera fades out towards the south and connects to the Andes of Ecuador (Fig. 1).

Concerning the geodynamics of the Eastern Cordillera, several hypotheses have been proposed. Colletta et al., (1990) suggested a continental subduction below the axial zone of the chain to explain its double vergence. The continental slab below the axial zone of the Eastern Cordillera would have produced a mechanical anisotropy yielding a double-verging system.

Dengo and Covey (1993) proposed that the Eastern Cordillera is a predominant east-verging structure formed during two main tectonic phases. The first phase induced a thin-skinned style that created east-verging thrust faults penetrating into Cretaceous and Paleogene sequences. In this model, the low-angle faults are rooted in the Central Cordillera, and a mid-crustal detachment links the Eastern Cordillera to the Nazca subduction zone. Roeder and Chamberlain (1995) inferred a structural style of low-angle faults penetrating the basement, with dominant east-verging tectonic transport.

Montes et al., (2005), based on structural data, proposed a dextral transpressive deformation of the southern Eastern Cordillera and Magdalena Valley SW of Bogota. Major transpressive systems generating en echelon–type structures along both Eastern Cordillera flanks and its SE margin were also postulated by Kammer (1999) and Velandia et al., (2005), respectively.

Taboada et al., (2000) proposed a geodynamic model for Colombia characterized by the North Andean Block, a deformable wedge moving E-SE and bounded by the Ibague Fault in the south and the Bucaramanga Fault in the northeast (Fig. 1). According to this model, the block progressive indentation would be absorbed along reverse faults located in the foothills of the Eastern Cordillera. Taboada et al., (2000) assumed this block to be dragged at depth by a remnant of the Caribbean Plate. Cortés et al., (2005), relying on paleostress

directions, identified an E-W to WSW-ENE stress regimes from late Cretaceous to late Paleocene, subsequently evolving to NW-SE, and finally WNW-ESE during the main Miocene Andean tectonic phase. They also assumed that the Eastern Cordillera is the consequence of the subduction of the Caribbean plate beneath South America.

2.2 Previous Paleomagnetic data from the northern Andes.

First paleomagnetic works in Colombia were focused on La Guajira (MacDonald and Opdike, 1972), the Bucaramanga zone (Creer, 1970), the Santander Massif (Hargraves et al., 1984), the Perijá Range (Maze and Hargraves, 1984), and the Santa Marta Massif of the Maracaibo block (MacDonald and Opdyke, 1984) (Figs. 1, 3 and Table 1). These works addressed Jurassic-Cretaceous sediments and volcanics, and evidenced rotations of variable magnitude and sign with respect to stable South America. A 30º counterclockwise (CCW) rotation was reported by a paleomagnetic study of Late Tertiary igneous rocks from the Romeral Fault zone (MacDonald et al., 1996). Paleomagnetic studies carried out in the Maracaibo block indicate no rotation of the Merida Andes (Castillo et al., 1991), 17°±12º CW rotation of the Santa Marta Massif (Bayona et al., 2010) and a post-Eocene ~40-50° clockwise (CW) rotation of the Perija Range as documented in the eastern flank by Gose et al., (2003) and in the western flank by Nova et al., (2011). Ayala-Calvo et al., (2005) and Bayona et al., (2006a, 2010) showed a post-late Jurassic translation of blocks from southern latitudes of several crustal domains assembled presently in the Eastern Cordillera and Maracaibo block. Bayona et al., (2010) also documented a (Maracaibo Block), while Jiménez et al., (2012) documented moderate CW rotations in the southern Upper Magdalena Valley. Finally, a widespread magnetic overprint in Cretaceous and Paleogene strata from the Merida Andes and Eastern Cordillera was reported by Bayona et al., (2006b).

Table 1. Previous paleomagnetic results from Colombia

		Geographic coodinates			In situ				tilt-corrected				
Area	Unit	Longitude	Latitude	Age	D (deg)	I (deg)	*k*	a95	D (deg)	I (deg)	k	a95	Rotation
[*Bayona et al*, 2010]													
Santa Marta massif	Guatapurí	73.7	10.1	Triassic-Jurassic	8.2	1.9	25.68	13.5	8.8	8.3	24.71	13.7	12 ± 14.3
	Guatapurí -Los clavos	72.9	10.9	Jurassic	24.4	-5.3	33.02	6.1	20.4	-18.2	46.9	5.1	17 ± 12.8
[*Bayona et al.*, 2006a]													
Bucaramanga	Jordán	73.15	7.25	Jurassic	15.1	-5.2	10.7	13.3	353.6	-27.1	15.0	11.1	
	Girón	73.07	6.97	Jurassic-Cretaceous	9.0	13.3	29.3	14.4	1.7	21.8	29.1	14.4	
Floresta massif	Girón-Tibasosa	72.79	6.06	Jurassic-Cretaceous	353.1	-14.8	12.8	22.2	352.6	14.8	33.0	13.5	
Upper Magdalena	Saldaña	75.41	3.84	Triassic-Jurassic	175.2	15.2	16.0	14.3	178.9	20.3	14.5	15.1	
	Yaví	74.96	3.46	Aptian	5.5	-5.4	34.6	10.4	5.2	6.2	40.2	9.6	
[*Bayona et al.*, 2006b]													
Cerrejon mine	Hato Nuevo-Manantia	72.80	11.00	Cretaceous-Paleocene	357.7	26.9	41.3	8.7	8.6	45.6	34.3	9.6	
Rio Loro	Mito Juan-catatumbo-Mirador	71.85	8.41	Cretaceous-Paleocene	359.3	28.1	22.8	7.4	359.9	-18.1	14.1	7.1	
Cosgua	Lower and Upper Socha- Cocentración	72.78	5.95	Paleocene	359.7	17	66.9	4.5	2.1	-21.6	33.7	6.4	
[*Castillo et al.*, 1991]													
Mérida Andes	La Quinta	71.8	8.1	Jurassic	172.8	-15.2	38.7	5.6	182.8	-17.4	36.2	5.8	
	La Quinta	71.8	8.1	Jurassic	352.1	16.1	39.1	6.4	351.6	0.1	51.7	5.6	
	La Quinta	71.5	7.8	Jurassic	356.2	-49.7	35.6	6.5	3.1	5.9	41.9	6	
	Rio Negro	71.5	7.8	Cretaceous	172.9	-7.9	74.4	6.5	170.4	-20.5	74.3	6.5	
[*Gose et al.* 2003]													
Perijá range	several units	72.70	10.50	Jurassic-Paleocene					47.4	26.1	14.6	12.4	50 ± 12
[Jiménez et al., 2011]													
Upper Magdalena	Saldaña	2.51	75.57	Aptian	19.3	37	17.34	11.9	28.5	34.8	19.04	11.4	31.7 ± 14.4
					336.4	-1.52	5.34	17.6	12	28.9	16	9.5	15.2 ± 11.4
				Jurassic	8.1	6.3	61.4	11.8	13.8	-27	61.4	11.8	
[*MacDonald et al*, 1996]													
Western Cordillera	Ingruma Andesite	5.4	-75.6	Neogene	13.0	-24.6	12.4	19.8					30.0
	Clavijo Andesite				3.0	83.7	9.7	25.9					
	Intrusive?				327.0	0.0							
	Intrusive?				355.0	14							
[*MacDonald and Opdyke*, 1984]													
Santa Marta massif	Guatapuri	73.7	10.1	Triassic-Jurassic	2.4	36.4		20.8	7.6	47.2		26.7	
	Los Clavos	73.4	10.4	Jurassic	344.6	34.7		29.1	351.2	41.3		21.1	
[*MacDonald and Opdyke*, 1972]													
Guajira	Ipapure-La Teta Lava	71.86	11.78	Jurassic	290	-3.1	4.7	39.6	273,6	-5,2	70,2	8,1	
					87.8	-11.3	175.6	7.0	89,6	-7,8	169,1	7,1	
					238.9	26.7	1.9	79.2	247,9	27,9	598,7	3,1	
					243.3	29.4	14.3	198.3	232,4	10,1	15,9	17,3	
					295.9	-5.8	81.6	7.5	291,5	-15,7	82,3	7,4	
					247.9	-18.5	1.9	68.1	268,1	-2,0	765,4	2,8	
					245.7	-24.8	43.4	10.3	249,4	-21,4	352,8	3,6	
					248.3	21.6	2.4	55.7	242,4	-2,8	16,5	19,4	
	Siapana Diorita	71.32	12.08	Paleozoic-Early-Triassic	315.6	45.8	1.8	57.6	337.5	61.8	2.8	37.9	
					233.6	53.4	1.2		262.5	53.1	2.1	51.1	
					359.9	43.6	1.4		251.2	69.2	2.1	53.1	
	Siapana dikes				300.8	-8.3	2.7	38.7	264.2	-38.2	4.2	30.8	
					289.1	28.3	1.5	74.3	245.1	-62.6	3.1	37.6	
	Parashi diorite				1.5	27.6	6.2	26.3	329.7	44.4	5.3	28.7	
					241.0	28.3	14.5	16.4	239.3	28.1	23.6	12.6	
					323.8	23.8	3.2	30.6	297.6	40.6	12.3	13.5	
	Parashi dikes	71.68	12.25	Eocene	25.6	36.6	4.7	26.5	264.3	44.3	7.2	20.5	
					46.6	33.6	52.5	6.7	56.8	33.9	27	9.4	
					103.7	13.7	9.9	18.5	91.1	57.2	12.1	16.6	
					18.0	28.6	20.7	15.1	345.4	37.5	55.2	9.1	
[*Maze and Hargraves*,, 1984]													
Perijá range	La Quinta	72.5	10.3	Jurassic	323	-2		28.4	319	9		35.9	
	La Quinta	72.5	10.3	Jurassic	311	0		36.1	309	3		35.7	
	La Quinta	725	10.3	Jurassic	354	36		10.4	6	27		16	

The geographic coordinates are referred to WGS84 datum. D and I, in situ and ttilt-corrected declination and inclination values respectively. K and a95 statistical parameters.

3. Sampling strategy and Methods

Our study was focused on lower to upper Cretaceous marine sediments and Maastrichtian-Cenozoic transitional to continental sedimentary successions from both the Eastern Cordillera and an area named the Cucuta zone, at the junction between the

Merida Andes and the Santander Massif (Tables 2 and 3). Marine Cretaceous strata sampled in the Eastern Cordillera include black shales, limestones, mudstones and fine to medium-grained sandstones. The continental deposits collected in the Eastern Cordillera include claystones, fine-grained quartzarenites, and local volcanoclastic layers of Maastrichtian to Miocene age. Three areas were sampled in the Eastern Cordillera: the first area is to the south of Bogotá, the second is in the hanging-wall of the Boyacá Fault, and the third is in the hanging-wall and footwall of the Soapága-Pesca fault system (Fig. 3). Structural trend is N-S in the first area, NE in the second areas, while in the third the strike changes northward from NE to N-S. Strata sampled in the Cucuta zone include upper Cretaceous marine black shales, Paleocene continental mudstones and fine-grained sandstones, Eocene to Oligocene quartzarenites and mudstones, and Miocene claystones and fine-grained sandstones (Fig. 3).

We collected lower Cretaceous to Miocene rocks in 58 localities (715 cores), using a petrol-powered portable drill cooled by water. At each site we collected 6–16 cores (12 on average), spaced in at least two outcrops in order to try to average out secular variation of the geomagnetic field. All samples were oriented in situ using a magnetic compass, corrected to account for the local magnetic field declination value at the sampling area (from -6º to -8° during 2010 according to NOAA's National Geophysical Data Center, http://www.ngdc.noaa.gov).

Cores were cut into standard cylindrical specimens of 22 mm height, and magnetic fabric, rock magnetic and paleomagnetic measurements were done in the shielded room of the paleomagnetic laboratory of the Istituto Nazionale di Geofisica e Vulcanologia (Roma, Italy). We first measured the low-field anisotropy of magnetic susceptibility (AMS) of a specimen per core by a spinner Multi-Function Kappabridge (MFK1-FA, AGICO) using the spinning method. For each sample the measurements allowed to reconstruct the AMS tensor, defined by three eigenvalues (i.e. the maximum, intermediate and minimum

susceptibilities) indicated as kmax ≥ kint ≥ kmin (or k1≥ k2≥ k3). The AMS parameters at both the specimen and the site levels were evaluated using Jelinek statistics (Jelinek, 1977, 1978).

Afterwards, all samples were thermally demagnetized through 11–12 steps up to 680°C by a shielded oven, and the natural remanent magnetization (NRM) of the specimens was measured after each step with a DC- SQUID cryogenic magnetometer (2G Enterprises, USA). On a set of selected specimens, magnetic mineralogy analyses were carried out to identify and characterize the main magnetic carriers using the thermal demagnetization of a three-component isothermal remanent magnetization (IRM) imparted on the specimen axes, according to the method of Lowrie (1990). Fields of 2.7, 0.6, and 0.12 T were successively imparted on the z, y, and x sample axes (respectively) with a pulse magnetizer (Model 660, 2G Enterprises). Thermal demagnetization data were plotted on orthogonal diagrams (Zijderveld, 1967), and the magnetization components were isolated by principal component analysis (Kirschvink, 1980). The site-mean directions were evaluated by Fisher's (1953) statistics.

4. Results

4. 1. Anisotropy of magnetic susceptibility

Only 35 out of 58 sites (mostly from clayey layers) gave interpretable AMS results (Fig. 3 and Table 2), while 23 sandy-silty sites did not give a clear magnetic fabric (Table 2). The AMS parameters are reported in Table 2. The site-mean susceptibility values range from 13 to 1640 × 10-6 SI (197 × 10-6 SI, on average). The low susceptibility values (below 200 x 10-6 SI on average) suggest the predominant contribution of the paramagnetic clayey matrix on both the low-field susceptibility and AMS (e.g., Rochette, 1987; Averbuch et al.,

1995; Sagnotti et al., 1998; Speranza et al., 1999).

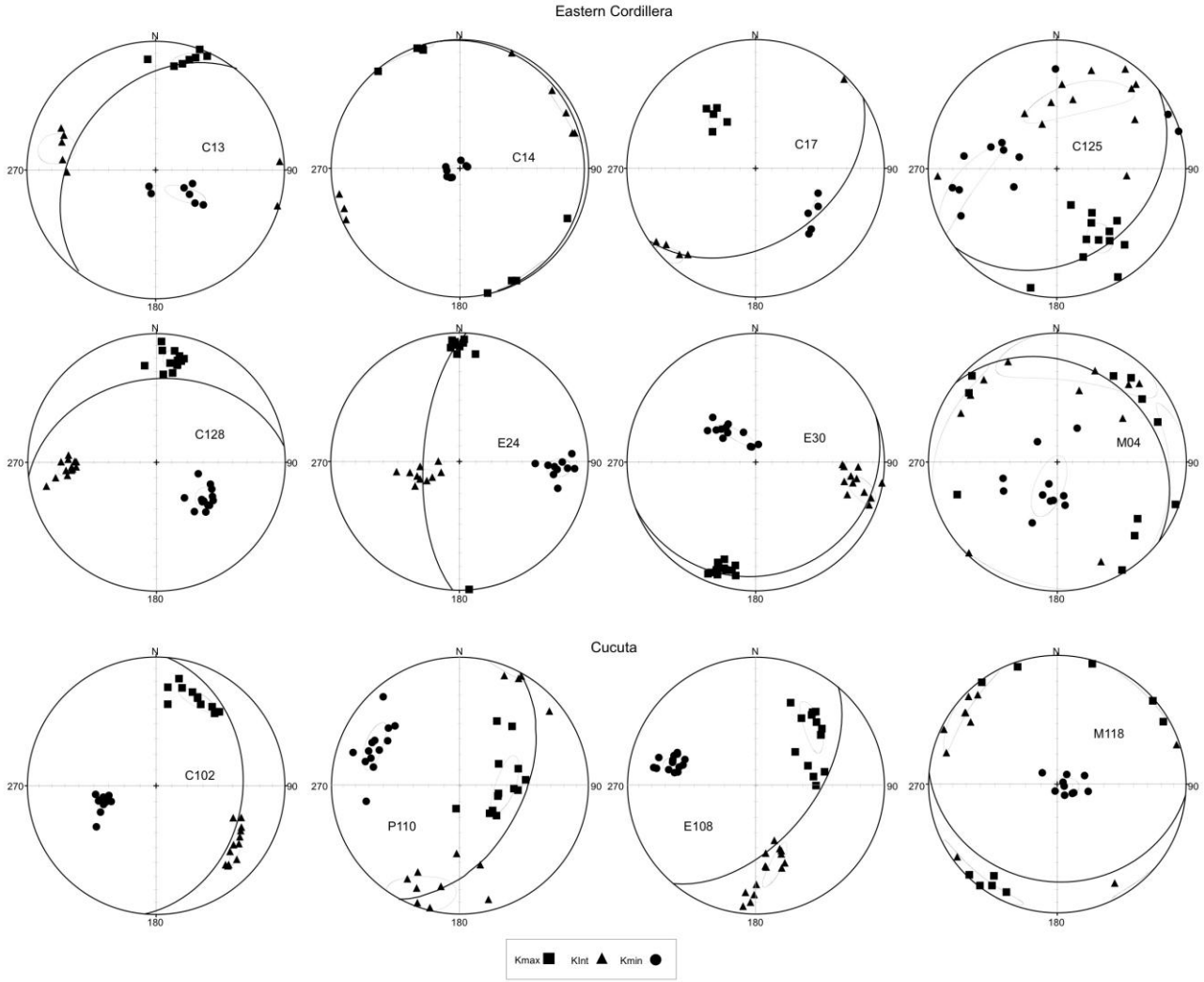

Figure 4. Schmidt equal-area projections, lower hemisphere, of the (in situ coordinates) principal axes of the AMS ellipsoid and their respective 95% confidence ellipses, for some representative sites (see Table 2). Bedding planes are also projected.

The shape of the AMS ellipsoid is predominantly oblate, with an average value of the shape factor (T) of 0.373, suggesting a prevailing sedimentary fabric (Hrouda and Janàk, 1976). Only in six Cretaceous-Paleocene sites, the AMS ellipsoid is prolate (T comprised between -0.015 and -0.353, Table 2). In addition, the low values of the P′ parameter (1.007–1.12) confirm that the studied sediments underwent only mild deformation.

Magnetic foliations are generally sub-parallel to layer attitudes measured in the respective

sites, confirming again the predominantly sedimentary-compaction magnetic fabric. At site C125, kmin directions are scattered along a plane orthogonal to Kmax (Fig. 4), indicating a "pencil-like" magnetic fabric (T= -0.282) typical for stronger compressive tectonic deformation (Hrouda, 1982). At site C17, both magnetic foliation and lineation are orthogonal to bedding. This is a typical case for inverse magnetic fabric (e.g. Rochette et al., 1992), testifying the occurrence of some given magnetic minerals (typically single-domain magnetite and several Fe carbonates) whose magnetic fabric does not correlate with mineral fabric. Site-mean susceptibility value of site C17 is low (252 x 10-6 SI, Table 2), thus excluding that, its susceptibility and AMS is controlled by ferromagnetic (sensu lato) minerals.

Table 2. Anisotropy of magnetic susceptibility results from Colombia.

												Kmax			Kmin	
Site	Formation	Longitude °W	Latitude °N	Age	Bedding (deg)	n/N	Km	L	F	T	P'	D (°)	I (°)	e12 (°)	D (°)	I (°)	e12 (°)
Eastern Cordillera																	
M04	Tilata	-73.342689	5.530168	Miocene	38/26	11/11	13.3	1.003	1.015	0.682	1.019	102.4	1.5	43.6	197.7	73.8	20.7
C13	Rosa Blanca	-73.330491	5.915324	Lower Cretaceous	308/35	7/7	16.1	1.012	1.017	0.168	1.030	16.2	10.4	9.5	130.1	65.6	13.8
C14	Rosa Blanca	-73.334881	5.901171	Lower Cretaceous	73/4	8/8	90.7	1.003	1.016	0.694	1.020	152.6	0.8	15.7	252.8	85.6	5.8
C15		-73.334882	5.893494	Lower Cretaceous	108/20	5/5	15.2	1.014	1.039	0.476	1.055	41.5	12.9	15.3	197.2	75.9	23.3
C16	Paja	-73.427929	5.789102	Lower Cretaceous	112/38	7/7	126.0	1.028	1.055	0.317	1.087	30.1	5.8	3.7	292.5	52.5	11.2
C17*		-73.514876	5.582867	Lower Cretaceous	146/42	5/5	252.0	1.013	1.006	-0.353	1.020	321.0	47.7	7.2	130.7	41.8	10.4
C18	Paja	-73.505705	5.575063	Lower Cretaceous	116/31	6/6	256.0	1.007	1.005	-0.183	1.012	198.6	4.4	5.1	295.9	59.0	15.0
P20	Guaduas	-74.146646	4.516292	Lower Paleocene	284/242	11/11	130.0	1.018	1.017	-0.024	1.036	350.4	12.9	10.1	89.4	34.3	14.4
E24	Bogotá	-74.140915	4.517505	Lower Eocene	273/247	10/10	544.0	1.032	1.042	0.132	1.076	359.3	9.0	5.7	93.3	23.7	9.0
E30	Lodolitas de Fusagasuga	-74.393850	4.411320	Lower Eocene	159/13	12/12	191.0	1.012	1.012	-0.015	1.025	198.2	12.6	5.9	325.2	69.6	14.0
C121	Rosa Blanca	-73.231126	6.888979	Lower Cretaceous	325/22	10/10	152.0	1.007	1.007	0.025	1.014	305.1	1.7	32.1	205.7	79.9	38.2
C122	San Gil	-72.957042	6.021034	Lower Cretaceous	300/25	10/10	89.0	1.003	1.018	0.724	1.023	334.2	11.5	69.3	127.4	77.2	39.6
C123	San Gil	-72.957042	6.021034	Lower Cretaceous	300/25	5/5	73.7	1.011	1.037	0.530	1.051	262.6	13.5	35.5	133.3	69.2	17.9
C124	San Gil	-72.916622	6.015778	Lower Cretaceous	300/25	13/13	128.0	1.015	1.052	0.547	1.071	215.9	16.2	35.7	72.5	70.1	17.0
C125	Churuvita	-72.895270	6.046642	Lower Cretaceous	142/30	12/12	144.0	1.016	1.009	-0.282	1.026	148.1	36.5	10.8	259.7	26.4	35.2
C127	Fomeque	-72.730003	5.494825	Lower Cretaceous	350/34	14/15	259.0	1.012	1.030	0.432	1.043	16.2	15.9	11.1	140.8	63.3	6.5
C128	Fomeque	-72.731990	5.496335	Lower Cretaceous	353/36	13/14	235.0	1.033	1.044	0.140	1.078	9.2	20.1	6.9	126.2	51.2	6.5
C129		-72.901842	5.611125	Lower Cretaceous	187/36	10/10	46.3	1.008	1.027	0.526	1.037	182.9	28.5	46.7	335.9	58.6	19.8
C130		-72.901489	5.614225	Lower Cretaceous	163/31	9/10	130.0	1.012	1.050	0.587	1.067	195.6	20.5	6.5	335.9	64.2	9.5
P131	Guaduas	-73.366118	5.559983	Lower Paleocene	106/21	5/5	68.2	1.021	1.009	-0.408	1.031	219.6	27.9	17.4	18.3	60.4	27.0
C134		-73.213538	5.628060	Lower Cretaceous	354/21	10/10	75.2	1.003	1.032	0.808	1.039	49.7	6.7	42.0	284.3	78.5	15.6
C135		-73.218409	5.627440	Lower Cretaceous	326/46	13/13	51.7	1.002	1.014	0.699	1.018	352.9	23.0	46.8	121.1	55.6	15.8
C137		-73.065814	5.580539	Lower Cretaceous	292/12	9/9	60.6	1.019	1.042	0.378	1.063	213.6	11.9	45.7	70.8	75.2	20.2
E138	Concentracion	-73.058511	5.564794	Eocene	280/34	14/14	42.0	1.003	1.004	0.240	1.007	199.0	31.7	35.8	81.7	36.6	22.6
P139	Guaduas	-72.995590	5.621390	Lower Paleocene	267/53	11/11	96.3	1.005	1.017	0.504	1.023	326.6	38.4	21.5	101.9	41.9	16.1
C152	Guadalupe	-73.885392	5.193317	Upper Cretaceous	144/57	6/6	32.8	1.006	1.046	0.780	1.056	230.4	4.9	32.6	323.7	34.9	8.3
Cucuta																	
C102	Catatumbo	-72.681961	7.905744	Upper Cretaceous	95/33	12/13	233.0	1.017	1.093	0.683	1.120	26.1	26.6	11.4	251.8	54.4	6.1
C103	Catatumbo	-72.681225	7.905711	Upper Cretaceous	70/37	12/12	188.0	1.007	1.034	0.633	1.044	79.9	33.4	48.8	240.1	55.0	18.4
P107	Cuervos	-72.664658	7.907975	Lower Paleocene	130/54	13/13	610.0	1.004	1.030	0.736	1.037	43.2	35.1	22.8	286.8	32.3	5.5
P108	Cuervos	-72.664658	7.907975	Lower Paleocene	130/54	14/14	155.0	1.005	1.019	0.578	1.026	43.8	36.4	16.3	284.7	33.4	6.9
P109	Cuervos	-72.664658	7.907975	Lower Paleocene	130/54	14/14	1640.0	1.003	1.004	0.101	1.007	39.6	32.1	38.0	274.1	42.7	58.3
P110	Cuervos	-72.662767	7.908377	Lower Paleocene	118/49	13/13	129.0	1.005	1.01	0.214	1.015	89.8	60.8	19.0	294.6	26.9	13.6
E112	Carbonera	-72.658308	7.910656	Eocene	122/62	9/10	124.0	1.007	1.036	0.677	1.047	24.9	57.9	19.8	272.2	13.6	12.1
M113	Guayabo	-72.587520	7.933685	Miocene	113/5	13/13	251.0	1.012	1.072	0.699	1.092	197.9	8.8	13.6	80.4	71.4	5.9
M118	Guayabo	-72.583551	7.940521	Miocene	185/25	10/10	233.0	1.005	1.021	0.629	1.028	220.2	4.0	24.3	89.9	83.9	8.1

The geographic coordinates are referred to WGS84 datum. Bedding is expressed in dip azimuth/dip values. n/N, number of samples giving reliable results/number of studied samples at a site. Km mean susceptibility in 10 $^{-6}$ SI. L, F, T and P' are magnetic lineation (Kmax/Kint), magnetic foliation (Kint/Kmin), shape factor and corrected anisotropy degree, respectively, according to Jelinek (1981). D and I are in situ site mean declination and inclination, respectively, of the maximunand minimum susceptibility axis. e12 is semi-angle of the 95% confidence ellipse around the mean kmax axis in the kmax-kint plane and Kmin axis in the kmin-kint plane. * Fabric of site C17 is inverse magnetic fabric (e.g. Rochette et al., 1992). Identification for each site C, P, E, M, for Cretaceous, Paleocene, Eocene, Miocene respectively.

We conclude that the inverse magnetic fabric of site C17 is due to peculiar minerals contained in its paramagnetic matrix, likely siderite or other Fe carbonates.

By selecting 20° as cut-off value of the e12 angle (semi-angle of the 95% confidence ellipse around the mean Kmax axis in the Kmax-Kint plane), we find that magnetic lineation is well defined for 19 out of 35 sites (Table 2 and Figs. 3 and 4). Magnetic

lineations frequently show significant dip values, reaching as high as ca. 60º for two sites from the Cucuta area. This may either imply non-cylindrical deformation, complex folding or be the result of extensional tectonics (e.g. Mattei et al., 1997). However, an extensional magnetic fabric can be excluded by both the lack of a significant extensional Cenozoic tectonics documented in the Eastern Cordillera, and the prolate AMS ellipsoid observed in six sites, which is definitely the result of compressive tectonics (Parés et al., 1999) or in a complex folding setting.

4. 2 Magnetic Mineralogy

The thermal demagnetization of a three-component IRM shows that for most of the samples both the medium coercivity and the hard fractions are demagnetized between 600 and 680°C (Fig. 5), pointing to hematite as the main magnetic carrier of our samples. A demagnetization of the hard fraction between room temperature and 200ºC in the samples P21 and C18 suggests the occurrence of goethite, besides hematite. In the sample C124, all coercivity components are demagnetized between 450 and 550°C (Fig. 5), indicating the presence of maghemite. Finally, the soft component of the sample E133 is demagnetized at ca. 400°C, suggesting the accessory occurrence of iron sulphides (likely pyrrhotite) besides hematite.

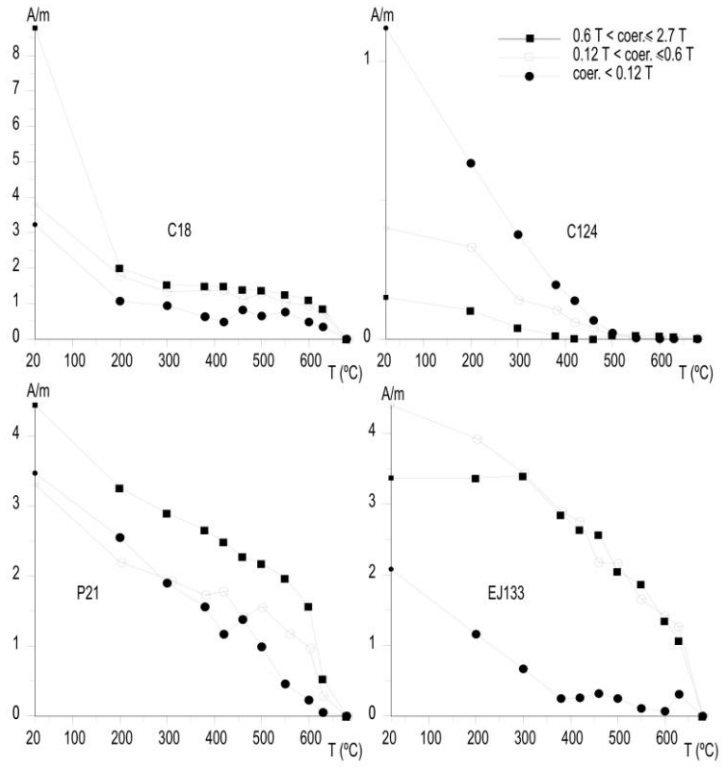

Figure 5. Thermal demagnetization of a three-component IRM according to the method of Lowrie (1990) for four representative specimens.

4. 3 Paleomagnetic Directions

Only 32 (out of 58) sites yielded reproducible paleomagnetic directions during cleaning, while the remaining 26 sites (Table 3) showed scattered demagnetization diagrams (Figure 6 and Table 3). From the 32 reliable sites, 25 were sampled in the Eastern Cordillera and 7 in the Cucuta zone. For most of the sites, a characteristic magnetization component (ChRM) was isolated between 550 and 680°C, confirming that hematite represents the main magnetic carrier.

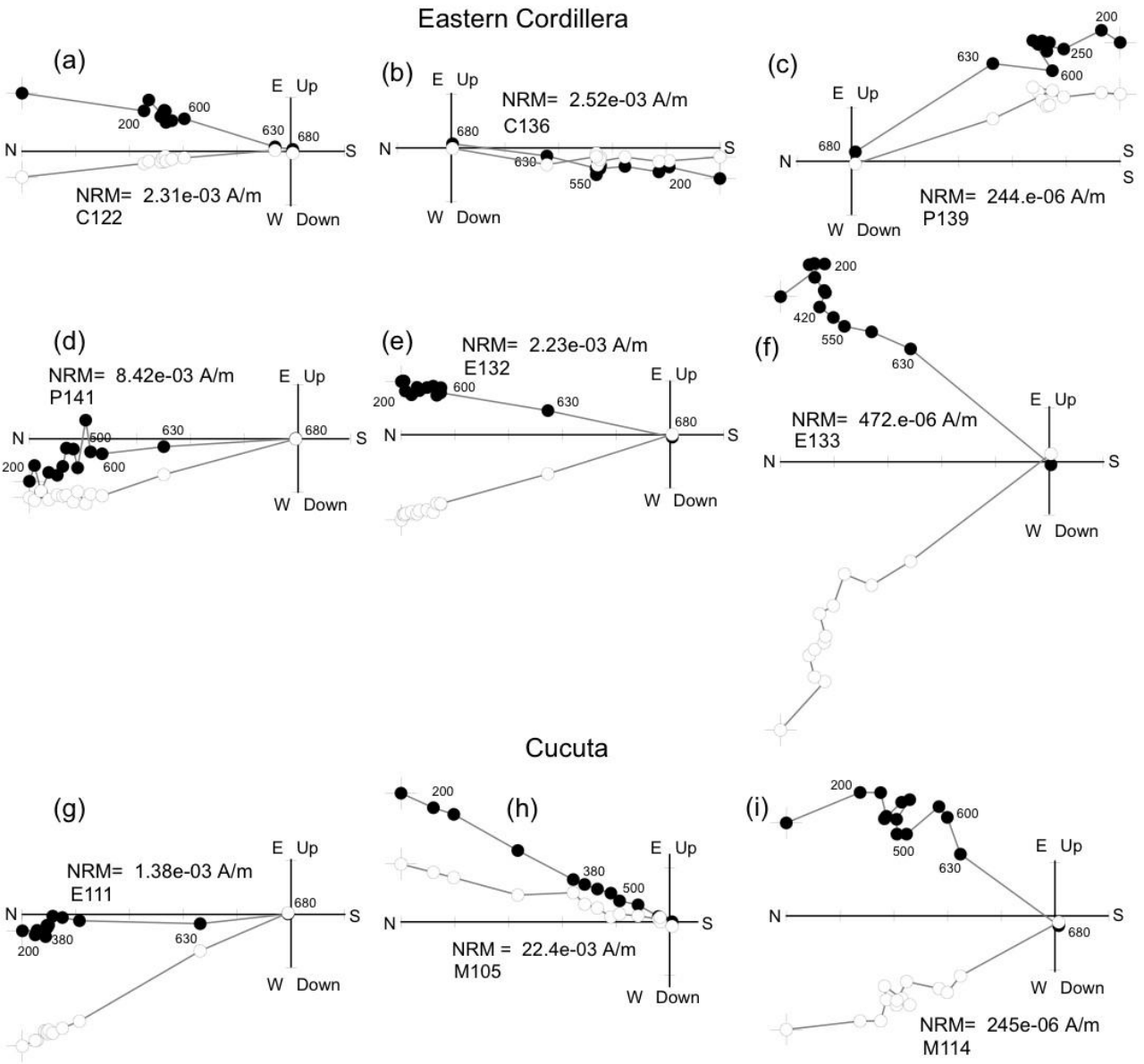

Figure 6. Orthogonal vector diagrams of typical demagnetization data, in situ coordinates for some representative sites (see Table 2). Solid and open dots represent projections on the horizontal and vertical planes, respectively. Demagnetization step values are in °C.

A ChRM is isolated between 380 and 680°C for about 10% of the samples, suggesting the coexistence of hematite and maghemite. Mean paleomagnetic directions are reasonably well constrained, the a95 values being comprised between 3.2° and 19.5° (9.8 on average, Fig. 7 and Table 3). The majority of the sites from the Eastern Cordillera (16 out of 25)

have reverse polarity, while 6 out of 7 sites from the Cucuta zone have normal polarity. The rotation and flattening values with respect to stable South America were evaluated according to Demarest (1983), using the reference South America paleopoles listed by Torsvik et al., (2007), (Table 3).

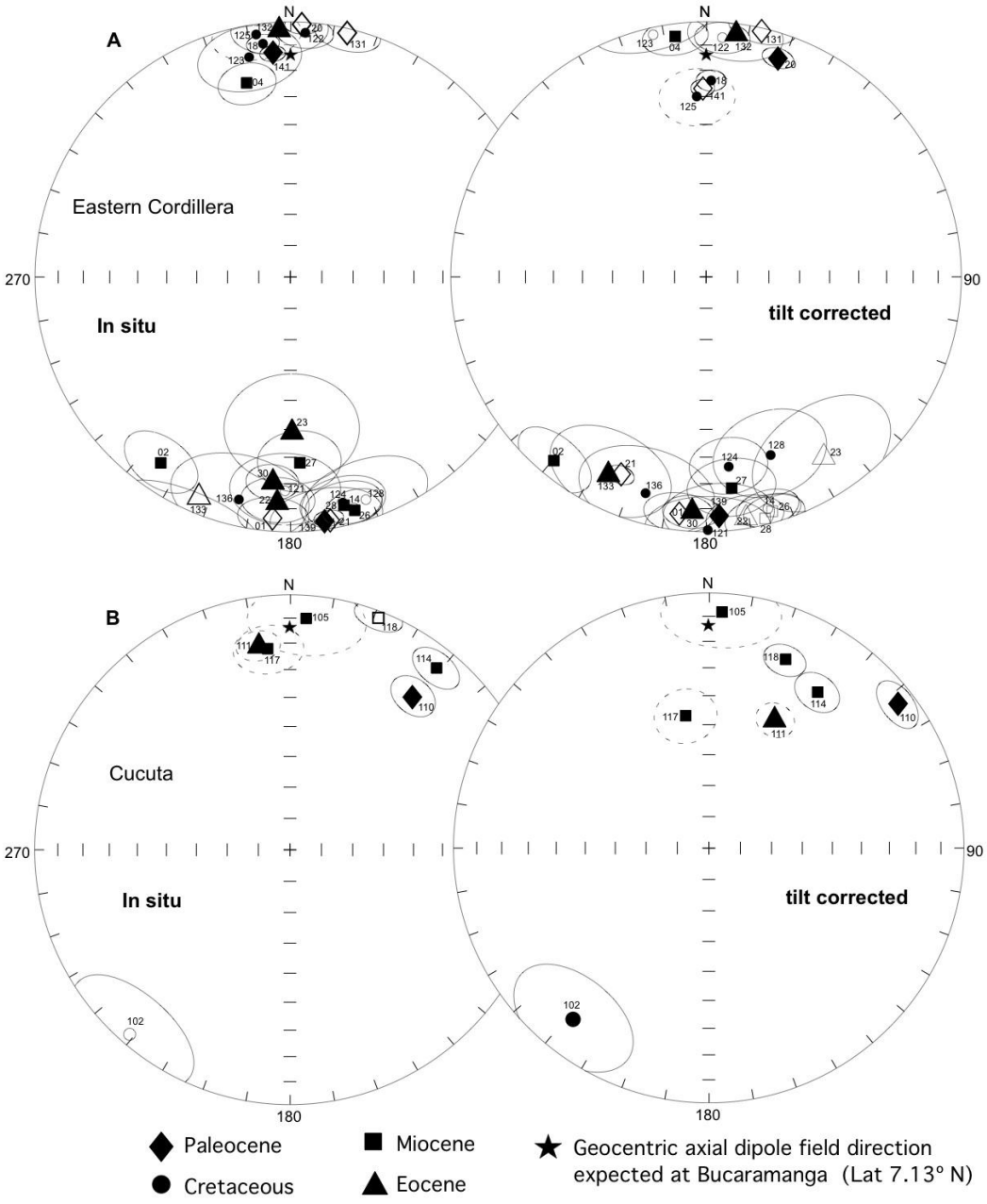

Figure 7. Equal-area projections of the site-mean paleomagnetic directions from the study area. Solid (open) symbols represent projection onto the lower (upper) hemisphere. Open ellipses (dashed for remagnetized and subsequently non-rotated sites) are the projections of the a95 cones about the mean directions. The star represents the normal polarity geocentric axial dipole (GAD) field direction (D=0°, I=14°) calculated for the Bucaramanga latitude (7.1° N). (A) Sites from the Eastern Cordillera, (B) sites from the Cucuta zone.

Considering the age window of our sampled sites, South America has not undergone significant rotations (Fig. 8). Paleolatitudes of Colombia were similar to present latitude during early Cretaceous, followed by a southward drift until ca. 3.25°S at the Eocene, and by a rather continuous northward drift until Present (Fig. 8). Flattening values are mostly <10° (Table 3), suggesting in general a primary origin of the observed ChRMs.

For the Eastern Cordillera, we discarded site C125 taken in lower Cretaceous rocks, characterized by relatively high inclination values (24.0° and 29.9°), negative flattening values (up to -25.9°), and in-situ directions close to the GAD field direction (Fig. 7 and Table 3).

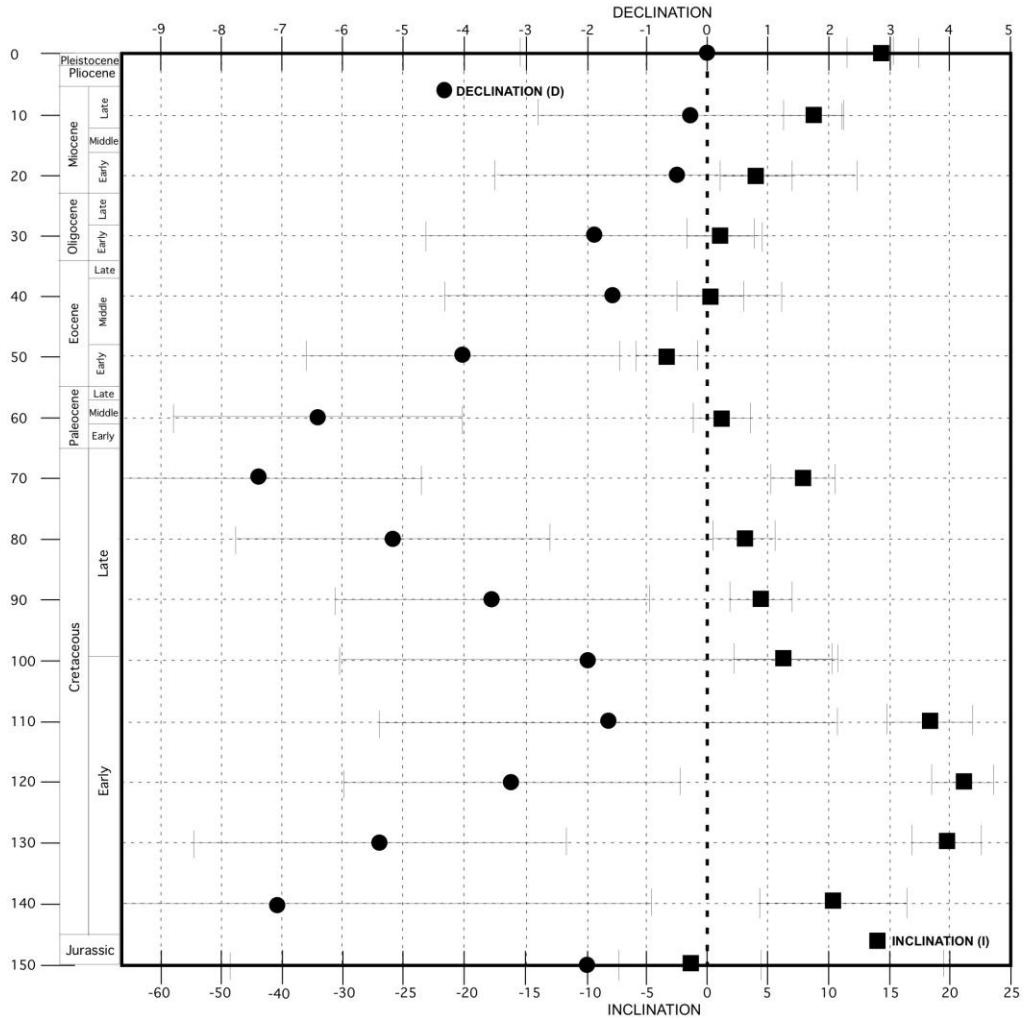

Figure 8. Expected declination and inclination values expected at Bucaramanga (7.1° N, 73.1° W) since 150 Ma considering South America paleomagnetic poles listed by Torsvik et al. (2007). Error bars for declination data are the respective a95 /cos(I) values; error bars for inclination data are the respective a95 values.

For the Eocene site E111 and Miocene site M117 from the Cucuta zone, flattening is negative and exceeds a -40° value, and the in-situ paleomagnetic directions are close to the geocentric axial dipole (GAD) field direction for the study area. Thus we infer that these sites (along with site M105, close to the GAD field direction in situ, and yielding very different rotation value than the other close sites) were magnetically overprinted, and discard them from further consideration. The McFadden, (1990) fold test was separately applied to reliable sites from the Eastern Cordillera and the Cucuta zone. The fold test is positive for the Eastern Cordillera (n=24; SCOS in situ=6.257; SCOS unfolded=0.642; 95% critical value SCOS95%=5.702), while it is negative for the Cucuta zone (n=4; SCOS in situ=0.225; SCOS unfolded=3.379; 95% critical value SCOS95%=2.335). The reversal test (according to McFadden and McElhinny, (1990)), solely performed on data from the Eastern Cordillera, was positive of Class C.

In summary, the results from the fold and reversal tests indicate that 24 sites from the Eastern Cordillera host a pre-tilting (and likely primary) remanent magnetization, and document on average a null rotation with respect to South America (R=4.04°±7.16°) (Table 3). Conversely, in the Cucuta zone a complex overprint occurred after Miocene times. Four sites were overprinted, and subsequently rotated CW by 20°-40° (34.8°±9.4° on average), while three sites were remagnetized more recently, and they did not subsequently rotate (Table 3).

Table 3. Paleomagnetic results from Colombia.

Paleomagnetic results from Colombia

		Geographic coodinates						Tilt Correct		In Situ					
Site	Formation	Longitude °W	Latitude °N	Age	Age (Ma)	N/n	Bedding (deg)	D (deg)	I (deg)	D (deg)	I (deg)	k	a95 (deg)	R (deg)	F (deg)
Eastern Cordillera															
P01	Cacho	-73.362311	5.55664	Lower Paleocene	60	7/5	99/21	186.6	-7.4	184.1	-6.0	84.31	8.4	13.0 ± 6.8	-5.6 ± 7.5
M02	Tilata	-73.381199	5.495502	Miocene	5	10/4	295/25	219.6	6.7	214.9	12.0	82.36	10.2	40.4 ± 8.2	-1.1 ± 8.8
M04	Tilata	-73.342689	5.530168	Miocene	5	13/4	38/26	352.5	5.7	347.4	23.3	60.13	7.8	-7.0 ± 6.4	-2.3 ± 7.2
C14	Rosa Blanca	-73.334881	5.901171	Lower Cretaceous	130	7/6	73/4	165.1	-6.6	164.6	-6.7	77.76	7.6	-9.5 ± 6.3	11.1 ± 7.2
C18	Paja	-73.505705	5.575063	Lower Cretaceous	120	6/4	116/31	1.5	24.0	353.3	8.8	520.79	4.0	4.6 ± 3.9	-5.5 ± 4.8
P20	Guaduas	-74.146646	4.516292	Lower Paleocene	60	12/12	284/62	18.2	10.6	2.7	-1.3	117.94	4.0	24.7 ± 3.6	-6.9 ± 4.8
P21	Cacho	-74.146934	4.517802	Lower Paleocene	60	14/10	281/68	203.2	-16.6	171	-4.6	194.64	3.5	29.7 ± 3.4	-12.9 ± 4.6
E22	Bogotá	-74.140915	4.517505	Lower Eocene	50	11/10	273/67	170.8	-4.9	183.2	13.1	28.75	9.2	-5.3 ± 7.4	3.3 ± 8.2
E23	Bogotá	-74.140915	4.517505	Lower Eocene	50	14/4	273/67	146.8	-16.9	179.5	39.3	23.26	19.5	-29.0 ± 16.0	-8.6 ± 15.7
M26	Honda	-74.375845	4.354329	Miocene	20	11/10	134/14	164.4	-4.9	164.5	7.2	49.89	6.9	-15.0 ± 5.8	-3.4 ± 7.1
M27	Honda	-74.375845	4.354329	Miocene	20	11/8	134/14	173.3	17.4	177.2	28.0	24.55	11.4	-6.1 ± 9.6	-15.9 ± 10.0
M28	Honda	-74.375845	4.354329	Miocene	20	11/10	134/14	166.4	-2.9	166.8	8.9	27.52	9.4	-13.0 ± 7.7	-1.4 ± 8.7
E30	Lodolitas de Fusagasuga	-74.39385	4.41132	Lower Eocene	40	11/11	159/13	183.6	8.3	185.0	20.1	44.26	6.9	5.3 ± 5.8	-3.1 ± 6.9
C121	Rosa Blanca	-73.231126	6.888979	Lower Cretaceous	130	12/10	325/22	179.6	0.8	181.4	-17.2	12.54	14.2	4.9 ± 11.3	18.7 ± 11.8
C122	San Gil	-72.957042	6.021034	Lower Cretaceous	110	12/11	300/25	3.9	-6.6	3.5	4.6	48.94	6.6	5.4 ± 5.9	9.9 ± 7.3
C123	San Gil	-72.957042	6.021034	Lower Cretaceous	110	12/9	300/25	347.7	-3.3	349.4	13.4	16.29	13.1	-10.7 ± 10.6	13.2 ± 11.5
C124	San Gil	-72.916622	6.015778	Lower Cretaceous	110	12/11	300/25	173.2	26.0	166.9	9.8	19.2	10.6	-5.1 ± 9.6	-9.4 ± 9.8
C125*	Churuvita	-72.89527	6.046642	Lower Cretaceous	100	12/11	142/30	357.1	29.9	352.0	4.5	20.05	10.5	-0.9 ± 9.9	-25.9 ± 10.3
C128	Fomeque	-72.73199	5.496335	Lower Cretaceous	110	12/8	353/36	160.1	26.6	161.4	-8.6	13.32	15.8	-18.2 ± 14.1	-11.0 ± 13.4
P131	Guaduas	-73.366118	5.559983	Lower Paleocene	60	12/12	106/21	12.7	-0.9	13.2	-2.0	32.73	7.7	19.1 ± 6.2	0.8 ± 7.0
E132	Concentracion	-73.353267	5.543719	Eocene	40	12/9	276/76	6.9	4.5	357.5	2.7	22.16	11.2	8.5 ± 9.0	-1.5 ± 9.6
E133	Bogota	-73.335193	5.539397	Lower Eocene	50	12/9	317/55	206.2	15.1	202.6	-7.6	10.91	16.3	30.2 ± 13.3	-8.7 ± 13.3
C136	Une	-73.065816	5.580539	Lower Cretaceous	110	12/9	292/12	195.6	13	193.0	11.4	9.78	17.3	17.1 ± 14.1	2.2 ± 14.5
P139	Guaduas	-73.065816	5.580539	Lower Paleocene	60	12/7	267/53	176.9	6.8	171.5	4.0	21.9	13.2	3.2 ± 10.5	-4.9 ± 10.9
P141	Socha Inferior	-72.998714	5.631126	Lower Paleocene	60	12/11	322/48	359	-26.8	355.5	13.2	202.21	3.2	5.3 ± 3.3	-25.0 ± 4.4
Cucuta															
C102*	Catatumbo	-72.681961	7.905744	Upper Cretaceous	70	12/8	95/33	218.5	14.5	220.9	-4.6	11.3	17.2 +	45.8 ± 14.0	-5.2 ± 14.0
M105*	Guayabo	-72.567018	7.916783	Miocene	20	12/10	290/8	3	7.9	4.2	10.1	12.06	14.5 +	3.4 ± 11.6	-2.2 ± 12.2
P110*	Cuervos	-72.662767	7.908377	Lower Paleocene	60	12/12	118/49	52.7	7.7	38.7	23.7	44.1	6.6 +	59.0 ± 5.5	-4.9 ± 6.3
E111*	Mirador	-72.661678	7.908694	Eocene	50	12/12	120/57	27.4	42.9	351.2	20.1	57.87	5.8 +	31.3 ± 6.5	-41.2 ± 6.0
M114*	Guayabo	-72.584389	7.932316	Miocene	20	12/11	252/21	34.8	26.5	38.8	9.3	49.36	6.6 +	35.2 ± 6.21	-20.8 ± 6.9
M117*	Guayabo	-72.583551	7.940521	Miocene	20	12/8	185/25	350	46.3	353.9	21.9	36.19	9.3 +	-9.5 ± 10.8	-40.5 ± 8.6
M118*	Guayabo	-72.583551	7.940521	Miocene	20	11/11	185/25	22	21.6	20.8	-2.4	62.91	5.8 +	22.4 ± 5.4	-15.9 ± 6.4

The geographic coordinates are referred to WGS84 datum. Bedding is expressed in dip azimuth /dip values. D and I are site mean declination and inclination calculated before and after tectonic correction; K and α95 are statistical parameters after Fisher (1953). Site mean rotation (R) and flattening (F) value, and relative errors (according to Demarest (1983)) are relative to coeval D and I South America values expected at the sampling area considering South America paleopoles from Torsvik et al., (2007). * Remagnetised site (see text). + Rotation values of sites from the Cucuta area were evaluated comparing in-situ declination values with the GAD field declination (see text). Rotation error values for these sites were equaled to (α95/cosI) in-situ values. Identification for each site C, P, E, M, for Cretaceous, Paleocene, Eocene, Miocene respectively.

4. 4 Oroclinal Test

We have performed an "oroclinal" test (e.g., Schwartz and Van der Voo, 1983; Eldredge et al., 1985; Hirt and Lowrie, 1988) on our paleomagnetic data, to verify whether in the Eastern Cordillera a statistically significant rotational difference (i.e., "oroclinal bending") exists at sites characterized by different structural attitude.

In Fig. 9 we compare the site mean paleomagnetic declinations (in tilt- corrected coordinates) to the local bed strikes, considered as proxies of structural directions. D0 = 0° and S0 = 40° were adopted as reference paleodeclination and structural direction values, respectively (reference values are trivial for the test result). The slope of the best-fit line attests the degree of correlation between paleomagnetic declinations and structural trends.

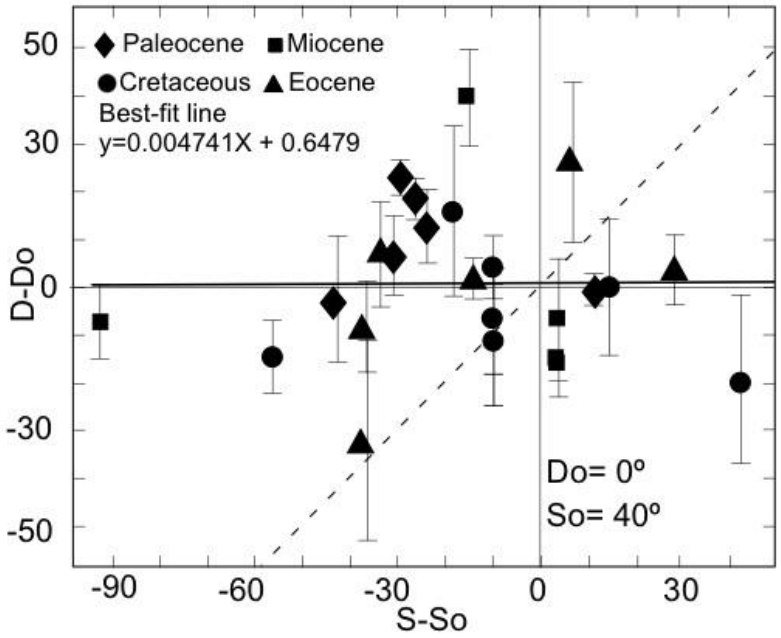

Figure 9. Paleomagnetic declination deviations versus relative bed strike deviation (e.g. Schwartz and Van der Voo, 1983). D is the observed paleomagnetic declination at a site, and D0 is the reference declination value. S is the observed bed strike at a site, and S0 is the reference bedding strike. Error bars for declination data are the respective a95 /cos(I) values.

A zero slope and a unitary slope of the best fit line imply that structural trend variability is not and is (respectively) related to paleomagnetic rotations. The statistical t test (according to Hirt and Lowrie, (1988)) is used to assess whether the slope values of the best-fit line calculated from our data set are significantly different from zero (indicating no paleomagnetic versus structural correlation). The t test on the slope of the regression line compared to zero slope gives t = 0.04. This value is smaller than the critical t value at the 99% significance level (t99 = 3.792), implying that the best-fit line is statistically indistinguishable from zero slope. The result of the oroclinal test indicates that local rotations observed in the Eastern Cordillera (as apparent in Fig. 10) are not due to oroclinal bending mechanisms, but are likely to be related to paleomagnetic data scatter and/or rotations arising from different local mechanisms (i.e. rotations occurring before orogen formation, rotations related to strike-slip fault activity).

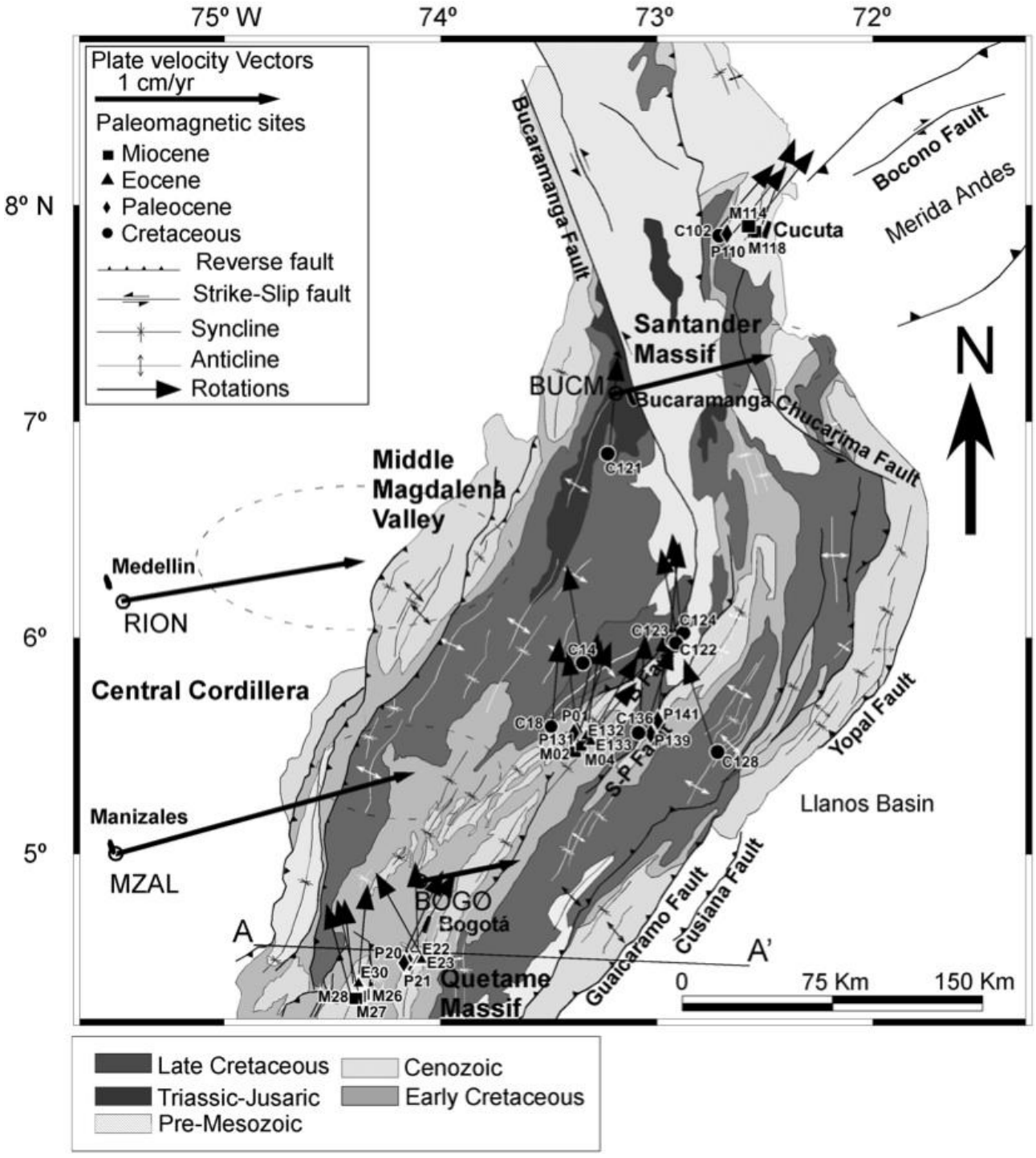

Figure 10. Same Geological map and plate velocity vectors of Fig. 3. Black arrows represent paleomagnetic site-mean rotations from this study calculated with respect to stable South America (numbers are site codes, see Table 3). S-P Fault = Soapága-Pesca Fault.

5.0 Discussion

Our paleomagnetic data demonstrate that the Eastern Cordillera of Colombia is a purely non-rotational belt and is defined as a primary arc. From a paleogeographic point of view, paleomagnetism documents that the chain lies above (and is subparallel to) a NNE Mesozoic rift basin inverted during the Miocene Andean tectonic phase. Therefore, our data support that shortening is relatively low, and thrust sheets are not transported from a long distance.

Conversely, the Cucuta zone, at the junction of the Santander massif with the Merida Andes, underwent a post-Miocene 30°-40° CW rotation. This rotation is consistent with the right-lateral displacement characterizing the Merida Andes and the Boconó fault, as recorded by geological, seismological, and GPS evidence (Kellogg and Vega, 1995; Trenkamp et al., 2002; Bermúdez et al., 2010, Bezada et al., 2010). Several studies have proven that right-lateral strike-slip faults yield significant CW rotations at fault walls; that rotations generally fade out at a distance comprised between few km and 20-30 km from the strike-slip fault, depending on displacement, crust rheology, and coupling between fault walls (Sonder et al., 1994; Piper et al., 1997; Randall et al., 2011; Kimura et al., 2011). But the Cucuta zone sites are located ca. 60-70 km from the supposed termination of the Boconó Fault (Fig. 10), thus their CW rotation cannot be the consequence of right-lateral displacement occurring along that fault. We conclude that right-lateral strike-slip shear is not solely concentrated along the Boconó fault, but characterizes also the external thrust fronts of the whole Merida Andes and Santander massif chain.

While the interpretation of paleomagnetic data from the Eastern Cordillera is relatively straightforward, the AMS results are rather puzzling, when compared to results normally obtained on orogens. In fact, magnetic lineation directions are considered a proxy for the maximum elongation axis (ε1) of the strain ellipsoid of a sedimentary rock. Thus they

generally trend sub-parallel to fold axes and thrust sheet directions, and in general to the main orogenic trend (e.g. Mattei et al., 1995; Sagnotti et al., 1998). But the pattern of magnetic lineation directions observed in the Eastern Cordillera (Fig. 3) is clearly different from that expected in a thrust-fold belt.

Magnetic lineations trend obliquely with respect to both local and regional orogenic trends south of Bogota as well as in the hanging-wall of the Soapága-Pesca fault (Fig. 3). On the other hand, in the hanging-wall of the Boyaca fault, several lineations seem to follow the general Eastern Cordillera trend, but two lineations (sites C14 and C125; Figs. 3 and 4) are almost orthogonal to the orogen (we remind that lineation of site C17 arises from inverse magnetic fabric, thus cannot be used for tectonic interpretations). It may be argued that lineation orthogonal to the orogenic trend arise from extensional tectonics, as several studies have proven that in an extensional tectonic regime magnetic lineation align orthogonal to normal faults (e.g. Mattei et al., 1995; 1999). However, we exclude here this possibility, as there is no evidence of main normal faults close to the sampling sites, and site C125 has a prolate magnetic fabric (negative T value, Table 2), definitely typical for compressive tectonics.

The sites yielding oblique magnetic lineations (and valuable paleomagnetic information) are not CW rotated (Figs. 3 and 10), whereas CW rotations would be expected in a right-lateral strike-slip zone. This suggests that right-lateral strike-slip displacement is accommodated along discrete shear zone, which are located far from our sampling sites (rotations may vanish in few km from a strike-slip fault, (e.g. Kimura et al., 2011). On the other hand, we note that four sites all located within ~20 km west of the Soapága-Pesca fault (C136, P01, E133, M02, Table 3 and Fig. 10), unfortunately do not yielding a reliable magnetic fabric, show significant (from 13° to 40°) CW rotations. The result of the oroclinal test (Fig. 9) shows that this rotation is not related to oroclinal bending, but most likely to strike-slip tectonics. Consequently, we suggest that further geological investigation should

ascertain whether the area west of the Soapága-Pesca fault is characterized by major right-lateral strike-slip fault(s).

Finally, four of the five reliable magnetic lineations gathered from the Cucuta zone are NE-directed (Fig. 3), consistent with the hypothesis derived by paleomagnetic data that the Cucuta zone is cut by NE-trending right-lateral strike-slip faults. In fact, the e1 axis of the strain ellipsoid, as well as magnetic lineation, are expected to become parallel to the fault trend, when located adjacent to the fault and/or located in the fault damage zone. The high inclination (reaching as high as ca. 60°, Table 2) of magnetic lineations confirms that this is a non-cylindrical fabric, incompatible with the magnetic fabric generally observed at external thrust fronts of the chains (Sagnotti et al., 1998; Speranza et al., 1999).

Summing up, paleomagnetic and structural data reveal some evidence that should be considered to unravel the tectonic scenario of the Eastern Cordillera: (i) the Eastern Cordillera is a non-rotational chain, whereas local clockwise rotations are limited to the vicinity of the Soapága-Pesca Fault (sites C136, P01, E133 and M02) and the Cucuta zone. (ii) The magnetic lineations are oblique to main fault and fold trend; in most cases those lineations have a significant plunge. (iii) Strain markers along faults show variability of the compressive strain field around E-W, in agreement with what may be inferred from present-day geodetic displacements (Trenkamp et al., 2002).

Two possible scenarios, schematically illustrated on Figure 11, may explain this structural setting: oblique/transpressional deformation and strain partitioning model.

The oblique/transpressional model (Fig. 11a) could be a viable solution to explain the non-rotational pattern and the E-W/WNW-ESE shortening direction as inferred from AMS. This model would imply an oblique re-activation at depth of the main thrust faults.

The strain-partitioning model (Fig. 11b) would imply an almost dip-slip motion on the external thrust belt and a strike-slip motion on the inner side of belt, as also apparent in some analogue models (Zweigel, 1998). This model could further explain the local

paleomagnetic CW rotations, possibly associated to the inferred Soapága-Pesca dextral strike-slip. Re-folding during strike slip could also explain the plunge of the fold axes as recorded by AMS.

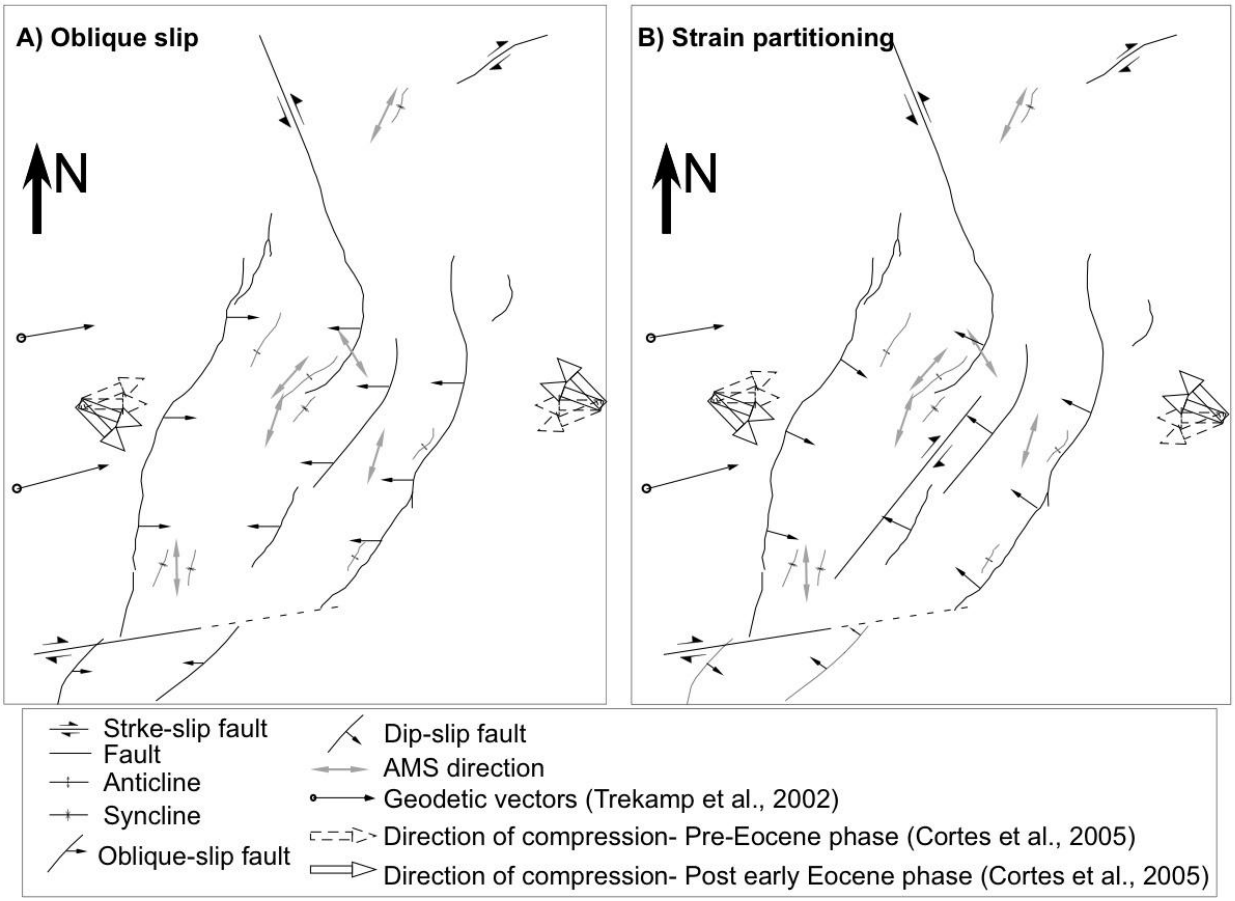

Figure 11. Schematic block diagram in map-view showing three possible models for evolution of the Eastern Cordillera. A) Oblique model; B) Strain partitioning model. (See text for more details).

In addition, the strain-partitioning model is supported by dip-slip thrust fronts (Colleta et al., 1990; Dengo and Covey, 1993; Cooper et al., 1995; Branquet et al., 2002; Cortés et al., 2006), and thrust sheet-type focal mechanisms for shallow earthquakes observed at both margins of the Eastern Cordillera (Taboada et al., 2000). Few focal mechanisms are available from the axial part of the Eastern Cordillera; two mechanisms reported by Taboada et al., (2000), however, show strike-slip shear compatible with the occurrence of N to NE right-lateral faults. Other studies propose the occurrence of right-lateral strike-slip faults in several Eastern Cordillera sectors; in the axial zone (Fajardo-Peña, 1998), and to

the southwest (Montes et al., 2005) and the South (Velandia et al., 2005) of our study area. Mora et al., (2010a) showed that some inverted faults as the Servitá Fault can absorb and focus transpressional deformation.

Therefore our data can support the occurrence in the axial zone of the Eastern Cordillera of structures with similar behavior that the Servitá Fault. In addition, Mora et al,. (2010b) suggested that if the Soapaga and Boyacá faults are the horsetail terminations of the Bucaramanga strike-slip fault, part of wrench deformation maybe focused around those faults.

Further structural data are necessary to validate the best solution for the Eastern Cordillera. Our preferred scenario implies an overall strain partitioning of the belt (Fig. 11b). Preliminary survey in the Santander massif indeed shows the presence of large-scale strike–slip fault zones cross-cutting previous thrust faults parallel to the belt. Those structures would be then reasonably explained within a “strain partitioning” model, where strike-slip fault zone are expected to be well expressed in the inner/higher portion of the belt during its late-stage phases of evolution and orogenic build up.

6.0 Conclusions

Paleomagnetism of Cretaceous to Miocene sediments shows that the Eastern Cordillera of Colombia is a non-rotational chain to be classified as a primary arc. Thus, we conclude that the orogen inverted a Mesozoic rift zone sharing the same orogenic N40° trend observed today. The curved orogenic shape apparent when considering also the Santander Massif to the north is not linked to any oroclinal bending mechanism. This in turn implies that shortening along different Eastern Cordillera transects remains rather constant, and does not increase significantly moving towards the north, i.e. towards the apex of this primary arc, unless the orogen is segmented by ~E-W strike-slip faults.

The magnetic lineation of the studied sediments unexpectedly trends NNE to NW, i.e. oblique to the Eastern Cordillera orogenic trend, while in other orogens it is routinely parallel to the chain direction. Since the observed magnetic fabric is rather consistent with the GPS evidence for a >1 cm/yr ENE shortening accommodated along the Eastern Cordillera, we infer that oblique convergence is partitioned in dip-slip thrust-sheet emplacement and right-lateral strike-slip shear along fault(s) subparallel to the chain, possibly located within its internal zone. Four CW rotated sites (C136, P01, E133 and M02) sampled west of the Soapága-Pesca faults (Fig. 10) yield the candidate area for strike-slip fault location. Strain partitioning is related to the obliquity between ENE convergence and NNE trend of the Mesozoic rift zone (Fig. 11), representing a mechanically weak zone of the crust, and reactivated by thick-skinned thrust fronts.

NE-trending right-lateral fault(s) within the Eastern Cordillera could be connected southward with the right-lateral Ibague fault (Montes et al., 2005; Fig. 1), and northward with the right-lateral system of the Boconó fault and Merida Andes (Schubert, 1981; Bermúdez et al., 2010). Here four sites in the Cucuta zone yielded a 30°-40° CW rotation that we relate to right-lateral shear occurring even along the more external NE-trending fronts of the Merida Andes. In our tectonic model, the right-lateral fault system of the Eastern Cordillera crosscuts the southern end of the Bucaramanga fault (Figs. 1 and 3), classically assumed to be an active left-lateral fault with significant displacement rate (Acosta et al., 2004; Cediel et al., 2003; Montes et al., 2005). Our data and model, as well as the lack of a significant shallow crustal seismicity associated with the fault (e.g. Taboada et al., 2000), imply minimal present-day relevance (if any existing, is necessary more data to accent this point) of the Bucaramanga fault within the tectonic puzzle of Colombian orogens.

References

Acosta, J., L. Lonergan, and M.P. Coward (2004), Oblique transpression in the western thrust front of the Colombian Eastern Cordillera, J. South Am. Earth Sci., 17, 181-194.

Arriagada, C., P. Roperch, and C. Mpodozis (2000), Clockwise block rotations along the eastern border of the Cordillera de Domeyko, northern Chile (22°450 – 23°300S),Tectonophysics, 326, 153 – 171, doi:10.1016/S0040-1951(00)00151-7.

Arriagada, C., P. Roperch, C. Mpodozis, G. Dupont-Nivet, P.R. Cobbold, A. Chauvin, and J. Cortés (2003), Paleogene clockwise tectonic rotations in the forearc of central Andes, Antofagasta region, northern Chile: Journal of Geophysical Research, v. 108p. 2032, doi: 10.1029/2001JB001598.

Arriagada, C., P. Roperch, C. Mpodozis, and R. Fernandez (2006), Paleomagnetism and tectonics of the south- ern Atacama Desert (25 – 28°S), northern Chile, Tec- tonics, 25, TC4001, doi:10.1029/2005TC001923.

Audemard, F. A., G. Romero, H. Rendon and V. Cano (2005), Quaternary faut kinematics and stress tensors along the southern Caribbean from microtectonic data and focal mechanisms solutions. Earth-Science Reviews 69, (3-4). 181-233.

Averbuch, O., M. Mattei, C. Kissel, D. Frizon de Lamotte, and F. Speranza (1995), Cinématique des déformations au sein d'un systéme chevauchant aveugle: l'exemple de la “Montagna dei Fiori” (front des Apenins centraux, Italie). Bull. Soc. Géol. Fr. 5, 451–461.

Ayala-Calvo, R.C., G. Veloza, G. Bayona, M. Gomez-Casallas, A. E. Rapalini, V. Costanzo-Álvarez and M. Aldana (2005), Paleomagnetismo y mineralogia magnetica en las unidades del Mesozoico de Bucaramanga y Macizo de Floresta: Geología Colombiana, v. 30, 49-66.

Ayala-Calvo, R.C.; G. Bayona, A. Cardona, V. Valencia, C. Ojeda, C. Padrón, F. Yoris, J.

Mesa and A. García (2009) Estratigrafia y procedencia de las unidades comprendidas entre el Campaniano y el Paleogeno en la subcuenca de Cesar-aportes a la evolución tectónica. Geología Colombiana 34, 3-33. Bogotá.

Ayala-Calvo, C., G. Bayona, A. Cardona, C. Ojeda, O. Montenegro, C. Montes, V. Valencia and C. Jaramillo (In press), The Paleogene synorogenic succession in the northwestern Maracaibo block: Tracking intraplate uplifts and changes in sediment-delivery systems. Submitted to Journal of South America Earth Sciences, Special Edition on Tectonic and climatic shaping of the northern Andes and southern Caribbean margin.

Bayona, G., A.E. Rapalini, and V. Costanzo-Álvarez (2006a), Paleomagnetism in mesozoic rocks of the northern Andes and its implications in mesozoic tectonics of northwestern Southamerica. Earth Planets and Space 58, 1255–1272.

Bayona, G., C. Jaramillo, and A. Reyes-Harker (2006b), Resultados Paleomagnéticos en unidades del Paleógeno de Colombia y Oeste de Venezuela y posibles usos para caracterización de contactos. Geología Colombiana 31, 57–72.

Bayona, G., M. Cortes, C. Jaramillo, G. Ojeda, J. Aristizabal, and A. Reyes-Harker (2008), An integrated analysis of an orogen-sedimentary basin pair: Latest Cretaceous-Cenozoic evolution of the linked Eastern Cordillera orogen and the Llanos foreland basin of Colombia.: Geological Society of America Bulletin, v. 120, 1171-1197.

Bayona, G., G. Jiménez, C. Silva, A. Cardona, C. Montes, J. Roncancio, and U. Cordani (2010), Paleomagnetic data and K- Ar ages from Mesozoic units of the Santa Marta massif: A preliminary interpretation for block rotation and translations, J. S. Am. Earth Sci., 29(4), 817–831, doi:10.1016/j.jsames.2009.10.005.

Bayona, G., C. Montes, A. Cardona, C. Jaramillo, G. Ojeda, and V. Valencia (2011), Intraplate subsidence and basin filling adjacent to an oceanic arc-continental collision; a case from the southern Caribbean-South America plate margin. Basin

Research, v. 23, p. 403-422, doi:10.1111/j.1365-2117.2010.00495.x

Bayona, G., A. Cardona, C. Jaramillo, A. Mora, C. Montes, V. Valencia, C. Ayala, O. Montenegro and M. Ibañez (2012), Early Paleogene magmatism in the northern Andes: insights on the effects of Oceanic Plateau-continent convergence. Earth and Planetary Science Letters, v. 331-332, p. 97-111; doi: 10.1016/j.epsl.2012.03.015

Barrero, D. (1979), Geology of the central Western Cordillera, west of Buga and Roldanillo Colombia, Publ. Geol. Espec. Ingeominas, 4, 75 pp.

Bermúdez, M. A., B. P. Kohn, P. A. van der Beek, M. Bernet, P. B. O'Sullivan, and R. Shagam (2010), Spatial and temporal patterns of exhumation across the Venezuelan Andes: Implications for Cenozoic Caribbean geodynamics, Tectonics, 29, TC5009, doi:10.1029/2009TC002635.

Bezada, M. J., A. Levander, and B. Schmandt (2010), Subduction in the southern Caribbean: Images from finite- frequency P wave tomography, J. Geophys. Res., 115, B12333, doi:10.1029/2010JB007682.

Branquet, Y., A. Cheilletz, P. R. Cobbold, P. Baby, B. Laumonier, and G. Giuliani (2002), Andean deformation and rift inversion, eastern edge of Cordillera Oriental (Guateque- Medina area), Colombia, J. S. Am. Earth Sci., 15, 391–407.

Boinet, T., J. Bourgois, H. Mendoza and R. Vargas (1985), Le poinçon de pamplona (Colombie): un jalon de la frontière meridionale de la plaque Caraïbe: Bulletin Societe Geologique de France, v. 8, 403-413.

Butler, R. F., D. R. Richards, T. Sempere and L. G. Marshall (1995), Paleomagnetic determinations of vertical-axis tectonic rotations from Late Cretaceous and Paleocene strata of Bolivia, Geology, 23, 799-802.

Carey, S. W (1955), The orocline concept in geotec- tonics, Proc. Royal Soc. Tasmania, 89, 255–288.

Case, J.E., R. Shagam, and R. F. Giegengack (1990), Geology of the northern Andes: an

overview. Geological Society of America, The Geology of North America, 177–200.

Castillo, J., W. A. Gose and A. Perarnau (1991), Paleomagnetic results from Mesozoic strata in the Mérida Andes, Venezuela: Journal of Geophysical Research, v. 96, p. 6011-6022.

Cediel, F., R. Shaw, and C. Cáceres (2003), Tectonic assembly of the northern Andean Block, in Bartolini, C., Buffler, R. T., and Blickwede, J., eds., The Circum-Gulf of Mexico and the Caribbean: Hydrocarbon habitats, basin formation and plate tectonics, American Association of Petrolum Geologists Memoir 79, p. 815-848.

Cifelli, F., M. Mattei, and M. Della Seta (2008), Calabrian Arc oroclinal bending: The role of subduction, Tectonics, 27, TC5001, doi:10.1029/2008TC002272.

Colletta, B., F. Hebrard, J. Letouzey, P. Werner, and J. L. Rudkiewicz (1990), Tectonic style and crustal struc- ture of the Eastern Cordillera (Colombia) from a balanced cross section, in Petroleum and Tectonics in Mobile Belts, edited by J. Letouzey, 81 – 100, Ed. Technip, Paris.

Cooper, M. A., F.T. Addison, R. Álvarez, M. Coral, R. H. Graham, A. B. Hayward, S. Howe, J. Martínez, J. Naar, R. Peñas, A. J. Pulham, and A. Taborda (1995), Basin development and tectonic history of the Llanos Basin, Eastern Cordillera, and Middle Magdalena Valley, Colombia, AAPG Bull., 79, 1421–1443.

Cortés, M., J. Angelier, and B. Colleta (2005), Paleostress evolution of the northern Andes (Eastern Cordillera of Colombia): Implications on plate kinematics of the South Caribbean region. Tectonics. 24. 1-27.

Cortés, M., B. Colletta, and J. Angelier (2006), Structure and tectonics of the central segment of the Eastern Cordillera of Colombia, Journal of South American Earth Sciences., 21, 437–465, doi:10.1016/j.jsames.2006.07.004.

Creer. K. M (1970), A paleomagnetic Survey of South American rock formations. PhilTrans. Roy.Soc.London. Ser. A, 267, 457-558.

Dengo, C. A., and M. C. Covey (1993), Structure of the Eastern Cordillera of Colombia: Implications for trap styles and regional tectonics, AAPG Bull., 77, 1315 – 1337.

Demarest, H. H (1983), Error analysis of the determination of tectonic rotation from paleomagnetic data, J. Geophys. Res., 88, 4321 – 4328.

Duque-Caro, H (1990), The choco block in the northwestern corner of South America: structural, Tectonostratigraphic, and Paleogeographic implications. Journal of South America Earth Sciences 3, 71–84.

Eldredge, S., V. Bachtadse, and R. Van der Voo (1985), Paleomagnetism and the orocline hypothesis, Tectonophysics, 119, 153 – 179.

Eldredge, S., and R. Van der Voo (1988), Paleomagnetic study of thrust sheet rotations in the Helena and Wyoming salients of the northern Rocky Mountains, in Schmidt, C. J. and W. J. Jr. Perry, eds, Interaction of the Rocky Mountain Foreland and the Cordilleran Thrust Belt: Geological Society of America Memoir 171, p. 319–332.

Evans, J (1977), Geological and Geochemical reconnaissance in the Central Santander Massif, Deparments of Santander and Norte de Santander, Colombia. U. S. Geological Survey (edits).

Fabre, A (1987), Tectonique et genéneration d'hydrocarbures: un modèle de l'evolution de la Cordillère Orientale de Colombie et du Bassin de Llanos pendant le Crétacé et le Tertiaire. Archives des Sciences Genève 40, 145–190.

Fajardo-Peña, G (1998), Structural analysis and basin inversion evolutionary model of the Arcabuco, Tunja and Sogamoso regions, Eastern Cordillera, Colombia (MSc. Thesis): Boulder, University of Colorado.

Farris, D.W., C. Jaramillo, G. Bayona, S.A. Restrepo-Moreno, C. Montes, A. Cardona, A. Mora, R.J. Speakman, M. D. Glasscock, P. Reiners,, and V. Valencia (2011), Fracturing of the Panamanian Isthmus during initial collision with South America. Geology, v. 39, 1007-1010; doi:10.1130/G32237.1

Fisher, R. A (1953), Dispersion on a sphere, Proc. R.Soc. London, 217, 295–305.

Gomez, E., T. Jordan, R. Almandiger, K. Hegarty, S. Kelly, and M. Heizler (2003), Controls on Archi- tecture of the Late Cretaceous to Cenozoic southern Middle Magdalena Valley Basin, Colombia, Geol. Soc. Am. Bull., 115, 131–147.

Gose, W.A., A. Perarnau, and J. Castillo (2003), Paleomagnetic results from the Perijá Mountains, Venezuela: an example of vertical axis rotation. In: Bartolini, C., Buffler, R., Blickwede, J. (Eds.), The Circum-Gulf of Mexico and the Caribbean, Hydrocarbon Habitats, Basin Formation and Plate Tectonics, 79. AAPG Memoir, 969–975

Hargraves, R. B., R. Shagam, R. Vargas, and G.I. Rodriguez (1984), Paleomagnetic results from rhyolites (early Cretaceous?) and andesite dikes at two localities in the Ocaña area, northern Santander massif, Colombia. GSA Memoir 162, 299- 302.

Hebrard. F (1985). Les foothills de la Cordillere Orientale de Colombie entre les rios Casanare et Cusiana. Evolution géodynamique depuis d'Eo Crétace. Ph.D. Thesis, Univ. Pierre et Marie Curie, Paris, 162pp.

Hey, R (1977), Tectonic evolution of the Cocos-Nazca spreading center, Geol. Soc. Am. Bull., 88, 1404– 1420.

Hirt, A. M., and W. Lowrie (1988), Paleomagnetism of the Umbrian-Marches orogenic belt, Tectonophysics, 146, 91 – 103, doi:10.1016/0040-1951(88)90084-4.

Hrouda, F (1982), Magnetic anisotropy of rocks and its application in geology and geophysics, Geophys. Survey, 5, 37-82.

Hrouda, F. and F. Janàk (1976), The changes in shape of the magnetic susceptibility ellipsoid during progressive metamorphism and deformation. Tectonophysics 34, 135–148.

Jelinek, V (1977), The statistical theory of measuring anisotropy of magnetic susceptibility of rocks and its application. Geofyzika, Brno. 88.

Jelinek, V (1978), Statistical processing of magnetic susceptibility on groups of specimens. Stud. Geophys. Geod. 22, 50–62.

Jelinek, V (1981), Characterization of the magnetic fabrics of rocks. Tectonophysics 79, 63–67.

Jiménez, G., J. Rico, G. Bayona, C. Montes, A. Rosero and D. Sierra (in press), Analysis of curved folds and fault/fold terminations in the southern Upper Magdalena Valley of Colombia. Submitted to Journal of South America Earth Sciences, Special Edition on Tectonic and climatic shaping of the northern Andes and southern Caribbean margin

Jolly, A.D. and S.D. Sheriff (1992), Paleomagnetic study of thrust sheet motion along the Rocky Mountain Front in Montana. Geological Society of America Bulletin, V. 104, 779-785.

Kammer, A (1999), Observaciones acerca de un origen transpresivo de la Cordillera Oriental, Rev. Geol. Colombiana, 24, 29–53.

Kellogg, J., and V. Vega (1995), Tectonic development of Panama, Costa Rica, and the Colombian Andes: Constraints from global positioning system geodetic studies and gravity, Spec. Pap. Geol. Soc. Am., 295, 75–90.

Kimura. H., N. Ishikawa and H. Sato (2011), Estimation of total lateral displacement including strike–slip offset and broader drag deformation on an active fault: Tectonic geomorphic and paleomagnetic evidence on the Tanna fault zone in central Japan, Tectonophysics 501. 87–97, doi:10.1016/j.tecto.2011.01.016.

Kirschvink, J. L (1980), The least-squares line and plane and the analysis of paleomagnetic data, Geo- phys. J. R. Astron. Soc., 62, 699–718.

Larrasoaña J. C., J. C. Parés, H. Millán H, J. del Valle J, and E. L. Pueyo (2003), Paleomagnetic, structural and stratigraphic constraints on the role of transverse fault development during basin inversion (Pamplona Fault, Pyrenees, N Spain). Tectonics. 22(6): 1071-1093.

Lowrie, W (1990), Identification of ferromagnetic minerals in a rock by coercivity and unblocking temperature properties, Geophys. Res. Lett., 17, 159 – 162.

MacDonald, W.D. and N.D. Opdyke (1972). Tectonic Rotations suggested by Plaeomagnetic results from northern Colombia, South America. Journal of Geophysical Research. 77, N 29 5720-5730.

MacDonald, W.D. and N.D. Opdyke (1984), Preliminary paleomagnetic results from Jurassic rocks of the Santa Marta Massif, Colombia. In: Bonini, W.E., R. B. Hargraves, R. Shagam. (Eds.), The Caribbean–South American plate boundary and regional tectonics, vol. 162. Geological Society of America Memoir, 295–298.

MacDonald, W.D., J. J. Estrada, G. M. Sierra and H. Gonzalez (1996), Late Cenozoic tectonic and paleomagnetism of North Cauca Basin intrusions, Colomba Andes: Dual rotations modes. Tectonophysics 261, 277-289.

Macedo, J. and S. Marshak (1999), Controls on the geometry of fold-thrust belt salient's, Geological Society of America Bulletin 1999;111;1808-1822

McFadden, P. L (1990), A new fold test for paleomagnetic studies, Geophys. J. Int., 103, 163–169.

McFadden, P. L., and M. W. McElhinny (1990), Classification of the reversal test in paleomagnetism, Geophys. J. Int., 103, 725–729.

McFadden, B. J., F. Anaya and C. Swisher (1995), Neogene paleomagnetism and oroclinal bending of the central Andes of Bolivia. J. Geophys. Res., 100, 8153–8167.

Maffione, M., F. Speranza, and C. Faccenna (2009), Bending of the Bolivian orocline and growth of the central Andean plateau: Paleomagnetic and structural constraints from the Eastern Cordillera (22 – 24°S, NW Argentina), Tectonics, 28, TC4006, doi:10.1029/2008TC002402.

Marshak, S (1988), Kinematics of orocline and arc formation in thin-skinned orogens: Tectonics, v. 7, p. 73–86.

Mattei, M., R. Funicello and C. Kissel (1995), Paleomagnetic and structural evidence for Neogene block rotations in the Central Apennines, Italy. J. Geophys. Res., 100 (B9), 17, 863-17,883, doi:10.1029/95JB0864.

Mattei. M., L. Sagnotti, C. Faccenna, R. Funniciello (1997), Magnetic fabric of weakly deformed clay-rich sediments in the Italian peninsula: relationships with compressional and extensional tectonics. Tectonophysics, 271, 107-122.

Mattei, M., F. Speranza, Argentieri. A, F. Rossetti, L. Sagnotti and R. Funicello (1999), Extensional tectonics in the Amatea basin (Calabria, Italia): a comparison between structural and magnetic anisotropy data. Tectonophysics 307, 33-49.

Maze. W, and R.B. Hargraves (1984), Paleomagnetic results from the jurassic La Quinta formation in the Perijá range, Venezuela and their tectonic significance. GSA Memoir 162, 287-293.

Monod, B., D. Dhont, and Y. Hervouët (2010), Orogenic float of the Venezuelan Andes. Tectonophysics, v. 490, p. 123–135, doi: 10.1016/j. tecto.2010.04.036.

Montes, C., P. A. Restrepo-Pace, R. D. Hatcher Jr (2003), Three- dimensional structure and kinematics of the Piedras–Girardot foldbelt: surface expression of transpressional deformation in the northern Andes. In: Bartolini, C., Buffler, R.T., Blickwede, J. (Eds.), The Circum-Gulf of Mexico and the Caribbean: Hydrocarbon Habitats, Basin Formation and Plate Tectonics. AAPG, Memoir 79, 849–873.

Montes, C., T. Robert, D. Jr Hatcher, P. A. Restrepo-Pace (2005), Tectonic reconstruction of the northern Andean blocks: Oblique convergence and rotations derived from the kinematics of the Piedras–Girardot area, Colombia, Tectonophysics 399. 221–250, doi:10.1016/j.tecto.2004.12.024

Mora, A., M. Parra, M. R. Strecker, A. Kammer, C. Dimate´, and F. Rodríguez (2006), Cenozoic contractional reactivation of Mesozoic extensional structures in the Eastern Cordillera of Colombia, Tectonics, 25, TC2010, doi:10.1029/2005TC001854.

Mora, A., M. Parra, M. R. Strecker, E. R. Sobel, H. Hooghiemstra, V. Torres and J. Vallejo-Jaramillo (2008), Climatic forcing of asymmetric orogenic evolution in the Eastern Cordillera of Colombia, Geol. Soc. Am. Bull., 120, 930–949, doi:10.1130/ B26186.1.

Mora, A., T. Gaona, J. Kley, D. Montoya, M. Parra, L.I. Quiroz, G. Reyes, and M. Strecker (2009), The role of inherited extensional fault segmentation and linkage in contractional orogenesis: A reconstruction of Lower Cretaceous inverted rift basin in the Eastern Cordillera of Colombia: Basin Research, v. 21, p. 111– 137.

Mora, A., M. Parra, M. R. Strecker, E. R. Sobel, G. Zeilinger, C. Jaramillo, S. Ferreira Da Silva and M. Blanco (2010a), The eastern foothills of the Eastern Cordillera of Colombia: An example of multiple factors controlling structural styles and active tectonics. Geol. Soc. Am. Bull., 122, 1846–1864, doi: 10.1130/B30033.1

Mora, A., B. K. Horton, A. Mesa, J. Rubiano, R. A. Ketcham, M. Parra, V. Blanco, D. Garcia and D. F. Stockli (2010b), Migration of Cenozoic deformation in the eastern Cordillera of Colombia interpreted from fission track results and structural relationships: Implications for petroleum systems. AAPG Bulletin, v. 94, 1543-1580. DOI:10.1306/01051009111

Muttoni. G., A. Argnani, D.V. Kent, N. Abrahamsen and U. Cibin (1998), Paleomagnetic evidence for Neogene tectonic rotations in the northern Apennines, Italy. Earth and Planetary Science Letters, 154. 25–40.

Nova, G., P. Montaño, G. Bayona, A. Rapalini, C. Montes and C. Silva (2011), Análisis Paleomagnético en rocas del Mesozoico para el flanco occidental de la Serranía del Perijá; Resultados preliminares. Resumen en CD, Segunda Reunión Bienal de la Asociación Latinoamericana de Paleomagnetismo y Geomagnetismo (LatinMag), Tandil, Argentina, Noviembre 23-26 2011, 6 p.

Parra, M., A. Mora, C. López, L.E. Rojas and B. K. Horton (2012), Detecting early

shortening and deformation advance in thrust-belt hinterlands: Example from the Colombian Andes, Geology (in press)

Parés., J.M., B. A.Van der Pluijm, J. Dinarés-Turell (1999), Evolution of magnetic fabrics during incipient deformation of mudrocks (Pyrenees, northern spain). Tectonophysiscs, 307, 1-14.

Pindell, J. L., S. C. Cande, W. C. Pitman III, D. B. Rowley, J. F. Dewey, J. LaBrecque, and W. Haxby (1988), Plate- kinematic framework for models of Caribbean evolu- tion: Tectonophysics, v. 155, p. 121–138.

Piper, J. D. A., O. Tatar and H. Gürsoy (1997), Deformational behavior of continental lithosphere deduced from block rotations across the North Anatolian fault zone in Turkey. Earth Planet. Sci. Lett. 150, 191–203.

Pilger., R (1983), Kinematics of the South American subduction zone from global plate reconstructions, in Geodynamics of Eastern Pacific Region. American Geophysical Union Geodynamics Series 9, 113–126.

Pueyo E.L., J. M. Parés, H. Millán, and A. Pocoví (2003), Conical folds and apparent rotations in paleomagnetism (A case studied in the Southern Pyrenees). In: Paleomagnetism applied to tectonics; a tribute to Rob Van der Voo. Edited by: Mac Niocaill C., T. H. Torsvik., B.A. Van der Pluijm., Tectonophysics. 362 (1-4): 345-366.

Randall, D. E., G. K. Taylor, and J. Grocott (1996), Major crustal rotations in the Andean margin: Pa- leomagnetic results from the Coastal Cordillera of northern Chile, J. Geophys. Res., 101, 15,783– 15,798, doi:10.1029/96JB00817.

Randall, D. E., A. Tomlinson, and G. K. Taylor (2001), Paleomagnetically defined rotations from the Pre- cordillera of northern Chile: Evidence of localized in situ fault-controlled rotations, Tectonics, 20, 235–254, doi:10.1029/1999TC001180.

Randall, K., S. Lamb and C. Mac Niocaill (2011), Large tectonic rotations in a wide zone of Neogene distributed dextral shear, northeastern South Island, New Zealand,

Tectonophysics 509 165–180

Rapalini, A. E., F. Hervé, V.A. Ramos and S. Singer (2001), Paleomagnetic evidence of a very large counterclockwise rotation of the Madre de Dios archipelago, southern Chile. Earth and Planetary Science Letters, 184 (2), 471-487.

Restrepo-Pace, P. A (1995), Late Precambrian to early Mesozoic tectonic evolution of the Colombian An- des, Based on new geochronological, geochemical and isotopic data, Ph.D. thesis, 194 pp., Univ. of Ariz., Tucson.

Rochette, P (1987). Magnetic susceptibility of the rock matrix related to magnetic fabric studies. J. Struct. Geol. 9, 1015–1020.

Rochette, P., M. Jackson, and C. Aubourg (1992) Rock magnetism and the interpretation of anisotropy of magnetic susceptibility, Rev. Geophys., 30, 209-226.

Roeder, D., and R. L. Chamberlain (1995), Eastern Cordillera of Colombia: Jurassic Neogene Crustal evolution. In: Tankr, R., Suarez, Welsink, H.J. (Eds.), Petroleum basins of South America. American Association of Petroleum Geologists Memoir 62, pp. 633–645.

Roperch, P., and G. Carlier (1992), Paleomagnetism of Mesozoic rocks from the central Andes of southern Peru: Importance of rotations in the development of the Bolivian orocline, J. Geophys. Res., 97, 17,233–17, 249.

Roperch, P., G. He´rail, and M. Fornari (1999), Magnetostratigraphy of the Miocene Corque basin, Boli- via: Implications for the geodynamic evolution of the Altiplano during the late Tertiary, J. Geophys. Res., 104, 20, 415–20, 429, doi:10.1029/ 1999JB900174.

Roperch, P., M. Fornari, G. He´rail, and G. V. Parraguez (2000), Tectonic rotations within the Bolivian Al- tiplano: Implications for the geodynamic evolution of the central Andes during the late Tertiary, J. Geophys. Res., 105, 795 – 820, doi:10.1029/ 1999JB900311.

Ross, I., P. Parra, C. Mora and C. Pimentel (2009), AFTA apatite fission track analysis constraints on the Mesozoic to Quaternary thermal and tectonic evolution of the Middle Magdalena Basin and Santander Massif, Eastern Cordillera, Bucaramanga area, Colombia. X Simposio Bolivariano: Exploración Petrolera en Cuencas Subandinas. Cartagena, Colombia. Memoir.

Sagnotti, L., F. Speranza., A. Winkler., M. Mattei, and R. Funiciello (1998). Magnetic fabric of clay sediments from the external northern Apennines (Italy). Phys. Earth Planet. Inter. 105, 73–93.

Sarmiento-Rojas, L. F (2001), Mesozoic rifting and Cenozoic basin inversion history of the Eastern Cordillera, Colombian Andes, Ph.D. thesis, 295 pp., Vrije Univ., Amsterdam.

Sarmiento-Rojas, L. F, J.D. Van Wess and S. Cloetingh (2006), Mesozoic transtensional basin history of the Eastern Cordillera, Colombian Andes: Inferences from tectonic models. Journal of South American Earth Sciences 21, 383–411

Schubert, C (1981), Are the Venezuelan fault systems part of the southern Caribbean plate boundary? Geologische Rundschau 70 (2), 542–551

Schwartz, S. Y., and R. Van der Voo (1983), Paleomagnetic evaluation of the orocline hypothesis in the central and southern Appalachians, Geophys. Res. Lett., 10, 505 – 508.

Somoza, R., and A. J. Tomlinson (2002), Paleomagnetism in the Precordillera of northern Chile (22°300S): Implications for the history of tectonic rotations in the central Andes, Earth Planet. Sci. Lett., 194, 369 – 381.

Sonder, L. J., C. H. Jones, S. L. Salyards, and K. M. Murphy (1994), Vertical-axis rotations in the Las Vegas Valley Shear Zone, southern Nevada: Paleomagnetic constraints on kinematics and dynamics of block rotations, Tectonics, 13 (4), 769-788.

Speranza, F., M. Mattei and L. Sagnotti (1997), Tectonics of the Umbria-Marche-Romagna Arc (central northern Apennines, Italy): new paleomagnetic constraints. J. Geophys.

Res. 102 (B2), 3153–3166.

Speranza, F., R. Maniscalco, M. Matte, A. Di Stefan, R.W.H. Butler, R. Funiciello (1999), Timing and magnitude of rotations in the frontal thrust systems of southwestern Sicily. Tectonics 18 (6), 1178–1197.

Sussman, A. J., R. F. Butler, J. Dinares-Turrell, and J. Verges (2004), Vertical-axis rotation of a fore- land fold: An example from the southern Pyre- nees, Earth Planet. Sci. Lett., 218, 435 – 449, doi:10.1016/S0012-821X(03)00644-7.

Taboada, A., L. A. Rivera, A. Fuenzalida, A. Cisternas, H. Philip, A. Bijwaard, J. Olaya, and C. Rivera (2000), Geodynamics of the northern Andes: Sub- ductions and intracontinental deformation (Colom- bia), Tectonics, 19, 787–813.

Taylor, G. K., B. Dashwood, and J. Grocott (2005), The central Andean rotation pattern: Evidence of an anomalous terrane in the forearc of northern Chile from paleomagnetic rotations, Geology, 33, 777–780.

Torsvik, T. H., R. D. Muller, R. Van der Voo, B. Steinberger, and C. Gaina (2007), Global plate motion frames: Toward a unified model, Rev. Geophys., 46.

Trenkamp, R., J. N. Kellogg, J. T. Freymueller, and H. P. Mora (2002), Wide plate deformation, south- ern Central America and northwestern South America, CASA GPS observations, J. S. Am. Earth Sci., 15, 157–171.

Velandia, F., J. Acosta, R. Terraza, and H. Villegas (2005), The current tectonic motion of the Northern Andes along the Algeciras Fault System in SW Colombia, Tectonophys., 399, 313-329.

Ward, D, R. Goldsmith, B. Cruz, C. Jaramillo and H. Restrepo (1973), Geología de los Cuadrángulos H-12, Bucaramanga y H-13, Pamplona, Departamento de Santander. U.S. Geological Survey e Ingeominas. Boletín Geológico XXI (1-3), 1-132.

Weil, A., and A. J. Sussman (2004), Classifying Curved Orogens Based on Timing Relationships, pp. 1 – 15, Geol. Soc. of Am., Boulder, Colo.

Zarifi, Z., J. Havskov, and A. Hanyga (2007), An insight into the Bucara- manga nest, Tectonophysics, 443(1–2), 93–105.

Zijderveld, J. D. A (1967), A.C. demagnetization of rocks: Analysis of results, in Methods in Palaeomagnetism, edited by D. W. Collinson, K. M. Creer, and S. K. Runcorn, pp. 254–286, Elsevier, New York.

Zweigel. P (1998), Arcuate accretionary wedge formation at convex plate margin corners: Results of sandbox analog experiments: Journal of Structural Geology, 20. 1597-1609.

Chapter 3

Magnetic stratigraphy of the Bucaramanga alluvial Fan: Evidence for a ≤ 3 mm/yr slip rate for the Bucaramanga-Santa Marta Fault, Colombia

Abstract

The 550 km long Bucaramanga-Santa Marta Fault is one of the main active tectonic features of NW South America. It is a left-lateral strike-slip fault bounding the Maracaibo block, and straddling northern Colombia from the Caribbean Sea to the Eastern Cordillera, where it crosses the Bucaramanga town. Variable total displacement values (from 40 to 110 km), and present-day slip rates (from 0.01 to 10 mm/yr) have been proposed so far for the Bucaramanga Fault. Here we report on the paleomagnetic investigation of a Plio-Pleistocene (?) continental alluvial fan juxtaposed to the Bucaramanga Fault, and horizontally displaced by 2.5 km with respect to its feeding river. Nine (out of fourteen) reliable paleomagnetic directions define a succession of six different magnetic polarity zones that, lacking additional age constraints, can be correlated with several tracks of the Plio-Pleistocene magnetic polarity time scale. If the youngest age model is considered, most recent sediments of the fan can be reasonably dated at 0.8 Ma (Brunhes-Matuyama chron transition), translating into a maximum 3 mm/yr slip rate for the Bucaramanga Fault. Older age models would obviously yield smaller slip rates. A 3 mm/yr slip rate is in rough agreement (although at the upper boundary of inferred magnitude) with previous estimates from paleoseismological evidence, documenting eight main seismic events in the last 8 ka, and earthquake sizes in the 6.5-7.0 M range. Our paleomagnetic sites, located at 4-10 km from the fault, do not show significant rotations, implying weak fault coupling and/or ductile upper crust behavior adjacent to the Bucaramanga Fault.

Keywords: Paleomagnetism, Bucaramanga Fan, Bucaramanga Fault, Slip rate.

1.0 Introduction

The NW margin of South America is characterized by a complex pattern of mountain ranges (Western, Central, and Eastern Cordillera of Colombia, Fig. 1), and by a puzzle of crustal blocks undergoing independent movements (Kellogg et al., 1982; Taboada et al., 2000; Trenkamp et al., 2002). The eastward subduction of the Nazca Plate beneath South America at a rate of 6 cm/yr is well documented (Trenkamp et al., 2002), while the existence of an ESE-ward directed subduction of the Caribbean plate is debated (Pindell et al., 1988), although a well-developed accretionary wedge (Fig. 1) is exposed at the boundary between the Caribbean and South American plate (e.g., Flinch et al., 2003).

The Maracaibo block, the biggest semi-rigid block of the Colombian tectonic puzzle, is bounded by three major wrench faults: the dextral Boconó and Oca faults, and the sinistral Bucaramanga-Santa Marta Fault (Fig. 1). The relevance, age, and displacement rate of these major strike-slip faults have been widely discussed in the past (Irving, 1971; Toro, 1990; Ujueta, 2003; Mora and Garcia, 2006; Lopez et al., 2008), and a consensus on the whole block and fault kinematics has not been reached so far.

The Bucaramanga-Santa Marta Fault system juxtaposes basement rocks to the east and sedimentary Jurassic to Cenozoic rocks to the west. This fault system extends for a distance of 550 km from the Caribbean coast to the Eastern Cordillera (Fig. 1), where it crosses the Bucaramanga town (ca. 500,000 inhabitants). It can be divided along strike into three major zones (Northern, Central and Southern zone), where it bounds several distinct geological provinces. The Northern zone, or Santa Marta section (Paris, 2000; Ingeominas, 2001a), corresponds to a 140 km long topographic lineament juxtaposing old crystalline rocks of the Santa Marta Massif to Neogene deposits of the Lower Magdalena Valley basin (Fig. 1). The 100 km long Central zone is covered by alluvial deposits of the

Lower Magdalena Valley basin (Ariguani graben) and Cesar Valley basin (Mora and García, 2006; Fig.1).

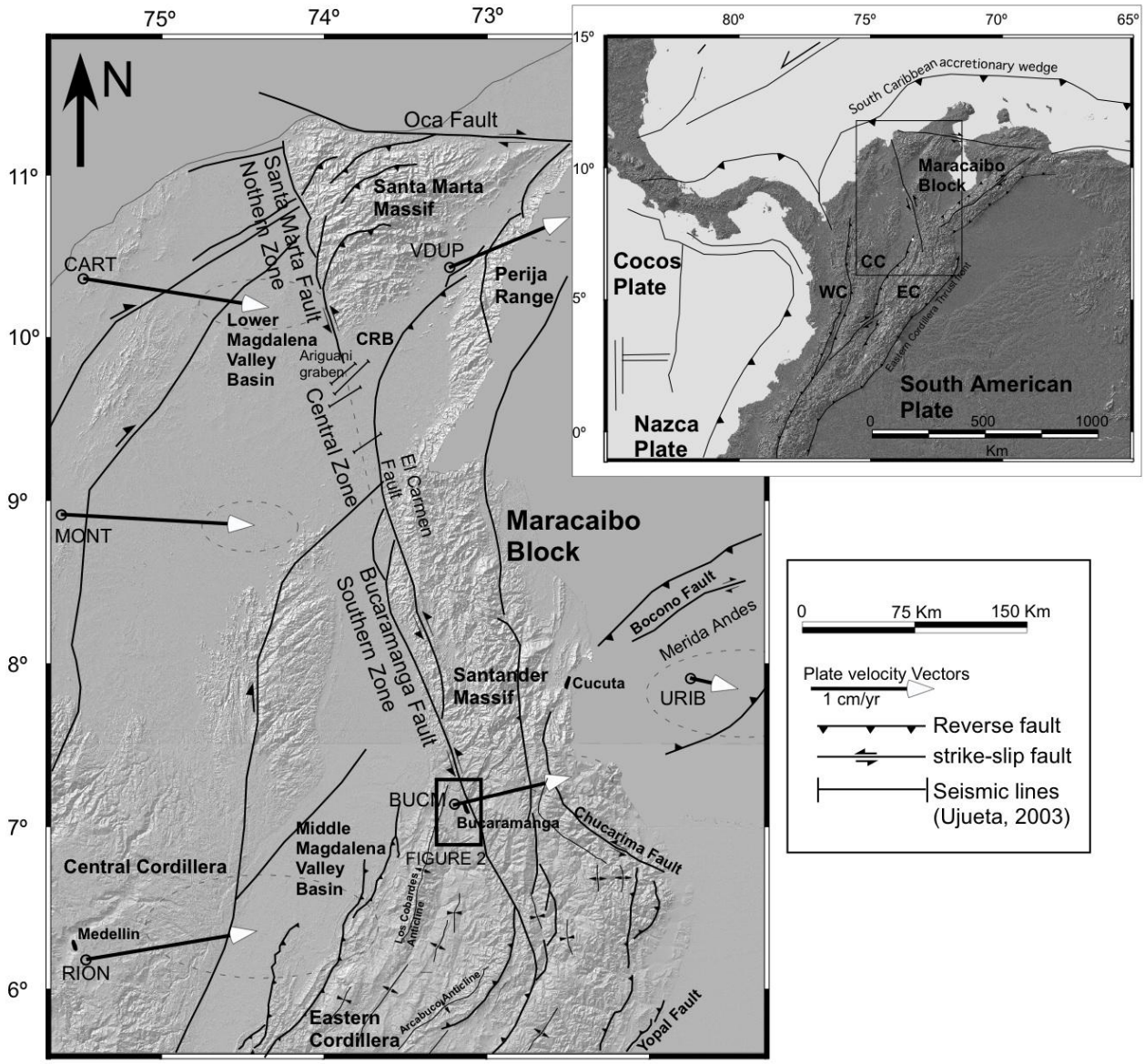

Figure 1. Major tectonic and structural features of the NW margin of South America. Plate velocity vectors with respect to stable South America are from Trenkamp et al. (2002). WC = Western Cordillera, CC = Central Cordillera, EC = Eastern Cordillera.

The Southern zone corresponds to Bucaramanga section (Paris, 2000; Ingeominas, 2001a), a 310 km long outstanding linear topographic feature separating the Santander Massif from the Middle Magdalena Valley basin (Fig. 1). At the Bucaramanga town, the fault clearly left-laterally displaces a 10-15 km wide continental alluvial fan of presumable

Plio-Pleistocene age, produced by debris carried by the Suratá river from the adjacent Santander Massif (Fig. 2). The zone is well known for the high seismic activity of the "Bucaramanga nest" (Taboada et al, 2000; Zarifi et al, 2007; Fig. 3), but earthquakes are deep (from 100 to 200 km), thus they should not be related to the activity of the Bucaramanga Fault.

In this paper we report on a paleomagnetic investigation of the Bucaramanga Fan to constrain its age by magnetic stratigraphy, one of the few viable method to date those gravel-size alluvial fan deposits. The results will allow the documentation of when fan displacement occurred, and unravel recent and present-day slip rate of the Bucaramanga Fault. The Bucaramanga town has not been struck by devastating earthquakes since when historical accounts are available (XVII century AD), thus it is unclear whether we are living a recurrence interval preceding a future strong earthquake, or in fact there is no significant present-day activity of the Bucaramanga Fault, as GPS data of Trenkamp et al. (2002) might suggest (Fig. 1).

2.0 Characteristics of the Bucaramanga-Santa Marta Fault

Previous work around the Bucaramanga town has been done in the frame of regional and local cartography projects (Servicio Geológico Nacional, 1977; Ingeominas, 2001b; Diedrix et al., 2009; Fig. 2). In the Santander Massif, which is bounded to the west by the Bucaramanga Fault system, Pre-Cambrian, Paleozoic, and Mesozoic intrusive and metamorphic rocks (schists and gneisses) are exposed. According to Cediel et al. (2003), the Bucaramanga-Santa Marta Fault was active during the Pre-Cambrian Grenville - Orinoco continental collision, and reactivated in the Aptian-Albian times. Pindell et al. (1988) proposed that the Bucaramanga – Santa Marta fault is the western limit of the

Maracaibo Block since Miocene times. Ross et al. (2009) using Apatite fission track (AFT) analysis of Precambrian to Neogene rocks from the Santander Massif and Middle Magdalena Valley proposed three paleothermal episodes (interpreted as erosional phases) in the Paleocene (65 to 60 Ma), Early Miocene (20 to 18 Ma) and Middle Miocene (12 to 9 Ma). This evidence provides age clues for the uplift of the Santander Massif with respect to the adjacent Magdalena Valley that likely occurred along the Bucaramanga Fault.

As the Bucaramanga Fault is a recent geomorphological feature, it is more likely that acted in the last phase of deformation of late Miocene age, as suggested by AFTA data. Paleocene movements may be related to other structures in the Cobardes Anticline (Parra et al, 2012, Fig. 1). Provenance analysis indicates that the Santander Massif, and its sedimentary cover, was uplifted since Paleogene time, (Ayala et al, 2012). The Bucaramanga Fault bounds a thick deposition of upper Jurassic and Cretaceous rocks to the south and west (Kammer and Sanchez, 2006), whereas to the north and east deposition of Jurassic rocks is thinner than in the other block of the fault and in some areas lowermost Cretaceous strata is absent (Ward et al, 1973)

Reported total displacement values of the Bucaramanga – Santa Marta fault vary from 45 to 110 km. Toro (1990) using structural reconstructions proposed for the southern fault portion a displacement of 45 km. According to Campbell (1968), the total displacement is more than 100 km, relying on a regional scale correlation between rocks from the Central Cordillera and the Santa Marta Massif. Other authors (Irving, 1971; Tschantz, 1974) proposed 110 km of displacement after the analysis of samples drilled in oil wells. Montes et al. (2010) and Bayona et al (2010) used the Bucaramanga-Santa Marta Fault systems as boundary of clockwise rotation of the Maracaibo block during the Cenozoic. Reported values for the fault slip rate range between 0.01-0.2 mm/yr, calculated on the basis of

geomorphic offset features (Paris, 2000; Ingeominas, 2001a), to 10 mm/yr, evaluated after regional geology considerations (Rivera, 1989).

López et al., (2008) reported the occurrence of Pseudotachylite associated to cataclasites in the southern sector of the Bucaramanga Fault, that they interpreted as an evidence for paleoseismicity along the fault. Diedrix et al. (2009) using paleoseismological investigation and radiocarbon dating of paleosoils trenched adjacent to the fault proposed eight Holocene seismic events during the last 8300 years and magnitudes in the order of 6.5-7.0, associated to the Bucaramanga Fault activity.

Ujueta (2003) made an extensive review of the previous works on the Bucaramanga Santa Marta Fault available since 1933, and observed that some authors consider the Bucaramanga Santa Marta fault as a reverse fault, others as left lateral strike-slip fault, while few works propose two different and independent faults. About the activity of the Bucaramanga Fault, a late Mesozoic, Paleocene, Eocene or Pliocene-Quaternary age are proposed (Diedrix et al, 2009).

Finally, using seismic profiles, he discussed the continuity of the fault Central zone, and proposed two different but related faults, with absence of connection between the southern and the northern zone. Mora and García (2006) using extensive seismic profile analysis and well data, proposed that the Bucaramanga-Santa Marta Fault in the Central zone was responsible for the intense structural deformation that affected pre-Oligocene units, indicating that it was an active boundary between the Lower Magdalena Valley and Cesar basins during the late Eocene-early Oligocene. They also suggested that fault activity ended after Oligocene, as the Lower Magdalena Valley and Cesar basins have been connected without tectonic disturbances.

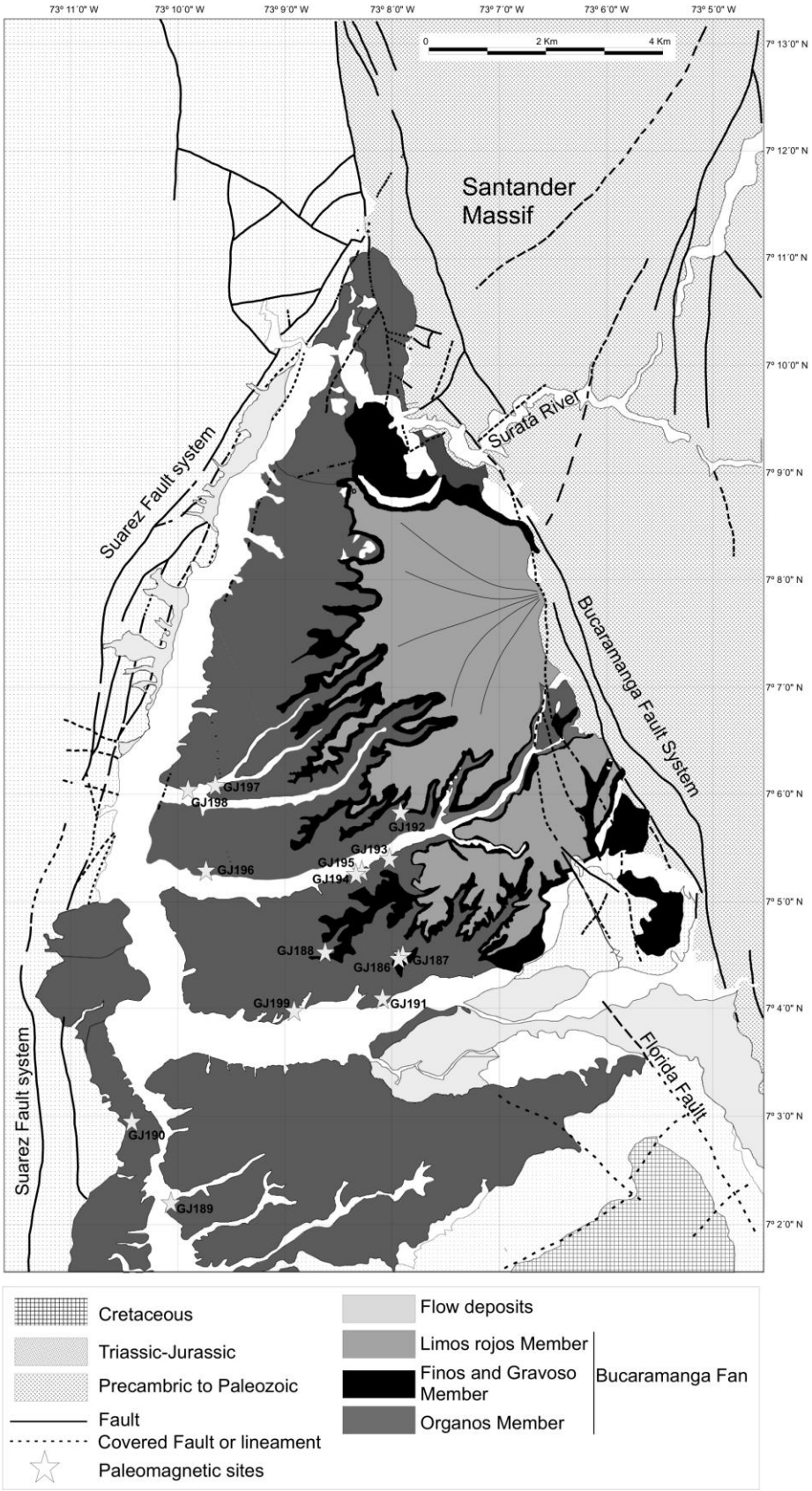

Figure 2. Geological map of the Bucaramanga Fan (modified from Ingeominas, 2001b and Servicio Geológico Nacional, 1977) with the location of the 14 paleomagnetic sites (see Figure 1 for location).

2.1 The Bucaramanga Fan

The Bucaramanga Fan is limited to the east by the Santander Massif and the Bucaramanga Fault, and to the west by the Suárez Fault (Fig. 2). The Suárez Fault is a west-dipping reverse fault with sinistral displacement and quaternary activity (Page, 1986; Paris et al., 2000; Ingeominas, 2001a) that terminates northward against the Bucaramanga Fault. In the study area, the Suárez Fault places in contact Jurassic and Cretaceous strata against the Bucaramanga Fault. Locally, the Bucaramanga Fan is folded with vertical to overturned beds by the effect of the Suárez Fault (Ingeominas, 2008).

De Porta (1958) defined the Bucaramanga Fan as a sedimentary deposit of Quaternary age with an alluvial fan morphological shape (Fig. 2). According to Ingeominas (2001b) the thickness of the Bucaramanga Fan increases from east to west with an average thickness of 250 m, and it was divided into, from base to top, the Organos, Finos, Gravoso, and Limos Rojos member (Fig. 2).

The Organos Member was defined by Hubach (1952), and according to Bueno and Solarte (1994) is a monotonous sequence of conglomerates with intercalations of fine sandstones. Conglomerate clasts are 10 - 30 cm in diameter (and in some cases more than 1 m) and includes gneisses and schists fragments. This member is clast supported, contains a clay matrix (Ingeominas, 2001b), and crops out to the west of the study area with a maximum thickness of 180 m (Mancera and Salamanca, 1994). The Finos Member (Hubach, 1952) is a continuous sub-horizontal 15 m thick bed overlying the Organos member along a net discontinuity, and it consists of clays evolving upsection into fine-grained sandstone beds (Ingeominas, 2001b). The Gravoso Member (Vargas and Niño, 1992) is an 8 to 30 m thick, matrix supported level of gravel-size clasts overlying the Finos Member along a net contact. The clasts are on average 15 cm in diameter (cobble size), and the matrix

includes a mixture of clay- and sand-size fragments. Finally, the Gravoso Member transitionally passes upward into the 15 m thick Limos Rojos Member (Julivert, 1963); this unit consists of argillaceous sandstones and conglomeratic sandstones, interbeded with layers of siltstones. Locally, block fragments (meter scale in diameter) of sandstone texture are supported by the red silty matrix (Ingeominas, 2001b).

The Bucaramanga Fan is generally inferred of Plio-Pleistocene in age (Ingeominas, 2001b), although no conclusive age constraints were gathered from the continental succession so far.

2.2 The deep seismicity of the Bucaramanga Nest

No significant shallow crustal seismicity has been recorded along the Santa Marta-Bucaramanga Fault (Fig. 3), but at depth a remarkable cluster of subcrustal earthquakes in the 100-200 km depth interval is observed in the so-called “Bucaramanga nest”, centered at 7°N 73°W. It differs from other worldwide nests by its high rate of activity in a volume much smaller than the other nests at similar intermediate depths (Schneider et al., 1987; Zarifi and Harsco, 2003; Prieto et al., 2012). The Bucaramanga nest has been mostly related to tectonic processes occurring in the oceanic subducting plates beneath Colombia (Zarifi and Havskov, 2003). Taboada et al. (2000) proposed that the Bucaramanga Nest is due to the interaction between the subducting Nazca and a remnant of the paleo-Caribbean plates, while Zarifi et al. (2007) suggested a simultaneous subduction process and collision between two subducted slabs. Alternatively, Cediel et al. (2003) propose that the seismic activity recorded in the Bucaramanga Nest represents a zone of tectonic detachment associated with NW-ward migration of the Maracaibo subplate, while Rivera (1989) proposed that there is a relationship between the Bucaramanga Fault and Nest.

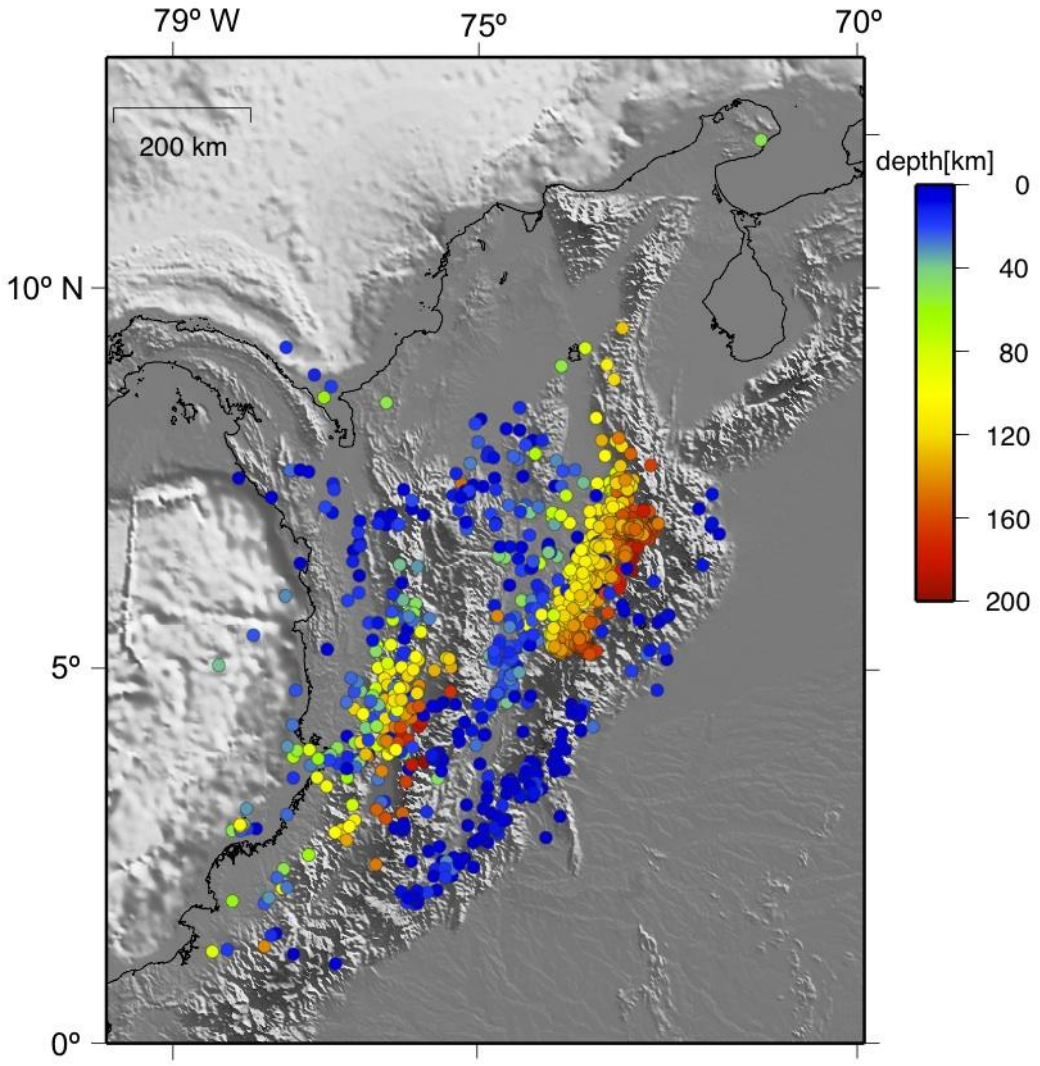

Figure 3. Seismicity in NW South American Plate recorded during 2006-2009 by the Red Sismica Nacional de Colombia (RSNC)-Ingeominas.

3.0 Sampling and Methods

We collected sandy-silty samples for paleomagnetic analysis in fourteen sites (154 cores, Table 1) from the Bucaramanga Fan, using a petrol-powered portable drill cooled by water. Ten sites were gathered in the Organos Member, two in the Finos Member, and two in the Gravoso Member (Figure 2 and Table 1). At each site we collected 6–12 cores (11 on average), spaced in at least two outcrops in order to try to average out secular variation of the geomagnetic field. All samples were oriented using a magnetic compass, corrected to account for the local magnetic field declination value at the sampling area (about 7° W)

according to NOAA's National Geophysical Data Center (http://www.ngdc.noaa.gov).

Cores were cut into standard cylindrical specimens of 22 mm height, and rock magnetic and paleomagnetic measurements were done in the shielded room of the paleomagnetic laboratory of the Istituto Nazionale di Geofisica e Vulcanologia (Roma, Italy). All samples were thermally demagnetized through 11–12 steps up to 680°C by a shielded oven, and the natural remanent magnetization (NRM) of the specimens was measured after each step with a DC- SQUID cryogenic magnetometer (2G Enterprises, USA). Thermal demagnetization data were plotted on orthogonal diagrams (Zijderveld, 1967), and the magnetization components were isolated by principal component analysis (Kirschvink, 1980). The site-mean directions were evaluated by Fisher's (1953) statistics

On a set of selected specimens, magnetic mineralogy analyses were carried out to identify and characterize the main magnetic carriers using the thermal demagnetization of a three-component isothermal remanent magnetization (IRM) imparted on the specimen axes, according to the method of Lowrie (1990). Fields of 2.7, 0.6, and 0.12 T were successively imparted on the z, y, and x sample axes (respectively) with a pulse magnetizer (Model 660, 2G Enterprises).

4.0 Results

4.1 Magnetic Mineralogy

The thermal demagnetization of a three-component IRM shows that for most of the samples both the medium coercivity and the hard fractions are demagnetized between 600 and 680°C (Fig. 4), pointing to hematite as the main magnetic carrier of our samples. In almost all sites, a drop of the medium coercivity and hard fraction occurring before 100º shows that a small amount of goethite is also associated to hematite

For most of the sites, a characteristic magnetization component (ChRM) was isolated

between 550 and 680°C, confirming that hematite represents the main magnetic carrier. For about 10% of the samples, a ChRM is isolated between 380 and 680°C, suggesting the coexistence of hematite and magnetite

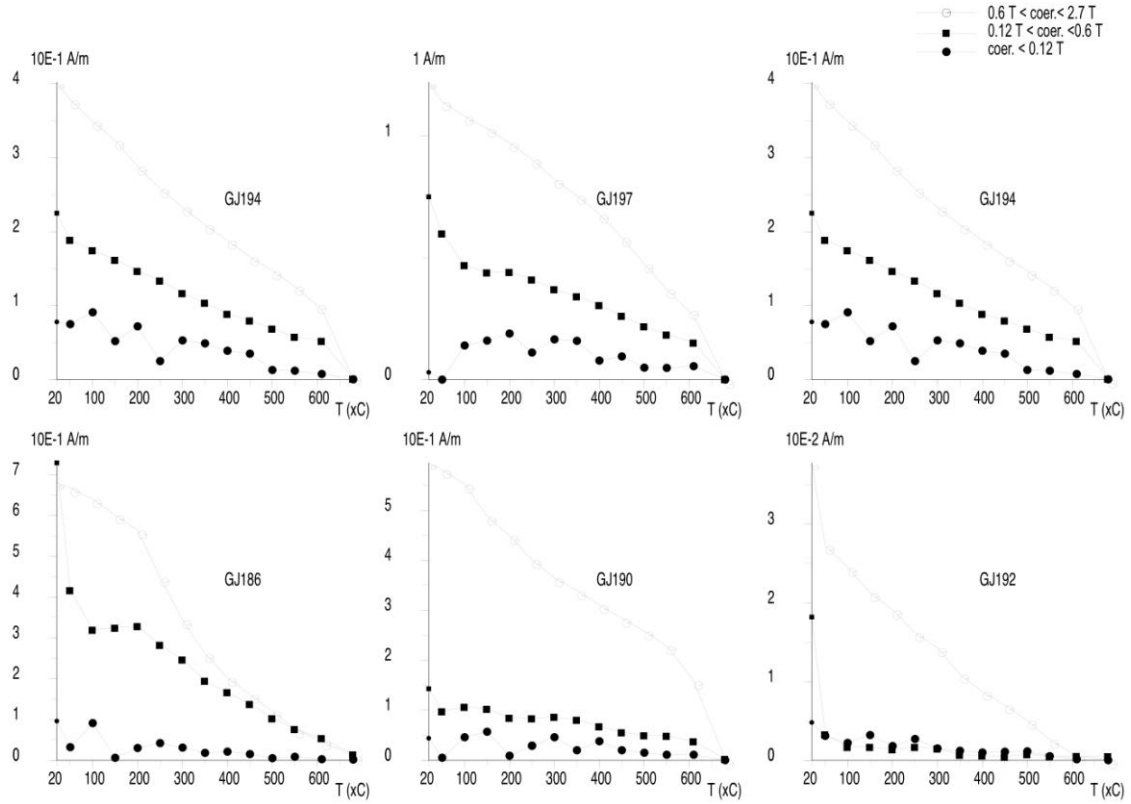

Figure 4. Thermal demagnetization of a three-component IRM according to the method of Lowrie (1990) for six representative specimens.

4.2 Paleomagnetism

Only 9 (out of 14) sites yielded reproducible paleomagnetic directions during cleaning, while the remaining 5 sites showed scattered demagnetization diagrams (Figure 5 and Table 1). Mean paleomagnetic directions are reasonably well constrained, the a95 values being comprised between 8.4° and 22.4° for all sites but one has a value of 48.2 (Fig. 6 and Table 1,). Three sites are of normal polarity (mean value) and the other six are of reverse polarity (mean value), the reversal test (according to McFadden and McElhinny

(1990), is positive of Class “c”.

Table 1. Paleomagnetic results

Paleomagnetic results from Bucaramanga Fan

Site	Member	Geographic coordinates		N/n	In Situ		k	α95 (º)
		Longitude ºW	Latitude ºN		D (º)	I (º)		
GJ186	Finos	73.132031	7.075061	10/8	179	13.4	7.8	21.2
GJ187	Finos	73.132031	7.075061	11/6	176.4	9.0	14.9	17.9
GJ188	Gravoso	73.143939	7.075496	12/0	-	-	-	-
GJ189	Organos	73.168091	7.036684	12/0	-	-	-	-
GJ190	Organos	73.174056	7.049284	11/9	353.5	4.0	9.1	18.0
GJ191	Organos	73.138192	7.067906	6/0	-			-
GJ192	Gravoso	73.132332	7.097189	12/5	176.7	9.2	12.6	22.4
GJ193	Organos	73.133936	7.090153	12/0	-	-	-	-
GJ194	Organos	73.138862	7.087891	11/0	-	-	-	-
GJ195	Organos	73.138862	7.087891	12/12	188.1	-19.0	12.8	12.6
GJ196	Organos	73.162533	7.088209	11/8	181.5	-0.6	11.6	18.5
GJ197	Organos	73.161192	7.101659	12/8	357.9	7.6	44.5	8.4
GJ198	Organos	73.165264	7.100704	12/8	356.9	16.7	13.4	15.7
GJ199	Organos	73.148797	7.066336	11/5	167.9	-1.3	3.5	48.2

The geographic coordinates are referred to WGS84 datum. Bedding is sub-horizontal. D and I are in situ declination and inclination; K and α95 are statistical parameters after Fisher (1953).

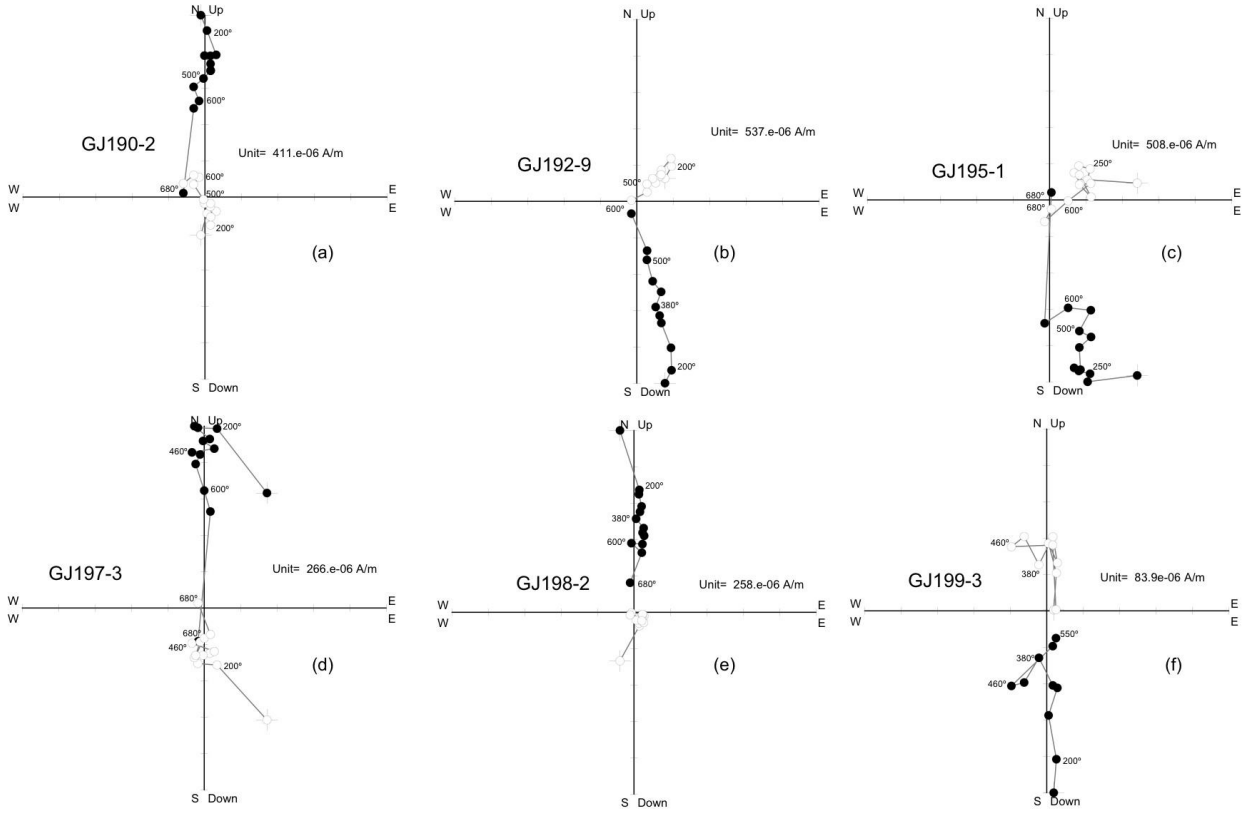

Figure 5. Orthogonal vector diagrams of typical demagnetization data, in situ coordinates. Solid and open dots represent projections on the horizontal and vertical planes, respectively. Demagnetization step values are in °C.

The fact that our results yielded reversal directions indicate that the Bucaramanga Fan should be older than the Bruhnhes polariry chron (0 to 0.8 Ma)

When plotted according to their stratigraphic position, the sites from the Bucaramanga Fan yield a succession of three normal- and three reverse-polarity magnetozones (Fig. 7).

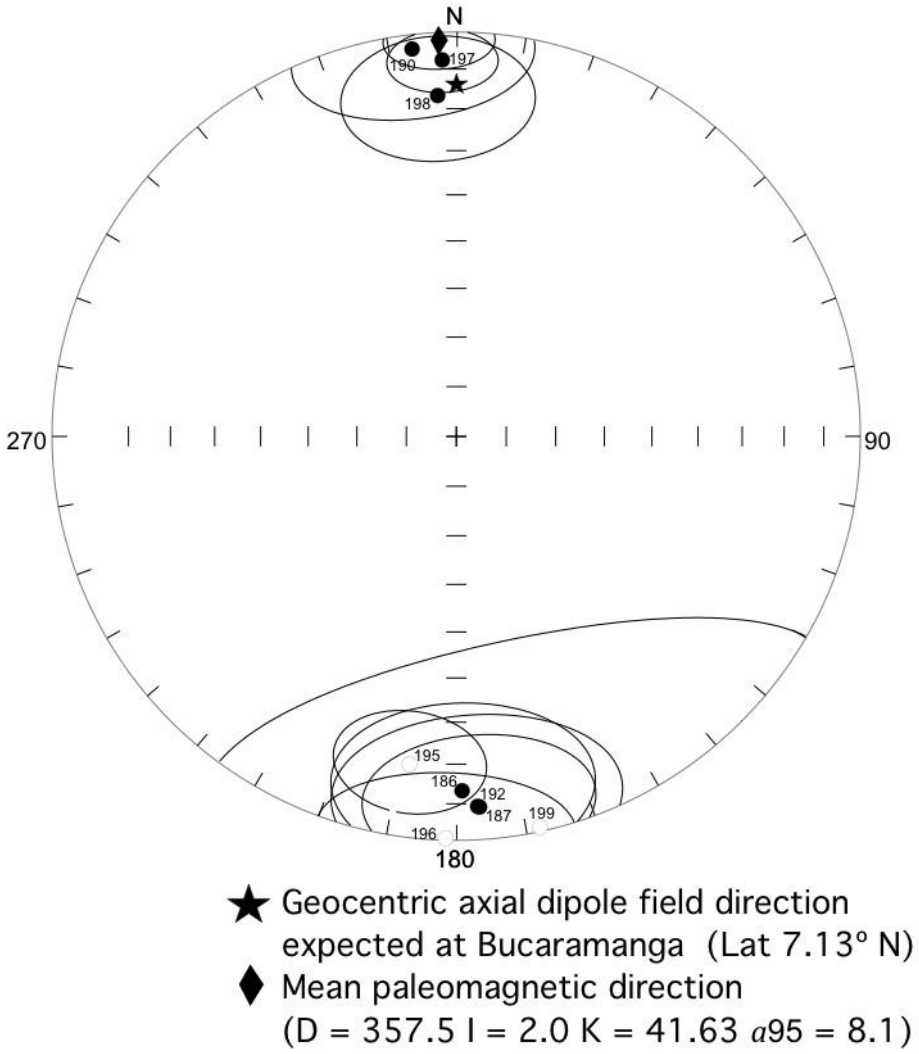

Figure 6. Equal-area projections of the site-mean paleomagnetic directions from the study area. Solid (open) symbols represent projection onto the lower (upper) hemisphere. Open ellipses are the projections of the a95 cones about the mean directions. The star represents the normal polarity geocentric axial dipole (GAD) field direction (D=0°, I=14°) calculated for the Bucaramanga latitude (7.1° N).

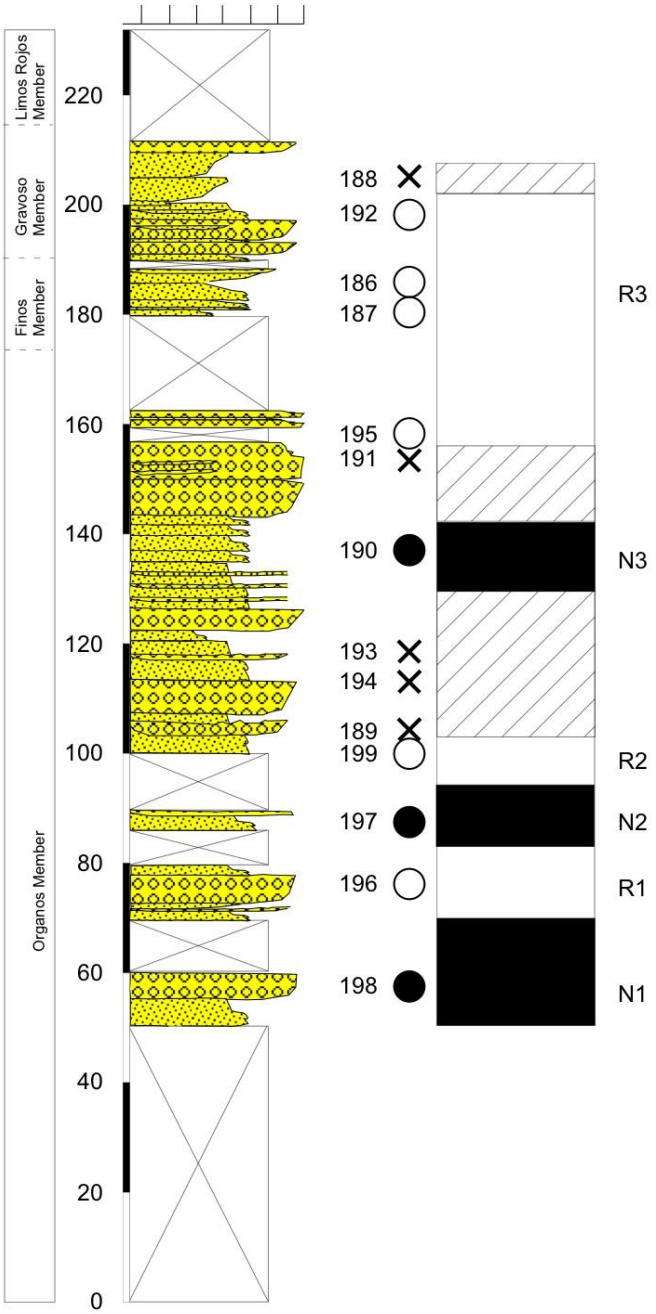

Figure 7. Stratigraphic column of the Bucaramanga Fan, and stratigraphic variation of magnetic polarity zones. Magnetic polarity zones are progressively numbered from the section bottom. Uncertain polarity intervals are grey and cross-hatched. The crosses indicate failed sites.

Each magnetozone is defined by one paleomagnetic direction, except the youngest magnetozone R3, which is corroborated by four different site results. As the age of the Bucaramanga Fan is vaguely inferred to be Plio-Pleistocene, several different correlations with the global magnetic polarity time scale (GPTS, Cande and Kent, 1995) are possible

(Fig. 8).

If we assign the youngest possible age to the succession (Fig. 8a), R3 correlates with upper Matuyama polarity chron C1r.1r, and N3, N2, and N1 with the Jaramillo, Olduvai, and Gauss chron, respectively. In a slightly older age model (Fig. 8b), R3 correlates with the mid Matuyama chron (C1r.2r), N3 with Olduvai chron, and N2 and N1 fall both within the Gauss chron. It is not possible at present to indicate a preferred age model using calculated sedimentation rates. In fact in this kind of deposits the sedimentation is expected to be highly irregular and discontinuous, and the thickness of some magnetozones (such as N3) is poorly constrained due to the occurrence of several failed sites located below and above it (Fig. 7). Hopefully, some further age constraints from the continental succession will enable in the future a safer match of our paleomagnetic data with the GPTS, and a careful age model for the Bucaramanga Fan.

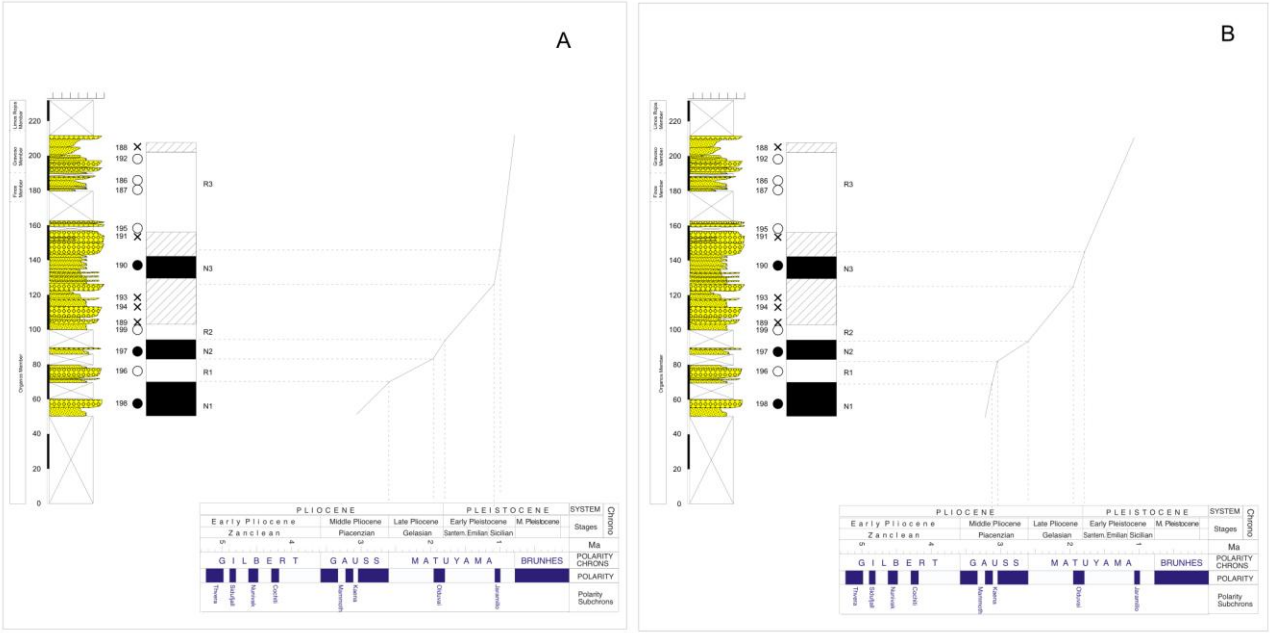

Figure 8. Stratigraphic distance versus age correlation plots. Magnetic polarity zones are correlated to polarity chrons from the GPTS (Cande and Kent, 1995). Sloping lines are average sediment accumulation rates. Two different possible correlations are shown (see text for explanation).

5.0 Discussion and Conclusions

The slip rate of the Bucaramanga fault can be in principle calculated by dividing its along-fault displacement by the age of the displaced rocks. Left-lateral displacement is well-known, and equates the 2.5 km distance from the mouth of the Suratá river to the apex of the Bucaramanga Fan (Figs. 9 and 10). Conversely, the age of the displaced sediments is not firmly constrained, as several different age models can equally fit the magnetozone succession gathered from the Bucaramanga Fan (Fig. 7).

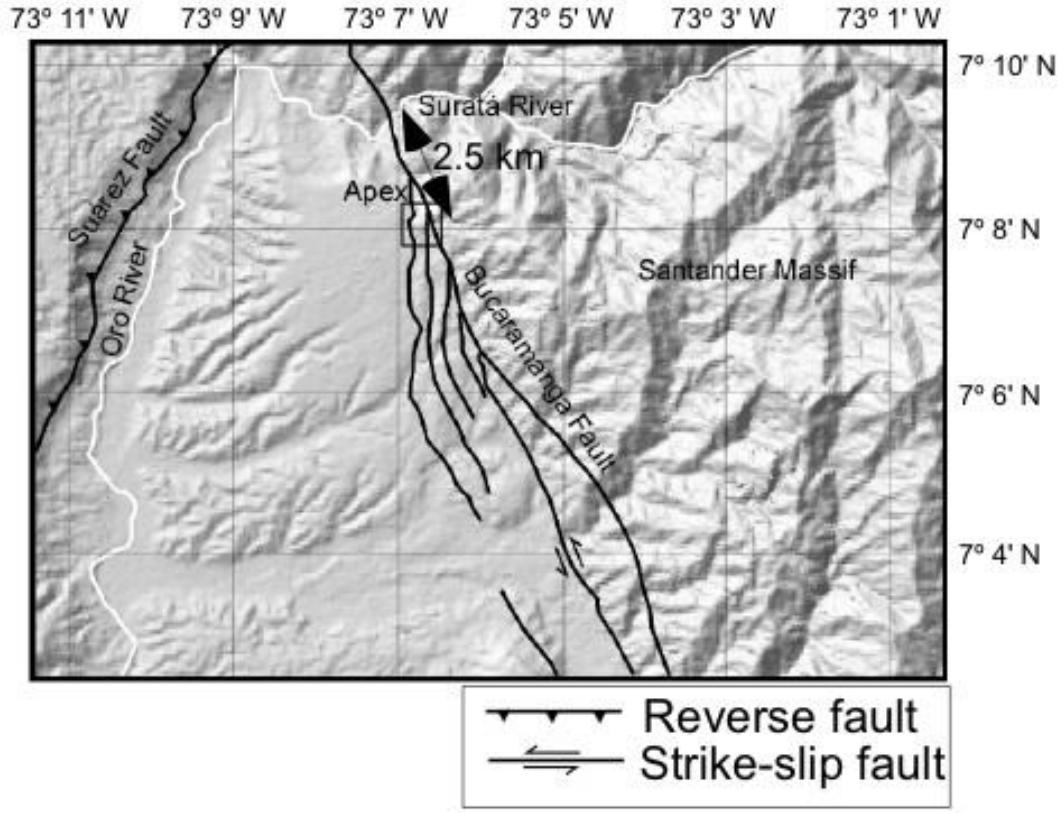

Figure 9. Geomorphological context of the zone, convergence between the Suárez and Bucaramanga faults. Details in locations and distance between the Bucaramanga Fan apex and the Suratá River (aprox 2.5 Km).

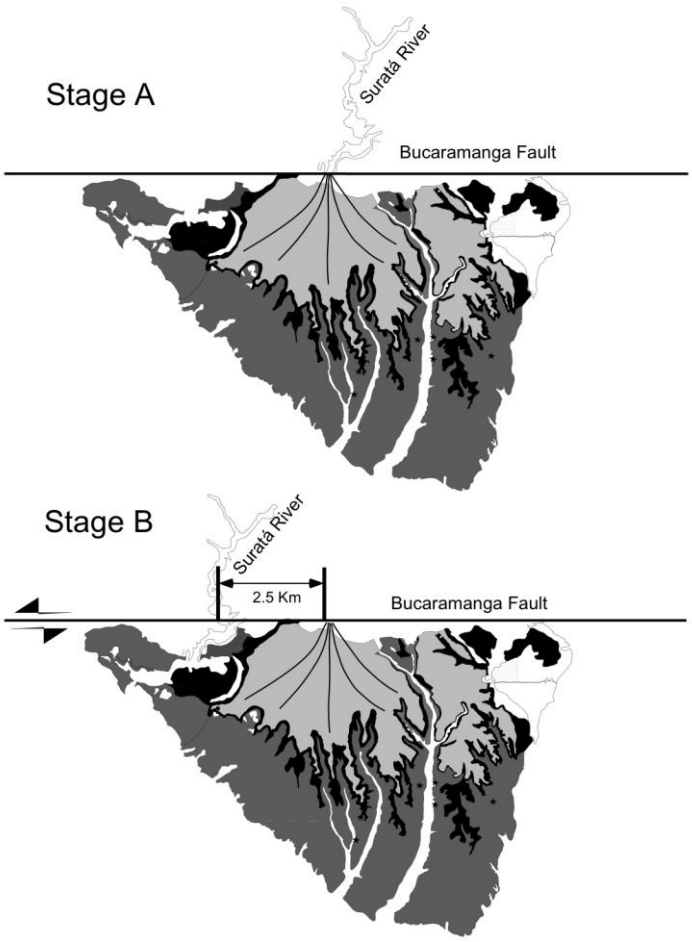

Figure 10. Scheme showing the displacement of the Bucaramanga Fan apex from its feeding Suratá River along the Bucaramanga Fault.

However, a maximum possible slip rate can be calculated assigning the youngest possible age of the succession, i.e. inferring that magnetozone R3 corresponds to the top of the Matuyama polarity chron (Fig. 8a). In this case, a 0.8 Ma age (Brunhes-Matuyama boundary, Cande and Kent, 1995) can be reasonably assigned to the youngest sediments of the Bucaramanga Fan, by considering that: 1) we did not reach the normal-polarity magnetozone above R3, thus the youngest sampled sediments (site GJ192) might fall in the lower-medium part of chron C1r.1r, and be 0.9-1 Ma old; 2) the upper member of the Bucaramanga Fan is the Limos Rojos Member, but the youngest paleomagnetic directions were obtained in the underlying Gravoso Member; 3) the Limos Rojos Member is only 15 m thick, and shares the same fan morphology with the underlying Finos-Gravoso members

(Fig. 2). This suggests that the Limos Rojos Member was rapidly emplaced, and that no significant time gap (and displacement of the fan feeding source) occurred with respect to the Gravoso Member.

A 0.8 Ma age of the top of the Bucaramanga Fan translates into a maximum slip rate of 3 mm/yr for the Bucaramanga Fault. Obviously, progressively smaller slip rates would arise by considering progressively older age models for the Bucaramanga Fan. Our slip rate estimate is in rough agreement with conclusions by Diedrix et al. (2009), who documented by paleosismology eight main earthquakes in the last 8300 years, with 400 to 1300 years recurrence intervals, and estimated magnitude values of 6.5 to 7.0. Average recurrence interval documented by Diedrix et al. (2009) is 1000 years, which would translate into an accumulated displacement of 3 m, if our 3 mm/yr spreading rate is considered. A 3 m displacement along a seismogenic fault is expected to be associated with 7-7.5 M earthquakes (Wells and Coppersmith, 1994), slightly greater than Diederix et al. (2009) estimates. We note however that older age models for the Bucaramanga Fan would give smaller slip rates, thus better agreement with Diedrix et al. (2009) calculated values. Considering that the Bucaramanga town has a documented history of 390 years without any catastrophic earthquake occurrence, a minimum 1.2 m displacement has been accumulated since then, when the 3 mm/yr slip rate is considered.

Sediments of the Bucaramanga Fan have been clearly displaced by left-lateral fault shear, thus counterclockwise rotations are expected at fault walls, as already observed in several strike-slip fault settings (Sonder et al., 1994; Kimura et al., 2011). On the other hand, our sites from the Bucaramanga Fan, located at 4-10 km from the fault, do not show significant rotations (Fig. 6).

Using the power law rheology model (England et al., 1985), in which the relation between distance from a fault trace y (km) and vertical-axis relative rotation θ (rad.) is expressed as:

$$\theta = \arctan\left(\left(\left(4Ds\pi\sqrt{n}\right)/L\right)\exp\left(\left(-4\pi\sqrt{n}y\right)L\right)\right)$$

Ds (km) is the displacement in one side of the fault, L/2 (km) is the length of the fault, and n is the stress exponent and describes the average mechanical behavior of the lithosphere (Sonder and England, 1986). Clearly, the lack of observed rotations may imply that 1) fault locking is extremely weak, whereas fault walls are extremely rigid and undergo minimal internal deformation, and/or 2) the upper crust west of the Bucaramanga Fault has a ductile behavior. Additional geophysical data (e.g. a dense GPS network) would be needed to fully understand this issue, and better constrain the seismic hazard assessment related to the Bucaramanga Fault activity.

References

Ayala-Calvo, C., G. Bayona, A. Cardona, C. Ojeda, O. Montenegro, C. Montes, V. Valencia and C. Jaramillo (2012), The Paleogene synorogenic succession in the northwestern Maracaibo block: Tracking intraplate uplifts and changes in sediment- delivery systems. Submitted to Journal of South America Earth Sciences, Special Edition on Tectonic and climatic shaping of the northern Andes and southern Caribbean margin.

Bayona, G., Jimenez, G., Silva, C., Cardona, A., Montes, C., Roncancio, J., and U. Cordani (2010), Paleomagnetic data and K.Ar ages from Mesozoic units of the Santa Marta Massif: A preliminary interpretation for block rotations and translations: Journal of South American Earth Sciences, v. 29, p. 817-831.

Bueno. E and A. Solarte (1994), Geología, Geotecnia y Comportamiento Erosivo del Área de Reserva Forestal de Bucaramanga. Tesis para optar al título de Geólogo. Escuela de Geología, UIS, Bucaramanga.

Cande, S.C. and D.V. Kent (1995), Revised calibration of the geomagnetic polarity timescale for the late Cretaceous and Cenozoic. Journal Geophys. Res., 100, 6,093-6,095.

Campbell, C. J (1965), The Santa Marta wrench fault of Colombia and its regional setting. Fourth Caribbean Geological Conference. Memoir: 247-261. Trinidad.

Cediel, F., R. Shaw, and C. Cáceres (2003), Tectonic assembly of the northern Andean Block, in Bartolini, C., Buffler, R. T., and Blickwede, J., eds., The Circum-Gulf of Mexico and the Caribbean: Hydrocarbon habitats, basin formation and plate tectonics, American Association of Petrolum Geologists Memoir 79, p. 815-848.

Diederix. H, C. Hernandez, M. T. Eliana, J. A. Osorio, P. Botero (2009), Memorias Congreso Colombiano de Geología, Paipa- Boyaca´. Resultados preliminares del primer estudio paleosismológico a lo largo de la falla de Bucaramanga.

England. P, G. Houseman and L. Sonder (1985), Length scales for continental deformation

in convergent, divergent, and strike–slip environments: analytical and approxi- mate solutions for a thin viscous sheet model. J. Geophys. Res. 90, 3551–3557.

Fisher, R. A (1953), Dispersion on a sphere, Proc. R.Soc. London, 217, 295–305.

Flinch, J.F. (2003), Structural evolution of the Sinu-Lower Magdalena area(Northern Colombia), in Bartolini, C., Buffler, R., and Blickwede, J., eds., The Circum-Gulf of Mexico and the Caribbean: Hydrocarbon Habitats, Basin Formation and Plate Tectonics, American Association of Petroleum Geologists Memoir 79, p. 776-796.

Hubach. E (1952), Interpretación Geológica de la erosión y de los deslizamientos en Bucaramanga y medidas de defensa, Serv. Geol. Nal. Bogotá. Informe 867 (inédito), 2-4.

Ingeominas (2008), Modelo de evolución morfotectónica cuaternaria basado en evidencias estructurales, neotectónicas y paleosismológicas de los principales sistemas de falla en la región de Bucaramanga. Diederix. H, Torres. E. M, Hernández. C and Botero. P. A. Bogotá

Ingeominas (2001a), Base de datos de fallas activas. Recopilación Bibliográfica. Proyecto Compilación y Levantamiento de la Información Geodinámica, Montes N., Sandoval A., Bogotá.

Ingeominas (2001b), Zonificación Sismo Geotécnica Indicativa del Área Metropolitana de Bucaramanga, Fase II. Convenio realizado entre la CDMB e Ingeominas, Bucaramanga.

Irving. E. M (1971), La evolución estructural de los Andes mas septentrionales de Colombia. Boletín Geológico, Ingeominas, Bogotá. 19 (2), 1-90

Julivert. M (1963), Nuevas observaciones sobre la estratigrafía y tectónica del Cuaternario de los alrededores de Bucaramanga. UIS. Bol. de Geología No. 15. p.p: 41-56, Bucaramanga.

Julivert. M (1968), Lexique Stratigraphyque International Amerique Latine Colombia

(Premiere Partie). Centre National de la Recherche Scientifique. 5, (4a). París. p.p:1-651.

Kammer, A., and J. Sanchez (2006), Early Jurassic rift structures associated with the Soapaga and Boyacá faults of the Eastern Cordillera, Colombia: Sedimentological inferences and regional implications: Journal of South American Earth Sciences, v. 21, p. 412-422.

Kellogg. J. N and W. E. Bonini (1982), Subduction of the Caribbean Plate and basement uplifts in the over- riding South American Plate: Tectonics, v. 1, no. 3, p. 251–276.

Kimura, H. N. Ishikawa, and H. Sato (2011), Estimation of total lateral displacement including strike-slip offset and broader drag deformation on an active fault; tectonic geomorphic and paleomagnetic evidence on the Tanna fault zone in central Japan Tectonophysics, 501(1-4):87-97 doi: 10.1016/j.tecto.2011.01.016

Kirschvink, J. L (1980), The least-squares line and plane and the analysis of paleomagnetic data, Geo- phys. J. R. Astron. Soc., 62, 699–718.

López. J. A, M. A. Cuéllar, J. A Osorio, L. E. Bernal and E. Cortés (2008), Pseudotaquilitas y el carácter paleosísmico de un segmento del Sistema de Fallas de Bucaramanga (SFB), noreste del Muncipio de Pailitas, Departamento del Cesar, Colombia. Boletín de Geología, Bucaramanga. 30 (2), 79-92.

Lowrie, W (1990), Identification of ferromagnetic minerals in a rock by coercivity and unblocking temperature properties, Geophys. Res. Lett., 17, 159 – 162.

Marcera. M and P. Salamanca (1993), Cartografía geológica y estratigráfica a detalle y Zonificación geotécnica del sector oriental del Área Metropolitana de Bucaramanga. Tesis para optar al título de Geólogo. Escuela de Geología, UIS, Bucaramanga.

McFadden, P. L., and M. W. McElhinny (1990), Classification of the reversal test in paleomagnetism, Geophys. J. Int., 103, 725–729.

Montes, C., Guzman, G., Bayona, G., Cardona, A., Valencia, V., and C. Jaramillo (2010),

Clockwise Rotation of the Santa Marta Massif and Simultaneous Paleogene to Neogene Deformation of the Plato-San Jorge and Cesar-Ranchería Basins: Journal of South American Earth Sciences, v. 29, p. 832-848.

Mora. A and Garcia. A (2006), Cenozoic Tectono-Stratigraphic Relationships between the Cesar Sub-Basin and the Southeastern Lower Magdalena Valley Basin of Northern Colombia. AAPG 2006 Annual Convention. Houston, Texas.

Parra, M., Mora, A., Lopez, C., Rojas, L.E., and K.B. Horton (2012), Detecting earliest shortening and deformation advance in thrust-belt hinterlands: Example from the Colombian Andes: Geology, v. 40, p. 175-178.

París, G. M, Machette. R, Dart and K. Haller (2000). Map and Database of Quaternary Faults and Folds in Colombia and its Offshore Regions. U.S. Department of the Interior U.S. Geological Survey. 66 p.

Pindell, J. L., S. C. Cande, W. C. Pitman III, D. B. Rowley, J. F. Dewey, J. LaBrecque, and W. Haxby (1988), Plate- kinematic framework for models of Caribbean evolution: Tectonophysics, v. 155, p. 121–138.

Prieto. G. A, Gregory C. Beroza . G. Cb, Barrett. S. A, López. G.A and M. Florez (2012), Earthquake nests as natural laboratories for the study of intermediate-depth earthquake mechanics. Tectonophysics 570-571, 42–56

Rivera. L. A (1989), Inversion du Tenseur des Contraintes et des Mechanismes au Foyer a partir des Donnees de Polarite pour une Population de Seismes: Applicaton a l'Etude du Foyer de Sismicite Intermediaire de Bucaramanga (Colombie): Doctoral Thesis, Universite de Strasbourg, France, 266 p.

Ross, I., P. Parra, C. Mora and C. Pimentel (2009), AFTA apatite fission track analysis constraints on the Mesozoic to Quaternary thermal and tectonic evolution of the Middle Magdalena Basin and Santander Massif, Eastern Cordillera, Bucaramanga area, Colombia. X Simposio Bolivariano: Exploración Petrolera en Cuencas

Subandinas. Cartagena, Colombia. Memoir.

Servivio Geólogico Nacional (1977), Mapa Geológico Del Cuadrángulo H-12, Bucaramanga. Escala 1:100.000. Bogotá.

Schneider, J., Pennington, W., Meyer, R., 1987. Microseismicity and focal mechanisms of the intermediate depth Bucaramanga nest, Colombia. J. Geophys. Res. 92, 13913–13926.

Sonder. L and P. England (1986), Vertical averages of rheology of the continental lithosphere: relation to thin sheet parameters. Earth Planet. Sci. Lett. 77, 81–90.

Sonder. L, J. Jones, C.H. Salyards, S.L and K. M. Murphy (1994), Vertical axis rotation in the Las Vegas Valley shear zone, southern Nevada: paleomagnetic constraints on kinematics and dynamics of block rotations. Tectonics 13, 769–788.

Taboada, A., L. A. Rivera, A. Fuenzalida, A. Cisternas, H. Philip, A. Bijwaard, J. Olaya, and C. Rivera (2000), Geodynamics of the northern Andes: Sub- ductions and intracontinental deformation (Colombia), Tectonics, 19, 787–813.

Toro, J. (1990), The termination of the Bucaramanga Fault in the Cordillera Oriental, Colombia: Masters Thesis, University of Arizona, Department of Geosciences, Tucson: 60.

Trenkamp, R., J. N. Kellogg, J. T. Freymueller, and H. P. Mora (2002), Wide plate deformation, south- ern Central America and northwestern South America, CASA GPS observations, J. S. Am. Earth Sci., 15, 157–171.

Tschanz. C, R. Marvin, J. Cruz, H. Mennert, and E. Cebula (1974), Geologic evolution of the Sierra Nevada De Santa Marta. Geol. Soc. Am. Bull., 85, 269-276.

Ujueta. G (2003), La Falla de Santa Marta-Bucaramanga no es una sola falla; son dos fallas diferentes: La Falla de Santa Marta y la Falla de Bucaramanga: Geología Colombiana No. 28, Universidad Nacional de Colombia, Bogotá.

Vargas, A., G and A. Niño (1992), Patrones de fracturamiento asociados a la Falla

Bucaramanga. Tesis, Universidad Industrial de Santander, Bucaramanga.

Ward, D., Goldsmith, R., Cruz, J., and H. Restrepo (1973), Geología de los Cuadrángulos H-12, Bucaramanga y H-13, Pamplona, Departamento de Santander, Boletín Geológico Ingeominas 21(1-3), 132 p.

Wells, D.L and K. J. Coppersmith (1994), New Empirical Relationships among Magnitude, Rupture Length, Rupture Width, Rupture Area, and Surface Displacement. Bulletin of the Seismological Society of America, Vol. 84, No. 4, pp. 974-1002

Zijderveld, J. D. A (1967), A.C. demagnetization of rocks: Analysis of results, in Methods in Palaeomagnetism, edited by D. W. Collinson, K. M. Creer, and S. K. Runcorn, pp. 254–286, Elsevier, New York.

Zarifi, Z, and J. Havskov (2003), Characteristics of dense nests of deep and intermediate-depth seismicity. Adv. Geophys. 46, 237–278.

Zarifi. Z, J. Havskov and A. Hanyga (2007), An insight into the Bucaramanga nest Tectonophysics 443, 93–10

Chapter 4

Emplacement of the Paleocene-Eocene Santa Marta Batholith (Santa Marta Massif-Northern Colombia): Constraining the Cenozoic tectonic evolution of the Caribbean arc.

1.0 Introduction

Mesozoic metamorphic rocks, Paleogene intrusives and Cenozoic sedimentary basins record the different stages of subduction evolution or arc-continent collision between the Caribbean plate and the NW margin South American plate (Sisson et al., 1997; Smith et al., 1999; Pindell et al., 1988, 2005, 2006, Weber et al., 2010). Evidences of this interaction are the Santa Marta Massif and surrounded areas. The Santa Marta Massif is an isolated and uplifted block of pre Cambrian and Mesozoic crystalline rocks with a mountain peak at 5800 m above sea level. The Santa Marta Massif has similar lithologies to those that crop-out in the Central Cordillera of Colombia (Villagomez, 2010). The Santa Marta Massif is limited by two major wrench fault Systems, northern the right-lateral Oca Fault displaces the continental Guajira block during the Cenozoic (Macellari, 1995; Cardona et al., 2009). Western the left-lateral Santa Marta-Bucaramanga Fault limits and separates the crystalline rocks of the Santa Marta Massif from the sedimentary Lower Magdalena Basin (Schantz et al, 1969, Ingeominas, 2007a; Ingeominas 2007b and Montes et al., 2010) (Fig 1). The Cesar lineament is the southeastern limit of the Santa Marta Massif, were the Cesar-Rancheria basin is exposed (Bayona et al., 2007). The Northwest margin of the Santa Marta Massif is composed by Late Cretaceous metamorphous rocks (Tschanz et al., 1969, 1974; Doolan, 1970, Cardona et al., 2010a) an divided into four units, Rodadero, Cinto, Punta Betin and Concha (Doolan, 1970, Bustamante et al., 2009, Cardona et al., 2010a), intruded by Paleogene granitic rocks (Cardona, et al. 2009, 2010a, 2010b and Duque, 2009).

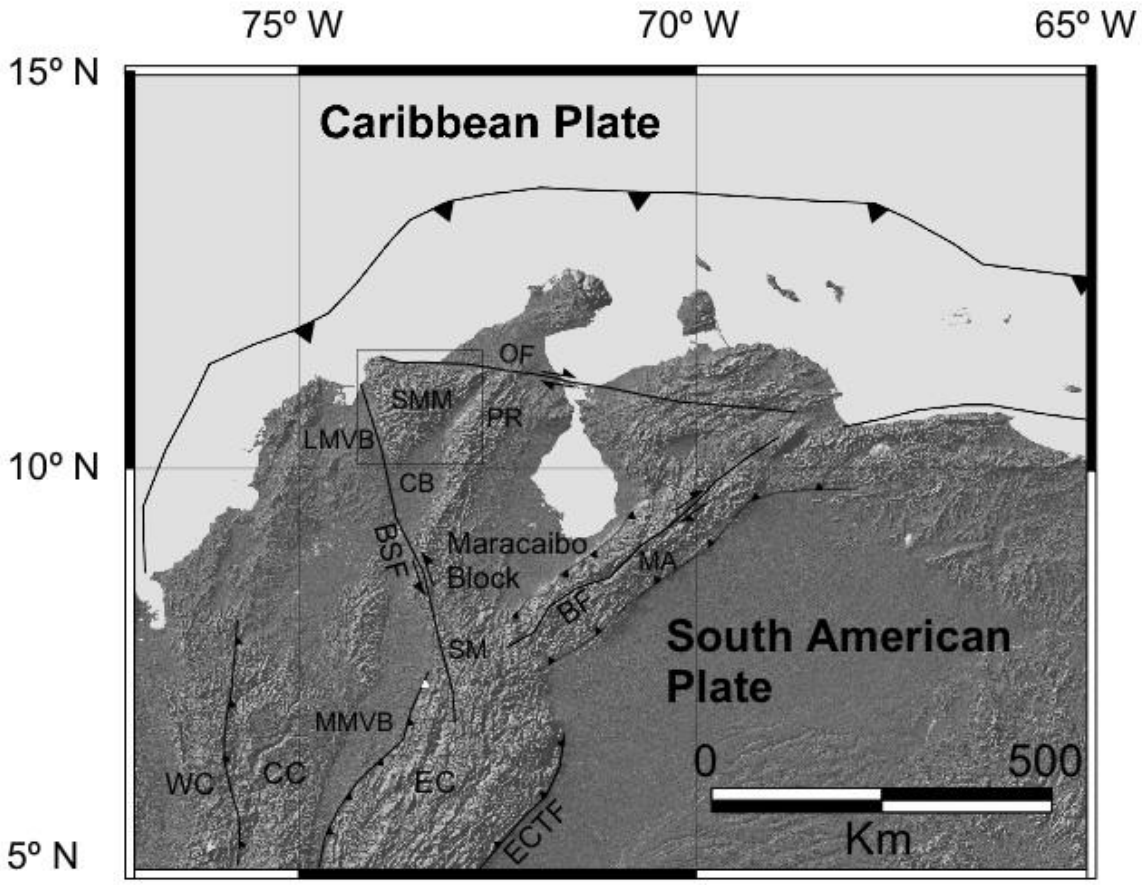

Figure 1. Major tectonic and structural features of the NW margin of South America. WC = Western Cordillera, CC = Central Cordillera, EC = Eastern Cordillera, SM = Santander Massif, SSM = Santa Marta Massif, PR = Perijá Range, MA = Merida Andes, ECTF = Eastern Cordillera thrust front, CB = Cesar Basin, LMVB = Lower Magdalena Valley Basin, MMVB = Middle Magdalena Valley Basin, BSF = Bucaramanga-Santa Marta Fault, OF = Oca Fault, BF = Boconó Fault.

The metamorphic sequence is related to volcanic-sedimentary protolite with an oceanic and continental affinity and variations from green schits facies to high anfibilite facies. (Bustamante et al, 2009) propose a metamorphism related to a collisional setting, and report P-T conditions for the Punta Betin and Concha units, between 3 to 5 Kbar and temperatures range from 300-500 ºC. For the Rodadero unit, the P-T conditions are between 7,6 to 9,5 Kbar and temperatures range from 565 to 665 ºC. According to (Duque, 2009), the arc-related granitoids are an extensive magmatic body composed by granodiorites and tonalites rocks with almost three different magmatic facies. The

magmatism takes place in 8 Ma, between 50-58 Ma into two major phases; At 55 Ma and 50 Ma, with a magmatic migration to NE (Duque, 2009). Cardona et al, (2011) propose for the Eocene granitoids, pressures between 4.9±0.6kbar and 6.4±0.6kbar with at least, 14.7-19.2 km of unroofing took place since 56-50Ma in the northwestern Santa Marta Massif. As well as propose three exhumation phases, the Late Eocene (ca. 45-40Ma), Late Oligocene (ca. 25Ma) and Miocene (ca. 15Ma), Villagomez et al., (2011), report for the NW belt an exhumation phases during 30-25 Ma and 25-16 Ma. The Paleogene magmatism in the Santa Marta Massif has been studied for detail mapping, geochonology, AFT, petrography and geochemistry data in previous works (Stchanz, 1969, Bustamante, et al, 2009, Cardona et al, 2009, 2010a, 2010b, Duque, 2009, Ingeominas, 2007a, 2007b and Villagomez et al., 2011). Montes et al., (2009), propose a translation- and vertical-axis clockwise rotation model for the Santa Marta Massif, starting during the Late Eocene. This model explains the opening at western of the Santa Marta Massif into the Lower Magdalena Valley (Plato-San Jorge Basin), the shortening into the Cesar-Rancheria and displacements of Santa Marta and Oca faults.

We report new Anisotropy of magnetic susceptibility (AMS) in Paleogene granitoids and structural data around the Oca and Santa Marta faults systems, showing ductile to brittle deformation and a reologic profile for metamorphic and intrusive rocks in the NW margin of the Santa Marta Massif. The goal of this work is propose a tectonic model for Paleogene-Eocene magmatic intrusions in the NW accreted belt of the Santa Marta Massif, integrating the available works and our new AMS and structural data.

2.0 Geological framework

Ages and lithologies let to divide the Santa Marta Massif into three tectonostratigraphic belts (Tschanz et al. 1969; 1974, Ingeominas, 2007a, 2007b; Villagomez et al., 2011 and Cardona et al. 2008a, 2010a, 2010b) (Fig. 2). At the southeastern zone of the Santa Marta

Massif crops out the first belt named Sierra Nevada Province (Tschanz, 1969; Villagomez et al., 2011). The Sierra Nevada Province is composed by the Proterozoic granulites, anorthosites and gneisses (Cordani et al., 2005; Cardona et al., 2006), intruded by Jurassic granites (Fig. 2). The Sierra Nevada Province is related to the Grenvillian province and could be correlated with rocks of the Garzón and Santander Massifs (Restrepo-Pace et al, 1997, Ordoñez-Carmona et al., 2006) (Fig. 2). The second belt, named Sevilla Province, located in the northwestern margin of the Santa Mart Massif. The Sevilla Province is composed of Paleozoic orthogneisses and schists, intruded by Permian to Late Triassic syntectonic granitoids (Cardona et al., 2006) and the Paleogene Buritaca granite (Tschanz et al., 1974; Ingeominas, 2007a). The Sevilla Province is correlated with the Macuira Schist Belt in the Guajira Peninsula (Cardona et al., 2006) (Fig. 2). The third belt named the Santa Marta Province is composed by Upper Cretaceous low-grade metamorphic rocks and is exposed in two bands, the inner-eastern band and the outer-western band, (Tschanz et al., 1974) (Fig. 2). The Santa Marta Province is overthrusted by the Sevilla Province and intruded by Paleogene granitoids called the Santa Marta Batholith (Fig. 2).

According to Cardona, et al (2010b) the trace element of the Santa Marta province are characterized by primitive island arc and MORB, with protoliths formed within a back-arc setting or at the transition between the intra-oceanic arc and the Caribbean oceanic crust. In samples of the inner band, Zuluaga and Stowell (2012) report a pressure increase of 1.5 kb and propose a subduction setting for the metamorphism.

Ages for the Santa Marta Batholith are reported in K/Ar of 58–44 Ma, (Tschanz et al., 1974) and in zircon U–Pb ages of 57-50 Ma, (Cardona et al., 2008). Cardona et al., (2010b) report in U-Pb ages, two major peaks of magmatic activity, at 65 Ma and 58–50

Ma.

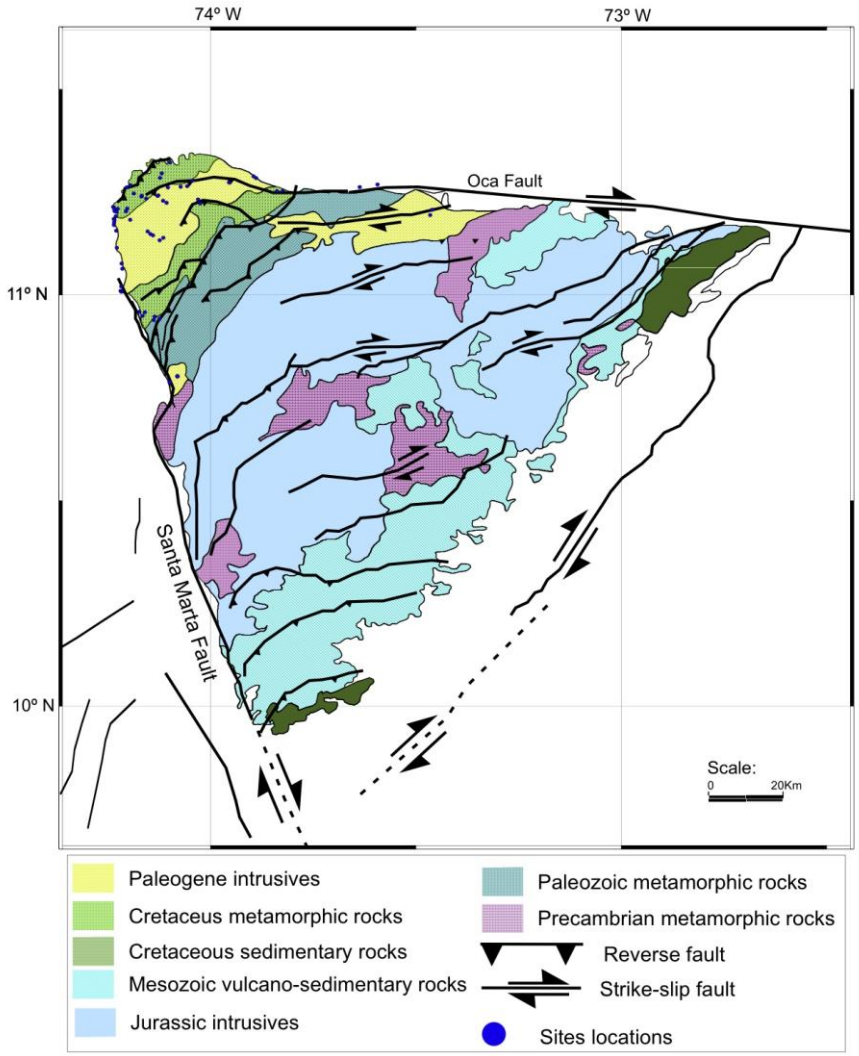

Figure 2. Geological map of the Santa Marta Massif and adjacent zones, (see Figure 1 for location). Sites sampled locations for AMS, structural data and control points.

Villagomez et al (2011), using AFT analyses report four pulses and exhumation rates, the Sierra Nevada Province exhumed at elevated rates (≥0.2 Km/My) during 65-58 Ma with second pulse of exhumation (≥0.32 Km/My) during 50-40 Ma. At 40-25 Ma (≥0.15 Km/My) proximal to the Santa Marta–Bucaramanga Fault. The northern regions of the Sierra Nevada Province exhumed rapidly during 26-29 Ma (~0.7 Km/My). The Santa Marta Province is exhumed during 30-25 Ma and 25-16 Ma. According to Villagomez et al (2011), after 16 Ma the exhumation is not-recorded. Clockwise rotations (17º±13°C) and latitude translations are reported in Middle–Late Jurassic and Early Cretaceous rocks (Bayona et

al., 2006, 2010), Montes et al. (2009) propose 30º clockwise rotations in the Santa Marta Massif and suggest that it´s an rigid block migrating, this block rotation-translation model is propose to explain contemporary extension, shortening and wrench displacements in basins and margins adjacent to Santa Marta Massif.

Vertical displacement of ~12 km over a lateral distance of ~50 km is proposed by (Cediel et al. 2003). Elevation and relief is testament to extensive surface and rock-uplift, which was probably driven by dextral and sinistral displacements of 50-100 km (Tschanz et al., 1974) along the Oca and Santa Marta faults. High positive gravity anomaly (+180 mGal) is reported for the Santa Marta Massif, which suggests that the summit is not isostatically compensated but is flexurally supported in place by the subducting slab (Kellogg and Bonini, 1982).

3.0 Sampling strategy and Methods

Fieldwork was carried out around of Santa Marta, El Rodadero town and Tayrona Park covering the northern and western margins of the Santa Marta Massif, in the interactions between the Santa Marta and Oca faults (Figure 1 and 2). The sampling and measures were focus on Upper Cretaceous metamorphic and Paleogene granitic rocks. Detail works and descriptions in Paleogene plutonic rocks (Duque, 2009), reports compositions of amphibole (90%) with plagioclase and dark minerals, locally, in the Latal plutonic body there are clinopiroxenes and olivine. According to Duque (2009), Late Paleocene to Early Eocene magmatic rocks are represented by the Santa Marta Batholith and related rocks as Buritaca, Toribio and Latal plutonic bodies. The magmatic body has a homogeneous composition from tonalite to granodiorite. (Duque, 2009) propose for the Santa Marta Batholith, a calcium-alkaline magmatic composition, with variations in SiO2, from 47 to 75

% in weight and identify three main groups 1) rocks with low silica values (47 a 57 % in weight), 2) Medium silica values from (57 a 70 % in weight), composed by tonalites and granodiorites and the third (>70 % in weight) related to late dikes.

We collected Late Paleocene to Early Eocene granodiorites rocks in 25 localities (312 cores), using a petrol-powered portable drill cooled by water for AMS analyses. At each site we collected 9–19 cores (13 on average). All samples were oriented in situ using a magnetic compass, corrected to account for the local magnetic field declination value at the sampling area (from -8° during 2011 according to NOAA's National Geophysical Data Center, http://www.ngdc.noaa.gov). Cores were cut into standard cylindrical specimens of 22 mm height, and magnetic fabric were done in the shielded room of the paleomagnetic laboratory of the Istituto Nazionale di Geofisica e Vulcanologia (Roma, Italy). We measured the low-field anisotropy of magnetic susceptibility (AMS) of a specimen per core by a spinner Multi-Function Kappabridge (MFK1-FA, AGICO) using the spinning method. For each sample the measurements allowed to reconstruct the AMS tensor, defined by three eigenvalues (i.e. the maximum, intermediate and minimum susceptibilities) indicated as kmax ≥ kint ≥ kmin (or k1≥ k2≥ k3). The AMS parameters at both the specimen and the site levels were evaluated using Jelinek statistics (Jelinek, 1977, 1978).

We measured striated fault planes and if present, the relative kinematic indicators, from late Cretaceous schist and Paleogene granitoids, around the Oca and Santa Marta faults. For each fault plane we recorded the dip and strike, the direction and pitch of the slickensides, and the sense of slip (if recognizable). As well as we measured the foliation and lineations in Cretaceous schits and locally in Paleozoic rocks. We measured and combined data in order to obtain a significant foliation and/or fault population. Results of fault planes and the relative slickensides were plotted using the free software Faultkin 5.2. Results of foliation-lineation were plotted using the free software Stereonet 7. All data were plotted in the Schmidt's lower hemisphere equal-area projection.

4.0 Results

4. 1Anisotropy of magnetic susceptibility

Using a 20° as cut-off value of the e12 angle (semi-angle of the 95% confidence ellipse around the mean Kmax axis in the Kmax-Kint plane and the Kmin axis in the Kmin-Kint plane), we find that 21 out of 25 sites gave interpretable AMS results (Fig. 3 and Table 1), while 4 did not give a clear magnetic fabric, AMS parameters are reported in Table 1. In the 15 interpretable sites, the site-mean susceptibility values have a range from 1.39 × 10-2 to 3.23 × 10-5 SI. The shape of the AMS ellipsoid in twelve sites is oblate, with range values of the shape factor (T) of between (0.233 to 0.942).

Table 1. Anisotropy of magnetic susceptibility results from Santa Marta Massif

Anisotropy of magnetic susceptibility results from Santa Marta Massif

Site	Formation	Longitude ºW	Latitude ºN	n/N	Km	Km	L	F	T	P'	D (º)	I (º)	e12 (º)
GJ204*	INTRUSIVE	-74.228395	11.124156	9/9	2.4E-4	2.4E-4	1.007	1.037	0.697	1.047	153	25.1	40.5
GJ205	INTRUSIVE	-74.230891	11.166817	11/9	3.06E-4	3.06E-4	1.019	1.033	0.281	1.053	208.1	21.3	19
GJ208	INTRUSIVE	-74.104205	11.264577	10/7	5.62E-3	0.562E-4	1.095	1.157	0.235	1.269	79.5	66.4	6.2
GJ212	INTRUSIVE	-73.95697	11.281796	12/10	1.07E-3	0.107E-4	1.022	1.062	0.466	1.088	195.3	30.8	16.3
GJ228*	INTRUSIVE	-74.061963	11.271157	12/12	2.02E-2	0.0202E-4	1.020	1.112	0.685	1.146	180.5	15.6	58.2
GJ229	INTRUSIVE	-73.465565	11.20955	12/11	3.03E-4	3.03E-4	1.065	1.025	-0.442	1.094	125.6	12.2	8.2
GJ230	INTRUSIVE	-73.464677	11.207925	12/10	2.48E-3	0.248E-4	1.022	1.052	0.394	1.078	180.4	35.5	17.2
GJ231*	INTRUSIVE	-74.115632	11.236651	14/14	3.14E-4	3.14E-4	1.006	1.008	0.155	1.014	173.4	35.2	50.6
GJ233	INTRUSIVE	-74.123771	11.142733	16/14	1.95E-3	0.195E-4	1.060	1.133	0.336	1.206	206.6	79.1	17.6
GJ234*	INTRUSIVE	-74.120839	11.145648	19/16	2.98E-4	2.98E-4	1.001	1.027	0,901	1.032	202.4	5,4	71.2
GJ235	INTRUSIVE	-74.105889	10.797306	15/15	2.52E-3	0.242E-4	1.064	1.007	-0.807	1.079	52.5	54.4	20.2
GJ237*	INTRUSIVE	-74.217873	11.085176	14/14	8.74E-4	8.74E-4	1.017	1.004	-0.641	1.022	183.7	6.4	30.9
GJ238	INTRUSIVE	-74.231075	11.200486	13/13	3.23E-5	32.3E-4	1.050	1.017	-0.483	1.070	71.5	65.4	10.6
GJ239*	INTRUSIVE	-74.234573	11.184942	12/10	5.21E-5	52.1E-4	1.025	1.034	0.146	1.061	248.2	57.3	29.4
GJ240	INTRUSIVE	-74.234355	11.180841	14/13	1.15E-4	1.15E-4	1.020	1.102	0.659	1.133	204.7	39.5	10.2
GJ241*	INTRUSIVE	-74.21794	11.018509	12/12	4.06E-4	4.06E-4	1.003	1.088	0.942	1.104	160.6	28.9	38.5
GJ242*	INTRUSIVE	-74.2159	11.073854	16/16	8.95E-4	8.95E-4	1.003	1.028	0.823	1.035	119.9	4.7	82.2
GJ243	INTRUSIVE	-73.894659	11.298865	12/12	7.87E-3	0.787E-4	1.072	1.022	-0.532	1.100	232.4	35.4	13
GJ244	INTRUSIVE	-73.895866	11.299719	12/10	6.26E-3	0.626E-4	1.037	1.014	-0.448	1.053	245.5	12.7	17.6
GJ245*	INTRUSIVE	-74.052362	11.278914	12/12	2.45E-2	0.0245E-4	1.011	1.227	0.885	1.275	17.7	5.9	49.1
GJ246	INTRUSIVE	-74.076418	11.271442	11/10	1.39E-2	0.0139E-4	1.066	1.105	0.233	1.179	294.4	84.1	11.4
GJ247	INTRUSIVE	-74.197826	11.192532	13/12	5.89E-4	5.89E-4	1.035	1.016	-0.383	1.053	103.1	25.8	14.4
GJ251	INTRUSIVE	-74.028278	11.232466	10/9	2.49E-3	0.249E-4	1.052	1.099	0.303	1.159	39.5	25.5	14.5
GJ235b	INTRUSIVE	-74.078722	10.810574	10/9	6.45E-3	0.645E-4	1.127	1.117	-0.04	1.259	353.8	57.5	10.6
CAS166*	INTRUSIVE	-74.097930	10.80097	9/9	5.44E-3	0.544E-4	1.020	1.023	0.049	1.043	124.9	57.3	38.6

The geographic coordinates are referred to WGS84 datu. n/N, number of samples giving reliable results/number of studied samples at a site. Km mean susceptibility in 10-4 SI. L, F, T and P' are magnetic lineation (Kmax/Kint), magnetic foliation (Kint/Kmin), shape factor and corrected anisotropy degree, respectively, according to Jelinek (1981). D and I are in situ site mean declination and inclination, respectively, of the maximun susceptibility axis. e12 is semi-angle of the 95% confidence ellipse around the mean kmax axis in the kmax-kint plane. * Sites with e12> 20º see text for datails

In nine sites, the AMS ellipsoid is prolate (T comprised between -0.04 and -0.807, Table 1). Low values of the P′ parameter (1.021–1.189) are present in 17 sites (Table 1). Four sites have High values of the P' parameter (1.206-1.275) (Table 1). Magnetic lineations in 17 sites is well defined (Fig 3), in most of the cases the lineations are N-NE. Four sites (GJ208, GJ233, GJ238 and GJ246) show vertical lineations with inclinations > to 65º (Fig 3 and Table 1). In one site (GJ229) the magnetic lineation shows a NW direction (Fig 3 and

Table 1). Three sites show a well defined magnetic foliation (GJ234, GJ241 and GJ245)

Two sites shows low inclinations values (12.2 – 12.7), seven sites shows moderate inclination values (21.3 – 39.5) and six sites shows high inclinations values (54.4 – 81.1), (Fig. 3 and Table 1).

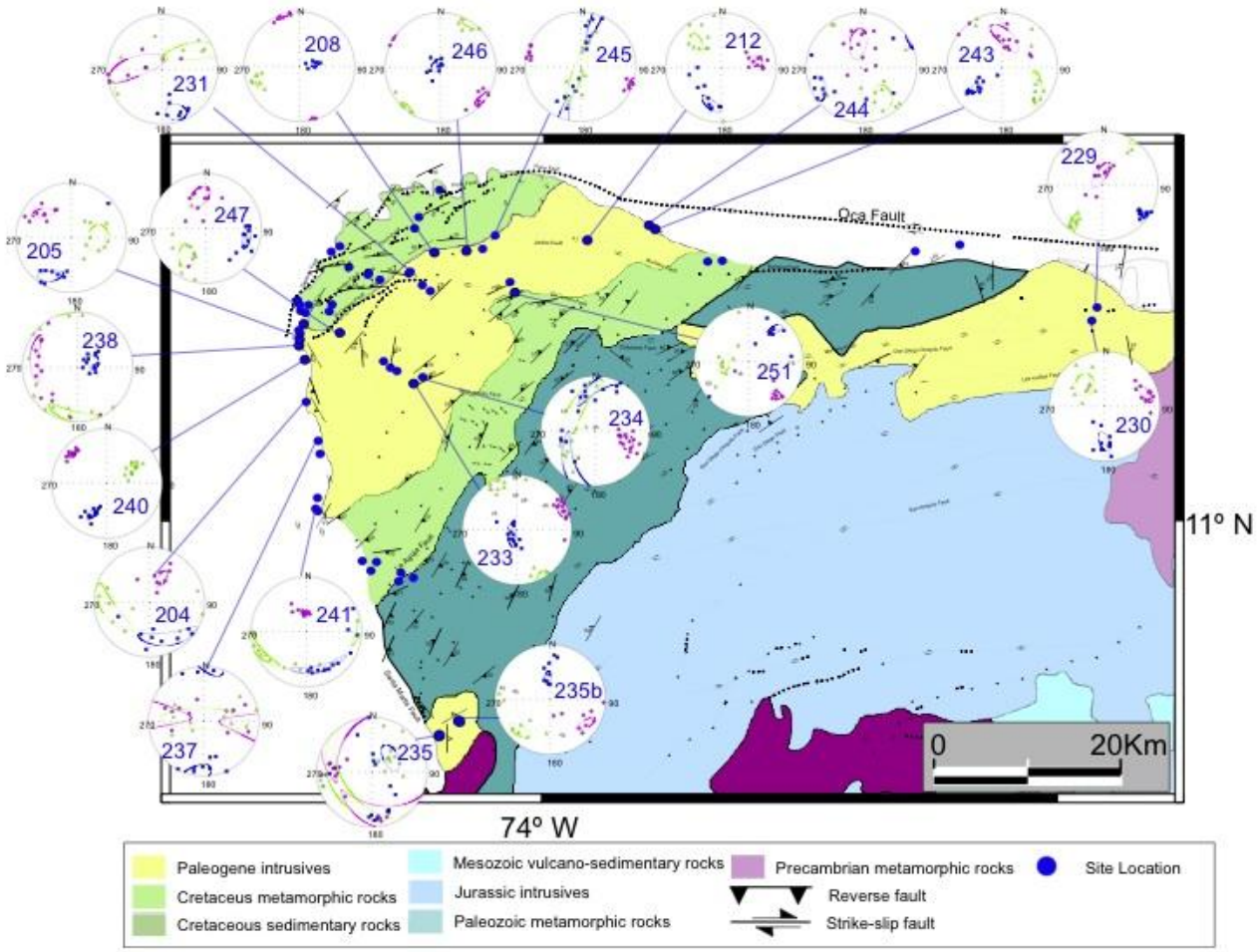

Figure 3. Geological map of the NW margin of Santa Marta Massif and adjacent zones (see Figure 2 for location). With schmidt equal-area projections, lower hemisphere, magnetic fabric projections of K1, K2 and K3. Lineation and foliation are defined for samples of the Santa Marta batholith. For all parameters values, see Table 1.

4. 2 Foliations and Lineations

Around the Santa Marta Fault the foliation strikes is NE to EW in the Cretaceous metamorphic sequence. Foliation into and in the granitic borders is NW. Dips values are randomly, mostly moderately to high. The trend lineation in different localities shows SW stretching directions, in one locality is defined by NE direction, locally the sites 56 and 256 shows lineations with a NW and SSE directions (Fig. 4). Foliation around the Oca Fault in the Cretaceous metamorphic rocks is NE, in the Paleozoic rocks is variable and disperse in three directions, NE, NW and EW. Foliations measured into the granitic rocks shows strikes EW. Dips values are lower to moderate, in the Paleozoic locality dips are randomly and disperse as the foliation strike.

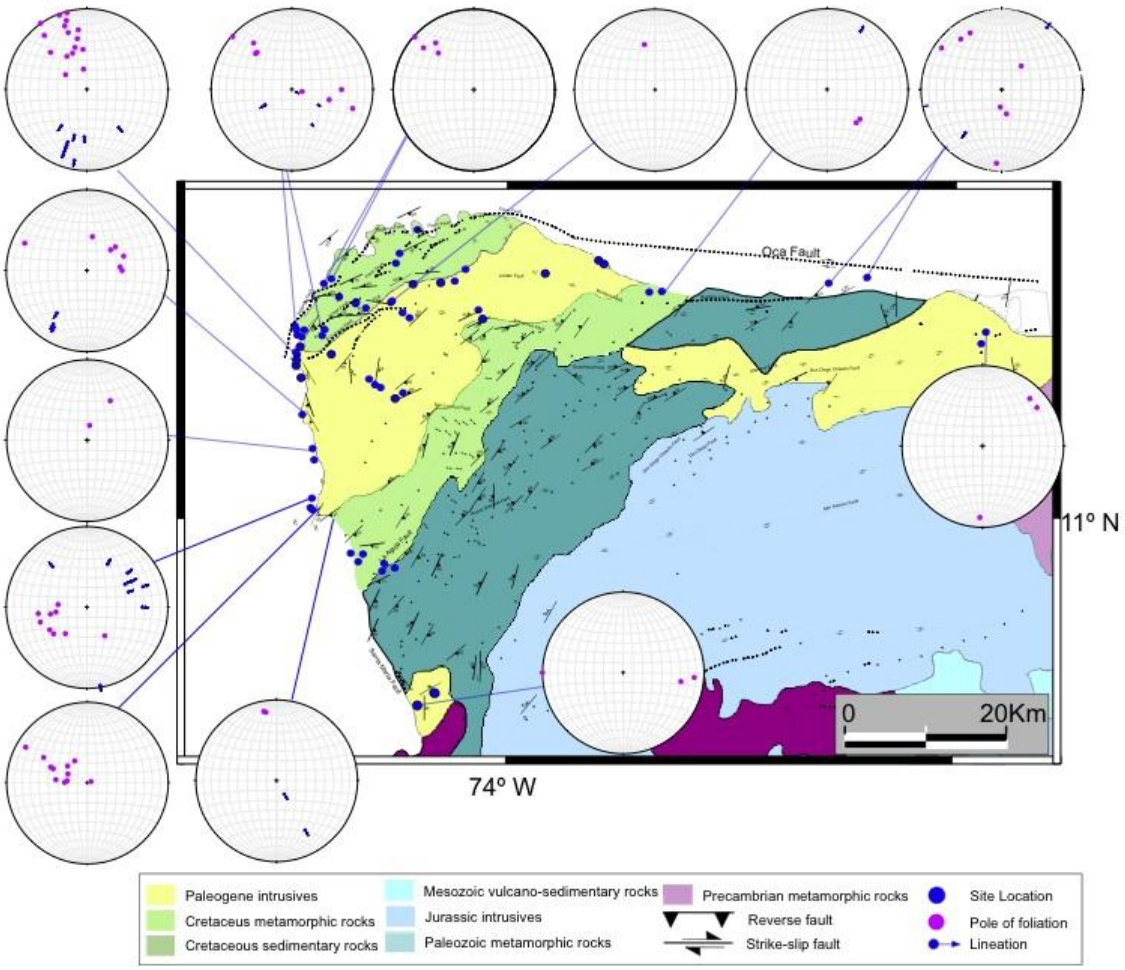

Figure 4. Structural map of the NW margin of Santa Marta Massif and adjacent zones (see Figure 2 for location). Schmidt equal-area projections, lower hemisphere, with poles of foliation. Blue arrows represent stretching lineations. (Blue pints and numbers are site codes, see Table 1).

4. 3 Faults

177 fault planes where measured around the Santa Marta and Oca Faults, in some cases sites were combined to obtain acceptable population for the fault plane solution, showing the P-T axis (Fig. 5). Fault plane solutions around the Santa Marta fault were plotted ten localities. Northern localities into the metamorphous sequence show a NW-SE compressive vector and tension vector sub-vertical (Fig. 5).

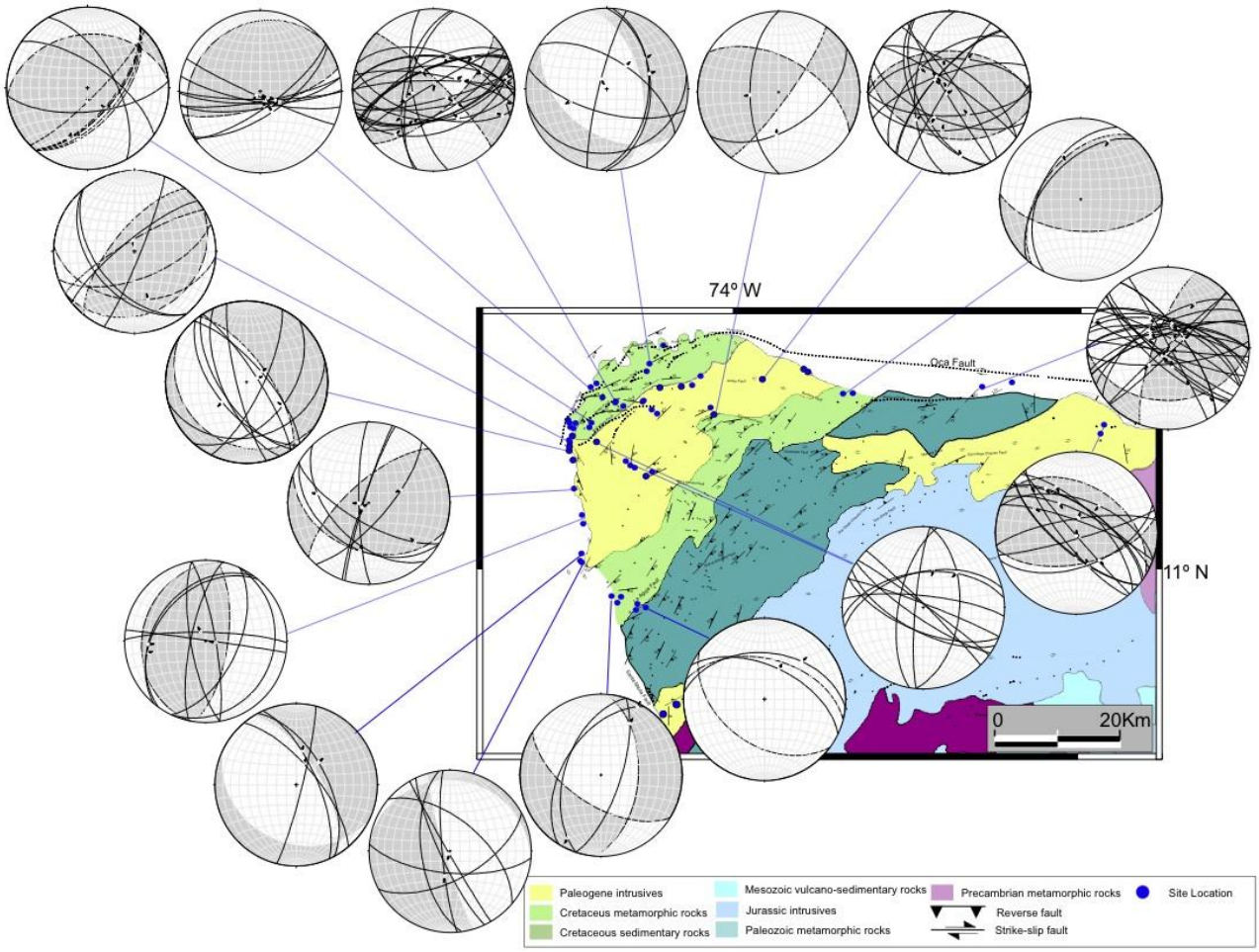

Figure 5. Geological map of the NW margin of Santa Marta Massif and adjacent zones (see Figure 2 for location) with schmidt equal-area projections, lower hemisphere, of fault populations and fault plane solutions, arrows represent fault kinematic. (Blue pints and numbers are site codes, see Table 1).

Southern the compressive vector is vertical and the tension vector sub-horizontal to E-W SW-NE. In three localities into the granitoids fault plane solutions, shows variations southern, from NS compression with sub-horizontal extension vector to sub-horizontal

extension vector SW-NE. For the Oca fault and related faults were plotted eight localities (Fig 5). Four localities show a horizontal compressive vector NNW-SSE with a vertical extension vector (Fig. 5). The other four localities around the Oca Fault, shows a NS compression vector with a subhorzontal EW extension vector.

5.0 Discussion and conclusions

The magnetic lineations obtained from AMS data, show magmatic fabrics with tectonic fabric modifications. In 17 of 25 sites are well defined magnetic lineations with direction N-NE, and vertical lineations >65º are in the most inner part of the intrusive body (Fig 3, Table 1).

Magnetic foliation is well defined only in four sites, in two sites (GJ204 and GJ241), around Santa Marta Fault the foliation plane is low-moderate. In other two sites (GJ234) at the inner zone of the intrusive and (GJ245) around the Oca Fault, the foliation planes are vertical (Fig. 3).

Foliation measured in the Cretaceous metamorphic sequence is coherent with a pattern NE of the Santa Marta belt and well correlated to foliations reported in detail maps (Ingeominas, 2007). These foliations develop a zonation around Paleogene granitoids with stretching lineations parallel to strike foliation NE (Fig. 4). Brittle deformation recorded in striated faults shows faults solutions in different localities around the Santa Marta and Oca faults (Fig 5). Striated faults measured in the Cretaceous metamorphic sequence have NW-SW compressive vector, coherent to the master wrench left-lateral Santa Marta Fault and right-lateral Oca Fault. Southern localities related to Santa Marta Fault develop a sub-horizontal extension vector at SSW-NNE direction (Fig. 5). In general fault localities measured around the Oca Fault show a NW-SE compression vector.

Our field data shows almost two deformation phases, first one a ductile deformation related to the emplacement of the granitoid cutting the Cretaceous metamorphic sequence in a tectonic setting of extension in a SW-NE directions, developing stretching lineations in the host rocks, parallels to the NE strike foliation (Fig. 3 and Fig 4). During this phase the intrusion develop a magmatic fabric vertical magnetic lineations in the inner zone of the intrusive body, NE magnetic and structural lineations are coherent at outer borders (Fig. 3) as well as magnetic foliation are tectonic modified and tend to be higher at the inner zone and lower at borders. The second phase is developed in a brittle deformation setting, related to wrench faulting of the Santa Marta and Oca faults (Fig. 5) with a constant NW-SE shortening direction. According to our field data and AMS distribution let us to propose a NE-SW extensional setting in a ductile regime for the Late Paleocene to Early Eocene granitoid (Cardona et al, 2008 and Duque, 2009). The intrusion deformation involves the host rock printing a well defined NE foliation with a SW stretching (Fig. 6).

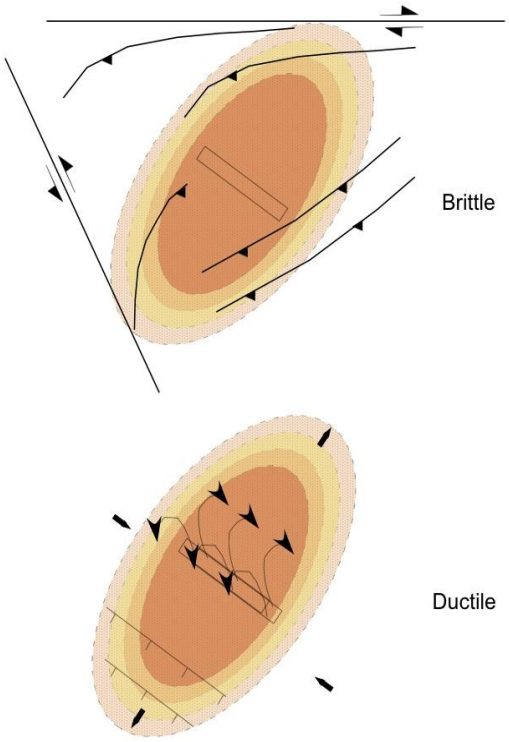

Figure 6. Schematic out scale graphic showing the intrusion-evolution from ductile to brittle regimens for the Santa Marta Batholith.

Our data is well correlated with an extensional phase recorded in the stratigraphic sequence in the Plato-San Jorge Basin (Lower Magdalena Valley) (Montes et al., 2009). Montes et al., (2009) propose the beginning of this extension during the Late Eocene with normal faults related with structural trend NNW-NW (Fig. 6).

References

Bayona, G., A. Rapalini, and V. Costanzo- Alvarez (2006), Paleomagnetism in Mesozoic rocks of the Northern Andes and its implications in Mesozoic tectonics of northwestern South America, Earth Planets Space, 58, 1255–1272.

Bayona, G., F. Lamus, Ochoa, A. Cardona, C. Jaramillo, C. Montes, and N. Tcheglilakova (2007), Procesos orogénicos del Paleoceno para la cuenca de Ranchería (Guajira, Colombia) y áreas adyacentes definidos por análisis de procedencia, Geol. Colombiana, 32, 21–46.

Bayona, G., G. Jiménez, C. Silva, A. Cardona, C. Montes, J. Roncancio, and U. Cordani (2010), Paleomagnetic data and K- Ar ages from Mesozoic units of the Santa Marta massif: A preliminary interpretation for block rotation and translations, J. S. Am. Earth Sci., 29(4), 817–831, doi:10.1016/j.jsames.2009.10.005.

Cardona, A., U. G. Cordani, and W. D. MacDonald (2006), Tectonic correlations of pre- Mesozoic crust from the northern termination of the Colombian Andes, Caribbean region, J. S. Am. Earth Sci., 21(4), 337–354, doi:10.1016/j.jsames.2006.07.009.

Cardona, A., Duque, J.F., Ruiz, J., Valencia, V., Bayona, G., Jaramillo, C., Ojeda, G., Orozco, M.T., 2008. Geochronology and tectonic implications of granitoids rocks from the northwestern Sierra Nevada de Santa Marta and surrounding basins, northeastern Colombia: Late Cretaceous to Paleogene convergence, accretion and subduction interactions between the Caribbean and South American plates. 24th–28th March 2008, Santo Domingo (Dominican Republic), Abstract Volume of the 18th Caribbean Geological Conference, 24-25.

Cardona, A., V. Valencia, G. Bayona, C. Jaramillo, G. Ojeda, and J. Ruiz (2009), U/Pb LA- MC- ICP- MS zircon geochronology and geochemistry from a postcollisional biotite granite of the Baja Guajira Basin, Colombia: Implications for Late Cretaceous and Neogene Caribbean- South American tectonics, J. Geol., 117(6), 685–692, doi:10.1086/605776.

Cardona, A., Valencia, V., Bustamante, C., Garcia-Casco, A., Ojeda, G., Ruiz, J., Saldarriaga, M., Weber, M., 2010a. Tectonomagmatic setting and provenance of the Santa Marta Schists, northern Colombia: Insights on the growth and approach of Cretaceous Caribbean oceanic terranes to the South American continent. Journal of South American Earth Sciences 29, 784e804.

Cardona, A., Valencia, V.A., Bayona, G., Duque, J., Ducea, M., Gehrels, G., Jaramillo, C., Montes, C., Ojeda, G., Ruiz, J., 2010b. Early-subduction-related orogeny in the northern Andes: Turonian to Eocene magmatic and provenance record in the Santa Marta Massif and Rancheria Basin, northern Colombia. Terra Nova 23, 26e34.

Cordani, U. G., A. Cardona, D. M. Jiménez, D. Liu, and A. P. Nutman (2005), Geochronology of Proterozoic basement inliers in the Colombian Andes: Tectonic history of remnants of a fragmented Grenville belt, Geol. Soc. London Spec. Publ., 246(1), 329–346, doi:10.1144/gsl.

Cediel, F., R. Shaw, and C. Cáceres (2003), Tectonic assembly of the northern Andean Block, in Bartolini, C., Buffler, R. T., and Blickwede, J., eds., The Circum-Gulf of Mexico and the Caribbean: Hydrocarbon habitats, basin formation and plate tectonics, American Association of Petrolum Geologists Memoir 79, p. 815-848.

Bustamante, C., Cardona, A., Saldarriaga, M., Garcı´a-Casco, A., Valencia, V. and Weber, M., 2009. Metamorfismo de los esquistos verdes y anfibolitas pertene- cientes a los Esquistos de Santa Marta, Sierra Nevada de Santa Marta (Colom- bia): ¿registro de la colisio´ n entre el Arco Caribe y la margen Suramericana? Bol. Cien. de la Tierr.,

25, 7–26.

Doolan, B. L., 1970. The structure and metamorphism of the Santa Marta area, Colombia, South America. Binghamton, State University of New York, Ph. D. Dissertation. 200 pp.

Duque, J.F., 2010. Geocronología (U/Pb y 40Ar/39Ar) y geoquímica de los intrusivos paleógenos de la Sierra Nevada de Santa Marta y sus relaciones con la tectónica del Caribe y el arco magmático circun-Caribeño. Tesis de Maestría, UNAM, 189 p.

Ingeominas (2007a), Geologic Map of the Sierra Nevada de Santa Marta, scale 1:200,000, Ingeominas- Invemar- Ecopetrol- ICP- Geosearch, Ltda., Bogota.

Ingeominas (2007b), Geología de las planchas 11, 12, 13, 14, 18, 19, 20, 21, 25, 26, 27, 33 Y 34. Proyecto “Evolución Geohistórica de la Sierra Nevada de Santa Marta,” 333 pp., Ingeominas- Invemar- Ecopetrol- ICP- Geosearch, Ltda., Bogota.

Jelinek, V. (1977). The statistical theory of measuring anisotropy of magnetic susceptibility of rocks and its application. Geofyzika, Brno. 88.

Jelinek, V. (1978). Statistical processing of magnetic susceptibility on groups of specimens. Stud. Geophys. Geod. 22, 50–62.

Kellogg, J., and W. Bonini (1982), Subduction of the Caribbean Plate and basement uplifts in the overriding South American Plate, Tectonics, 1, 251–276, doi:10.1029/TC001i003p00251.

Macellari, C. E. (1995), Cenozoic sedimentation and tectonics of the southwestern Caribbean pull- apart basin, Venezuela and Colombia, in Petroleum Basins of South America, edited by A. Tankard, S. Suarez, and H. Welsink, AAPG Mem. 62, 757–780.

Mantilla, A., 2007. Crustal structure of the southwestern Colombian Caribbean margin. Jena. Friedrich-Schiller-Universität, Ph D.Thesis.

Montes, C., Guzmán, G., Bayona, G., Cardona, A., Valencia, V., 2010. Clockwise Rotation of the Santa Marta Massif and Simultaneous Paleogene to Neogene Deformation of

the Plato-San Jorge and Cesar-Ranchería Basins. Journal of South American Earth Sciences, 29, 832-848.

Ordóñez Carmona, O., J. J. Restrepo Álvarez, and M. M. Pimentel (2006), Geochronological and isotopical review of pre- Devonian crustal base- ment of the Colombian Andes, J. S. Am. Earth Sci., 21(4), 372–382, doi:10.1016/j.j0073ames.2006.07.005.

Pindell, J. L., S. C. Cande, W. C. Pitman III, D. B. Rowley, J. F. Dewey, J. LaBrecque, and W. Haxby (1988), Plate- kinematic framework for models of Caribbean evolu- tion: Tectonophysics, v. 155, p. 121–138.

Pindell, J., Kennan, L., Maresch, W., Stanek, K., Draper, G. and Higgs, R., 2005. Plate kinematics and crustal dynamics of circumCaribbean arccontinent interactions: Tectonic controls on basin development in ProtoCaribbean margins. In: AveLallemant and Sisson (eds) Geological Society of America Special Paper 394, pp. 752.

Restrepo- Pace, P. A., J. Ruiz, G. Gehrels, and M. Cosca (1997), Geochro- nology and Nd isotopic data of Grenville- age rocks in the ColombianAndes: New constraints for Late Proterozoic- Early Paleozoic paleoconti- nental reconstructions of the Americas, Earth Planet. Sci. Lett., 150(3–4), 427–441, doi:10.1016/S0012-821X(97)00091-5.

Sisson, V.B., Ertan, I.F., AvéLallemant, H.G., 1997. High Pressure (~2000 MPa) glaucophanebearing pelitic schist and eclogite from Cordillera de la Costa belt, Venezuela. Journal of Petrology 38, pp. 6583.

Smith, C.A, Sisson, V.B., AvéLallemant, H.G., 1999. Two contrasting pressure temperaturetime paths in the Villa de Cura blueschist belt, Venezuela: Possible evidence for Late Cretaceous initiation of subduction in the Caribbean. Geological Society of America Bulletin: Vol. 111, No. 6, pp. 831848.

Tarling, D.H.; Hrouda, F. 1993. The Magnetic Anisotropy of Rocks. Chapman and Hall: 217 p. London.

Tschanz, C. M., Jimeno, A., Cruz, J., 1969. Geology of the Santa Marta area (Colombia). In- stituto Nacional de Investigaciones Geológico Mineras. Informe 1829. 288 p.

Tschanz, C., Marvin, R., Cruz, J., Mehn- ert, H. and Cebula, E., 1974. Geologic evolution of the Sierra Nevada de Santa Marta. Geol. Soc. Am. Bull., 85, 273– 284.

Villagómez, D. (2010), Thermochronology, geochronology and geochem- istry of the western and central cordilleras and Sierra Nevada de Santa Marta, Colombia: The tectonic evolution of NW South America, Ph.D. thesis, 143 pp., Univ. de Genève, Geneva.

Villagómez, D. Spikings, R, Mora. A, Guzmán. G, Ojeda. G, Cortés. E and R. Van der Lelij (2011), Vertical tectonics at a continental crust-oceanic plateau, plate boundary zone: Fission track thermochronology of the Sierra Nevada de Santa Marta, Colombia. Tectonics, V. 30, TC4004, 18 PP.

Weber, M., Cardona, A., Valencia, V., Garcı´ a-Casco, A., Tobo´ n, M. and Zapata, S., 2010. U／Pb detrital zircon provenance from Late Cretaceous metamorphic units of the Guajira Peninsula, Colombia: tectonic implica- tions on the collision between the Caribbean arc and the South American margin. J. S. Am. Earth Sci., 29, 805– 816.

Zuluaga, C and H. Stowell (2012), Late CretaceousePaleocene metamorphic evolution of the Sierra Nevada de Santa Marta: Implications for Caribbean geodynamic evolution. Journal of South American Earth Sciences 34 (2012) 1-9

Chapter 5

Rift inversion during oblique convergence insight from analog modeling

1.0 Introduction

Extensional sedimentary basins become reactivated during compression, in a convergent plate margins setting in response to horizontal compression. Tectonic inversion describes basins that have been initially controlled by extensional faults and later reactivated with a reverse movement during a tectonic compression (Cooper and Williams, 1989). Previous works related to the evolution of thrust belts and rift inversion process has been deep developed analog models. First works focus to orthogonal compression of elementary extensional fault patterns such as simple listric normal fault or tilted blocks (e.g., Koopman et al., 1987; McClay, 1989; Buchanan and McClay, 1991; McClay and Buchanan, 1992). Basin inversion experiments in oblique setting have been performed (Brun and Nalpas, 1996; Keep and McClay, 1997 and Dubois et al., 2002). According to Brun and Nalpas (1996) and Gartrell et al., (2005) inversion along high-angle normal structures in brittle system a non-coaxial angle between the compressive and extensive stresses is required, the optimum angle for inversion close to 15º (Brun and Nalpas, 1996). Inversion can be occurred with higher angles even with orthogonal compression, using ductile silicone basal layers (Brun et al., 1994; Corti et al., 2003; Del Ventisette et al., 2006).

There are nature examples where extension has been followed by tectonic inversion. In the northern Andean subduction margin the classic example of this process is well know in the Eastern Cordillera of Colombia. The evolution of this mountain chain can be summarize as a Jurassic to Early Cretaceous back arc basin, Late Cretaceous passive margin to Paleogene foreland basin which underwent tectonic inversion during Miocene

(Cooper et al., 1995; Sarmiento-Rojas, 2001; Cortés et al, 2006 and Mora et al., 2008;). Inversion, in these cases, occurred during major changes of plate dynamics that resulted in modification of the stress regime affecting the continental margin (Cortés et al, 2006 and Montes et al, 2005). The aim in this paper is to understand and explore the mechanisms involved during the inversion of crustal-scale grabens in different scenarios (orthogonal to oblique), focus in the map-view geometry evolution (Fig .1 and 2).

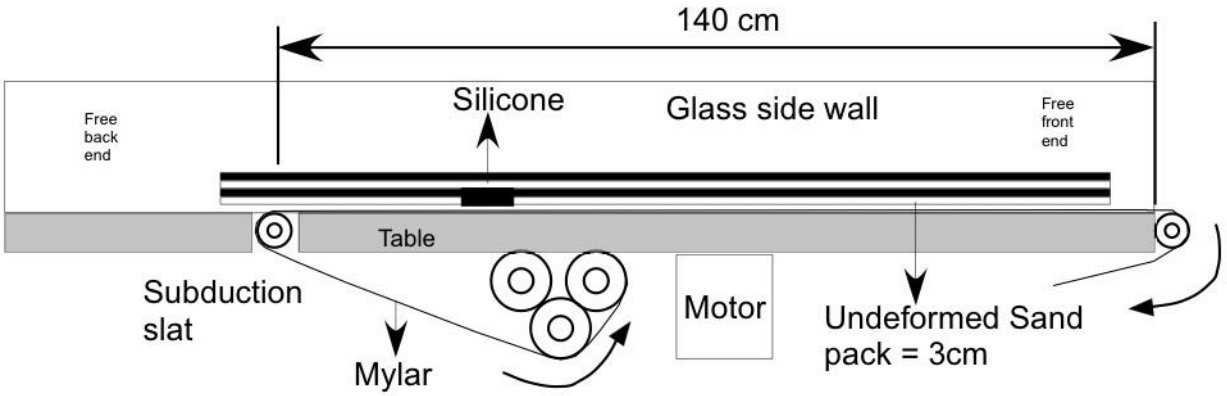

Figure 1. Diagram of the experimental sand box. The thickness of the sand and sand-silicone pack is 3 cm. The two glass side walls were positioned at a constant distance of 58 cm each other for all the experiments.

2.0 Methods

2.1 set up

The modeling set up are similar to previous experiments on brittle-ductile systems (e.g.,Faugbre and Brun, 1984; Vendevilleet al., 1987; Davy and Cobbold, 1991) (Fig 2 and Fig 2). Brittle basement and sedimentary cover are represented by sandwich layering with a mean friction coefficient ß of 0.6 (Table 1). Ductile behavior is represented by Newtonian silicone putty with a viscosity of 1.90 E 5 Pa-S (Table 1).

Table 1. Experimental parameters for brittle and ductile materials.

Brittle parameters	
Longitud (m)	0.01
Sand density (Kg/m3)ρ_b	1686
Coefficient of friction (u)	0.6
Gravity [m/s2]	9.8
Velocity (cm/h)	5
Ductile parameters	
Longitude (m)	0.01
Silicone density (Kg/m3)ρ_d	1409
Silicone Viscosity [Pa s] η	1.90 E 5
Gravity [m/s2]	9.8
Velocity (cm/h)	5

Eight different scenarios in normal to oblique convergence where analyzed. Four experiments in brittle and four experiments in ductile regime. For every regime convergence variation was 0º, 15º, 30º and 45º with a constant velocity of 5 cm/h (Table 1)

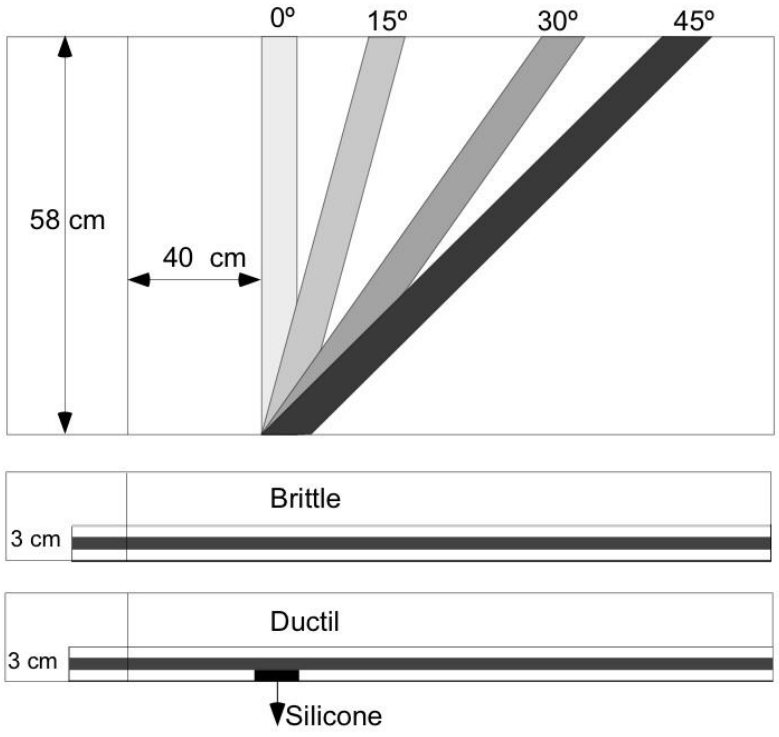

Figure 2. Set up experiments showing the top view and side view set up in two scenarios, Brittle and ductile.

In top view are the four rifts from normal to oblique (0º, 15º, 30º and 45º). Side view showing homogenous layering in brittle experiments and silicone-sand layering in ductile experiments.

3.0 Results

3.1 Brittle-ductile 0º

Following the parameters reported in (Table 1) the 0º experiments in brittle regimen can be summarized in a homogeneous rift with two major normal faults. Red sand marker used during rifting (Fig. 3) let us to see that the inversion in the 0º brittle experiment is focused on the major normal fault. Experiments in ductile regimen shows an extensive deformation area around the rift zone, normal fault are more developed (Fig 3). During the compression the silicone (ductile layer) created a positive flower in the rift zone in a synchronous way.

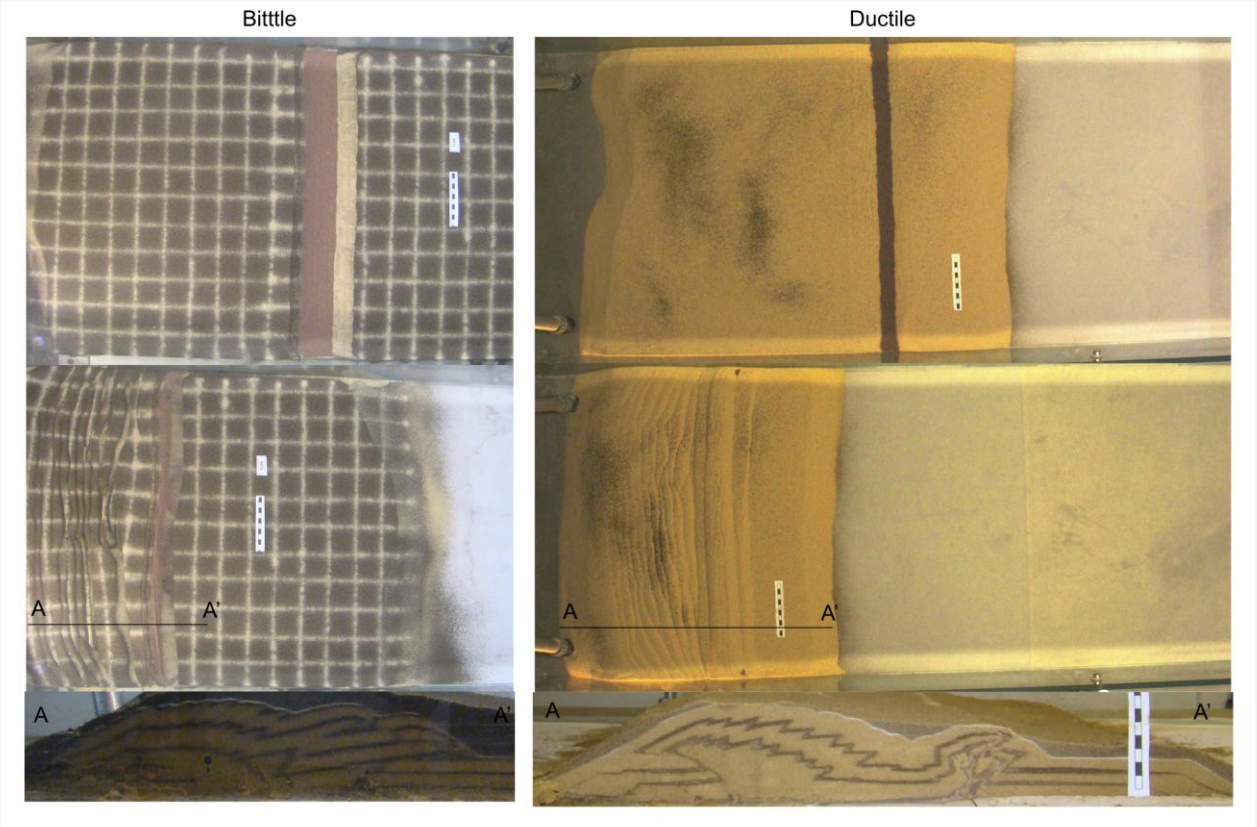

Figure 3. Brittle-Ductile experiments for 0º parallel extension-compression setting. Top view of final rifting and final top view of compression, cross section A-A' showing the structures after rift inversion.

3.2 Brittle-ductile 15º

The 15º experiments in brittle regimen are a continuous homogeneous rift with two major

normal faults (Fig. 3). Rift inversion in the 15º brittle experiment is focused on the major normal fault during the inversion. Ductile experiments shows an extensive deformation area around the rift zone, normal fault are more developed (Fig 4). During the rift inversion the ductile layer develop a positive flower in the rift zone, and exhumed the red sand market. The rift inversion occurred in synchronous phases.

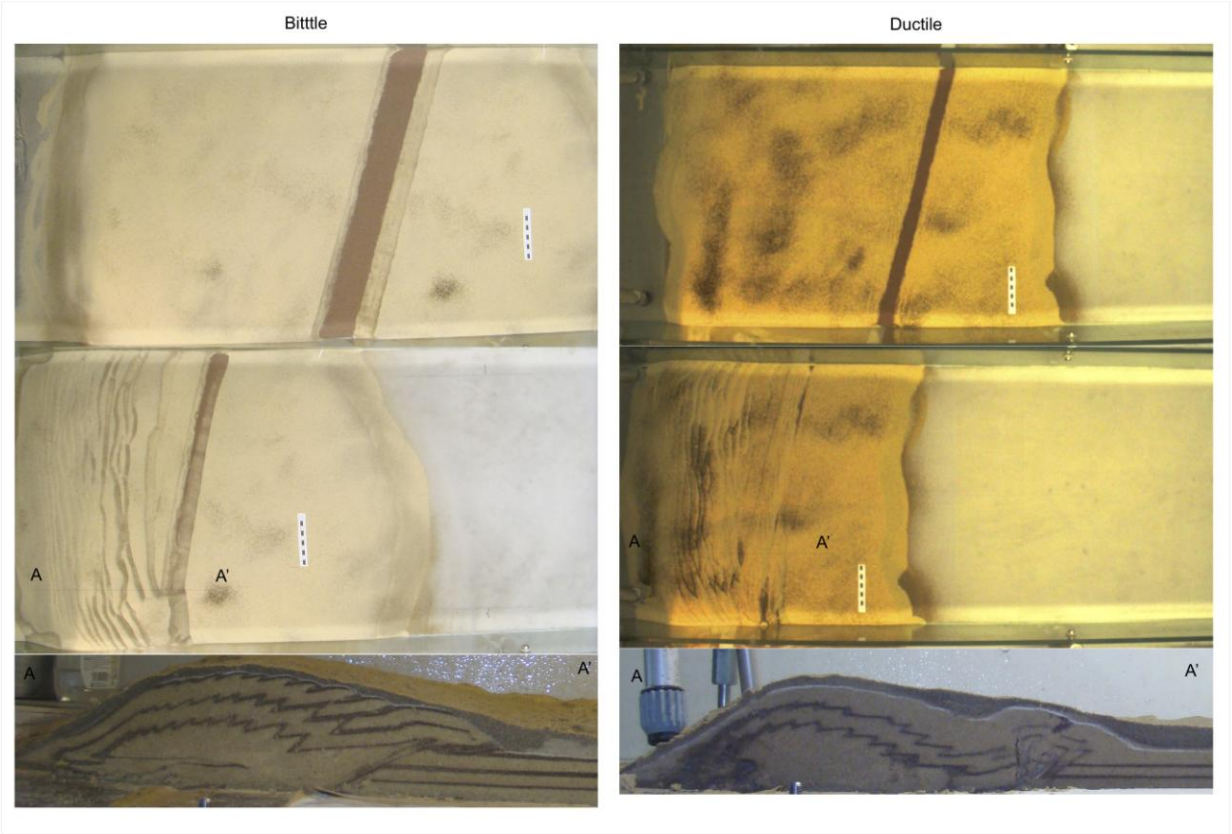

Figure 4. Brittle-Ductile experiments for 15º oblique extension-compression setting. Top view of final rifting and final top view of compression, cross section A-A' showing the structures after rift inversion.

3.3 Brittle-ductile 30º

The 30º brittle experiments are a homogeneous rift with two major normal faults (Fig. 5). Rift inversion in the 30º brittle experiment is focused on the major normal fault, but the inversion is divided by panels or in oblique structures, causing a diachronous inversion (Fig 5). Ductile 30º experiments show the extensive deformation area around the rift zone, with normal oblique faults (Fig 4). Rift inversion is diachronous with oblique structures

developing panels (Fig 5), during the oblique convergences the panel's inversion start with dextral strike slip component, compression and the inversion migrate to next panel (Fig. 5). In cross section the ductile layer develop a positive flower in the rift zone, foreland verging.

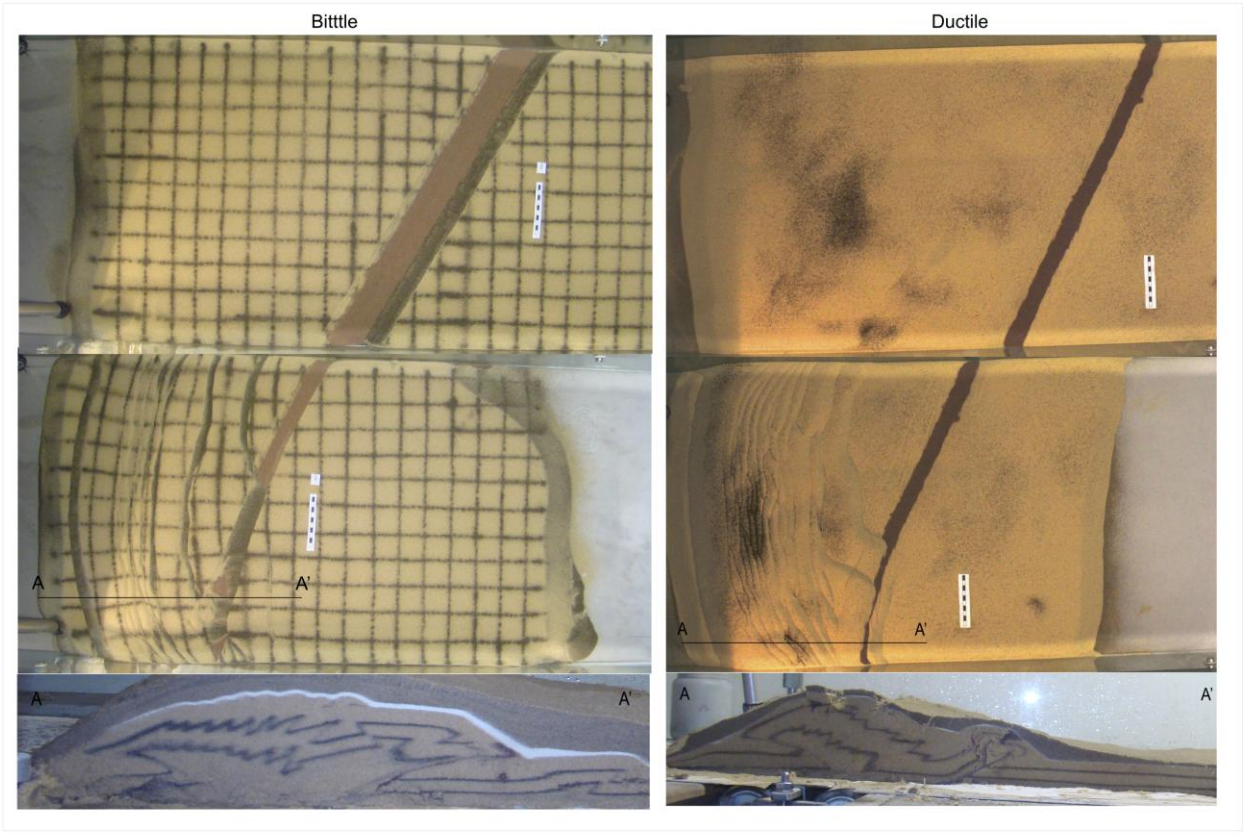

Figure 5. Brittle-Ductile experiments for 30º oblique extension-compression setting. Top view of final rifting and final top view of compression, cross section A-A' showing the structures after rift inversion

3.4 Brittle-ductile 45º

The 45º brittle experiments are a constant homogeneous rift with the common two major normal faults (Fig. 6). Rift inversion in the 45º brittle experiment is a complex combination between oblique convergence and dextral strike -slip component. During the brittle inversion the 45º experiment develop almost three panels and in the same process that in the 30º experiments the inversion diachronous and after every panel inversion, migrate to next one (Fig 6).

Ductile 45º experiments develop clearly oblique extensional faults around the rift zone (Fig

6). Rift inversion in ductile regimen develop panels (Fig 6), during the oblique convergences the panel's inversion start with dextral strike-slip component is diachronous and more evident that after every panel inversion the inversion migrate to next panel (Fig. 6). In cross section the ductile layer develop the typical positive flower in the rift zone.

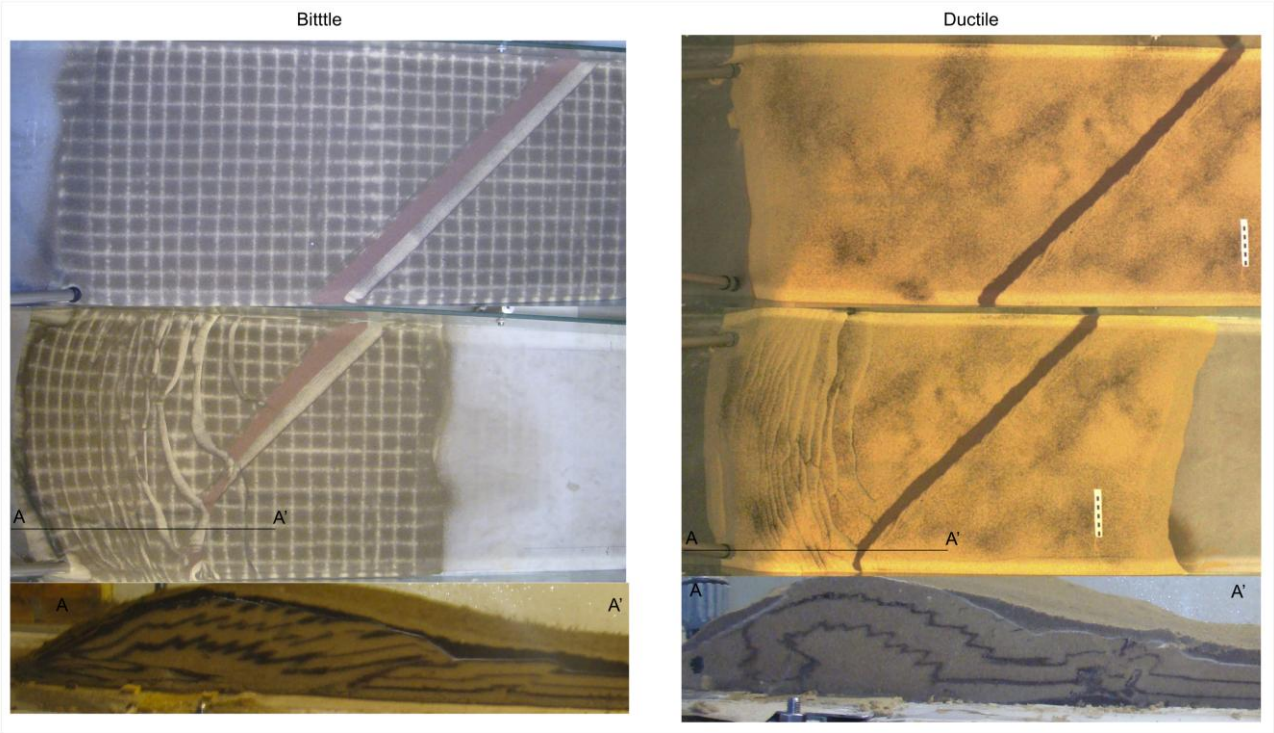

Figure 6. Brittle-Ductile experiments for 45º oblique extension-compression setting. Top view of final rifting and final top view of compression, cross section A-A' showing the structures after rift inversion.

References

Buchanan, P.G and K.R. McClay. (1991), Sandbox experiments of inverted listric and planar fault systems. In: Cobbold, P.R. (Ed.), Experimental and Numerical Modelling of continental Deformation: Tectonophysics, 188, pp. 97–115.

Brun, J.P., D. Sokoutis, and J. Van Den Driessche. (1994), Analogue modeling of detachment fault systems and core complexes. Geology 22, 319-322.

Brun, J.P and T. Nalpas. (1996), Graben inversion in nature and experiments. Tectonics 15, 677–687.

Corti, G., M. Bonini, S. Conticelli, F. Innocenti, P. Manetti, and D. Sokoutis. (2003), Analogue modelling of continental extension: a review focused on the relations between the patterns of deformation and the presence of magma. Earth-Science Reviews 63, 169–247.

Cooper, M.A and G.D. Williams. (1989). Inversion Tectonics, 44. Geological Society of London Special Publication. 375 pp.

Cooper, M. A., F.T. Addison, R. Álvarez, M. Coral, R. H. Graham, A. B. Hayward, S.

Howe, J. Martínez, J. Naar, R. Peñas, A. J. Pulham, and A. Taborda (1995), Basin development and tectonic history of the Llanos Basin, Eastern Cordillera, and Middle Magdalena Valley, Colombia, AAPG Bull., 79, 1421–1443.

Cortés, M., B. Colletta, and J. Angelier (2006), Structure and tectonics of the central segment of the Eastern Cordillera of Colombia, Journal of South American Earth Sciences., 21, 437–465, doi:10.1016/j.jsames.2006.07.004.

Davy, P., and P.R. Cobbold (1991), Experimentson shorteningof a 4-layer model of continen- tal lithosphere,Tectonophysics1,88, 1-25.

Del Ventisette. C, D. Montanari, F. Sani, and M. Bonini. (2006), Basin inversion and fault reactivation in laboratory experiments. In: Tavarnelli, E., Butler, R., Grasso, M. (Eds.),

Tectonic Inversion Processes and Structural Inheritance in Mountain Belts: Journal of Structural Geology, 28, pp. 2067–2083.

Dubois, A. F. Odonne, G. Massonnat, T. Lebourg, and R. Fabre. (2002), Analogue modeling of fault reactivation: tectonic inversion and oblique remobilisation of grabens. J. Struct. Geol. 24, 1741e1752.

Faugre, E and J.P. Brun. (1984), Mode1isation experimentale de la distension continentale, C R. Acad.Sci.,299, Ser.II, 365-370.

Keep, M and K.R. McClay. (1997), Analogue modelling of multiphase rift systems. Tectonophysics 273, 239-270.

Koopman, A, A. Speksnijder and W.T. Horsfield. (1987) Sandbox model studies of inversion tectonics. In: Ziegler, P.A. (Ed.), Compressional Intra-plate Deformations in the Alpine Foreland: Tectonophysics, 137, pp. 379–388.

McClay, K.R. (1989), Analogue models of inversion tectonics. In: Cooper, M.A., Williams, G.D. (Eds.), Inversion tectonics, 44. Geological Society of London, Special Publication, pp. 41–62.

McClay, K.R and P.G. Buchanan. (1992), Thrust faults in inverted extensional basin. In: McClay, K.R. (Ed.), Thrust Tectonics. Chapman and Hall, London, pp. 93–104.

Montes, C., T. Robert, D. Jr Hatcher, P. A. Restrepo-Pace (2005), Tectonicreconstruction of the northern Andean blocks: Oblique convergence and rotations derived from the kinematics of the Piedras–Girardot area, Colombia, Tectonophysics 399. 221–250, doi:10.1016/j.tecto.2004.12.024

Mora, A., M. Parra, M. R. Strecker, E. R. Sobel, H. Hooghiemstra, V. Torres and J.Vallejo-Jaramillo (2008), Climatic forcing of asymmetric orogenic evolution in the Eastern Cordillera of Colombia, Geol. Soc. Am. Bull., 120, 930–949,doi:10.1130/ B26186.1.

Sarmiento-Rojas, L. F (2001), Mesozoic rifting and Cenozoic basin inversion history of the

Eastern Cordillera, Colombian Andes, Ph.D. thesis, 295 pp., Vrije Univ.,Amsterdam.

Vendeville, B.C. (1988), Modeles experimentaux de fracturation de la couverture contre le par des failles normales dans le socle, C. R. Acad. Sci., Ser. II, 307, 1013-1019.